Mechanics of growth and remodeling in native and engineerd cardiovascular tissues

Oomen, P.J.A.

Accepted/In press: 15/10/2018

Document Version
Publisher's PDF, also known as Version of Record (includes final page, issue and volume numbers)

MECHANICS OF
GROWTH AND REMODELING
IN NATIVE AND ENGINEERED CARDIOVASCULAR TISSUES

PIM J.A. OOMEN

MECHANICS OF
GROWTH AND REMODELING
IN NATIVE AND ENGINEERED CARDIOVASCULAR TISSUES

PIM J.A. OOMEN

A catalogue record is available from the Eindhoven University of Technology Library

ISBN 978-90-386-4593-3

Cover design by Pim J.A. Oomen

Printed by Gildeprint, Enschede

Financial support by the Dutch Heart Foundation and ETB-BISLIFE for the publication of this thesis is gratefully acknowledged.

The work in this thesis was supported by the European Union's Seventh Framework Programme for research, technological development and demonstration under grant agreement no. 604514 (ImaValve), and the Netherlands Cardiovascular Research Initiative (CVON 2012-01): The Dutch Heart Foundation, Dutch Federation of University Medical Centers, the Netherlands Organization for Health Research and Development and the Royal Netherlands Academy of Sciences.

Mechanics of growth and remodeling in native and engineered cardiovascular tissues

Proefschrift

ter verkrijging van de graad van doctor aan de Technische Universiteit Eindhoven, op gezag van de rector magnificus prof.dr.ir. F.P.T. Baaijens, voor een commissie aangewezen door het College voor Promoties, in het openbaar te verdedigen op donderdag 15 oktober 2018 om 13:30 uur

door

Pim Jacobus Andreas Oomen

geboren te Rotterdam

Dit proefschrift is goedgekeurd door de promotoren en de samenstelling van de promotiecommissie is als volgt:

Voorzitter	prof. dr. ir. Frank P.T. Baaijens
Promotor	prof. dr. Carlijn V.C. Bouten
Co-promotor	dr. ir. Sandra Loerakker
Leden	prof. dr. med. dr. rer. nat. Simon P. Hoerstrup (Universität Zürich)
	prof. dr.-ing. Gerhard A. Holzapfel (Graz University of Technology)
	prof. dr. ir. Hans van Oosterwijck (Katholieke Universiteit Leuven)
	prof. dr. ir. Frans N. van de Vosse

Het onderzoek of ontwerp dat in dit proefschrift wordt beschreven is uitgevoerd in overeenstemming met de TU/e Gedragscode Wetenschapsbeoefening.

Biomechanics aims to explain the mechanics of life and living. From molecules to organisms, everything must obey the law of mechanics. Clarification of mechanics clarifies many things. Biomechanics helps us to appreciate life. It sensitizes us to observe nature. It is a tool for design and invention of devices to improve the quality of life. It is a useful tool, a simple tool, a valuable tool, an unavoidable tool. It is a necessary part of biology and engineering.

Y.C. Fung – Biomechanics: Motion, Flow, Stress, and Growth, 1990

Contents

Summary

Mechanics of growth and remodeling in native and engineered cardiovascular tissues

Cardiovascular tissues have the intriguing capacity to actively change their form and function. While these changes are most prominent during embryonic development, most living tissues are in a continuous state of adaptation through growth and remodeling. Since the time of Galileo Galilei, it has been believed that tissue growth and remodeling are strongly influenced by mechanical factors. Now, almost four centuries later, these processes are still only partially understood. From a biomechanical perspective, it is well accepted that growth and remodeling occur at least partly in response to changes in the tissue's mechanical environment, in order to maintain a certain mechanical tissue homeostasis. To date, it remains unclear what mechanical measure(s) determine(s) mechanical homeostasis in cardiovascular tissues. Growth and remodeling are of key importance to the functioning of human cardiovascular tissues during both health and disease. Furthermore, they are pivotal to the field of tissue engineering, which aims to create living tissue replacements that last a lifetime and should therefore be capable of functional growth and remodeling.

If engineered cardiovascular tissues are to be successful in the long term, further research on and, eventually, control of growth and remodeling and mechanical homeostasis in engineered cardiovascular tissues is required. In this thesis, a wide range of experimental and numerical techniques were used to (1) to identify what mechanical quantity determines mechanical homeostasis in native cardiovascular tissues, in this case heart valves, and (2) to investigate if a mechanical homeostasis could also be established in engineered cardiovascular tissues.

We first outline the importance and challenges of studying growth and remodeling in native and engineered cardiovascular tissues (Chapter 1). Next, age-related changes in native heart valves were studied to unravel which mechanical quantity determines mechanical homeostasis in native tissues during postnatal development (Chapter 2). To this end, an extensive data set was compiled of paired human aortic and pulmonary valves of fetal to adult age. Each valve was structurally, geometrically, and mechanically characterized. The outcomes were used to predict age-dependent changes in stress and stretch in the heart valves via finite element modeling. We predicted that the aortic valve stress increases with age, whereas remarkable small differences were found in stretch with age and between the aortic and pulmonary valve. These results suggest that mechanical homeostasis in human native heart valves is driven by tissue stretch.

Since growth and remodeling occur simultaneously during postnatal development, we developed finite element models, informed by the experimental data from the previous chapter, to elu-

cidate the roles of growth and remodeling during postnatal development (Chapter 3). The models indicated that growth and remodeling play opposing roles in preserving tissue stretch homeostasis during physiological development. During early development (infant to adolescent) excessive tissue stretch was prevented by tissue growth and increased by remodeling, while this was the other way around during late development (adolescent to adult).

Next, the focus was shifted from native to engineered cardiovascular tissues. In order to systematically study the mechanics of growth and remodeling in these engineered tissues, a bioreactor system was developed and validated. It was demonstrated that this bioreactor is capable of culturing engineered cardiovascular tissues for a prolonged time period under physiologically relevant dynamic loading conditions (Chapter 4), while the mechanical state of the engineered tissues during culture can be nondestructively quantified (Chapter 5). This latter was achieved by means of a classical inflation test in combination with ultrasound imaging and a custom two-step inverse analysis to estimate the tissues' material properties. From the material properties, a range of relevant mechanical constituents, such as stretch, stress, and stiffness, could be quantified during dynamic tissue culture.

Using the novel bioreactor system and nondestructive mechanical characterization method, we then aimed to determine if a geometrical and mechanical homeostasis can be reached in engineered cardiovascular tissues, and how this depends on the initial scaffold thickness (Chapter 6). To this end, engineered cardiovascular tissues were dynamically cultured with two different initial scaffold thicknesses. A mechanical equilibrium was reached in both thickness groups, although at different magnitudes of the investigated mechanical quantities. Interestingly, a geometrically stable state was only established in the thicker constructs, while the thinner construct's length increased continuously. These results indicate that a mechanically and geometrically stable state can be established in engineered cardiovascular tissues, albeit depending on scaffold design parameters such as initial scaffold thickness.

Summarizing, a wide range of experimental and numerical techniques were used to study the mechanics of growth and remodeling in native and engineered cardiovascular tissues. Most importantly, we found strong evidence that tissue growth and remodeling in human native heart valves occur, from a biomechanical perspective, to maintain a stretch homeostasis. Moreover, we demonstrated that a geometrical and mechanical stable state could be established in engineered cardiovascular tissues, dependent on the scaffold design. Evidence of such a stable state in engineered cardiovascular tissues, similar to the native tissues that they ought to replace, is promising for the field of tissue engineering.

CHAPTER 1

Either write something worth reading or do something worth the writing.

Benjamin Franklin – Poor Richard's Almanack, 1738

General introduction

1.1 Preface

Cardiovascular tissues exhibit a remarkable intrinsic capability of adaptation to environmental changes. The main processes responsible for this hallmark of living tissues are referred to as growth and remodeling. Cardiovascular growth can be defined as addition of tissue mass or volume through an increase in cell number or size, and/or an increase in the amount of extracellular matrix (ECM). Remodeling, on the other hand, can be defined as a change in the tissue's structural and/or mechanical properties. While the structural and mechanical properties of cardiovascular tissues are well-characterized, our understanding of postnatal cardiovascular growth and remodeling to achieve these properties remains incomplete. Many studies have been dedicated to the genetic aspects of growth and remodeling, yet it has also become clear that mechanical factors are pivotal for tissue adaptation. This thesis concerns the mechanical aspects of postnatal growth and remodeling in cardiovascular tissues.

1.2 Biomechanics of cardiovascular growth and remodeling

1.2.1 Early findings on the mechanical aspects of growth and remodeling

For many centuries, it has been believed that postnatal growth and remodeling in all biological tissues occur to maintain tissue function, and are strongly influenced by mechanical factors. The link between tissue adaptation and mechanics can be dated as far back as Galileo Galilei in the 17th century[8,75], who discovered that the animal's size and weight changed bone structure to allow for optimal function (Fig. 1.1). Three centuries later, Juliuis Wolff postulated that the achitecture of bones is dictated by the direction of external loading[194,240], perhaps the most clear concept of the influence of mechanics on growth and remodeling.

Around the same period, Thoma [217] appeared to be the first to report a similar relationship in cardiovascular tissues, when he noticed that an increased volumetric blood flow led to an increase in inner artery diameter.

1.2.2 The concept of mechanical homeostasis

Despite the long existing realisation that postnatal growth and remodeling are strongly influenced by mechanical factors, the exact relationship between these factors and cardiovascular growth and remodeling and mechanical factors remained elusive. Initial mechanistic insights into the mechanical aspects of cardiovascular growth and remodeling originate from in vivo observations of tissue adaptation in response to non-physiological mechanical environments.

For instance, in hypertensive rats, thoracic aortic wall thickness was found to increase in response to a rising blood pressure[146,241]. Conversely, the wall thickness of carotid arteries in rabbits was

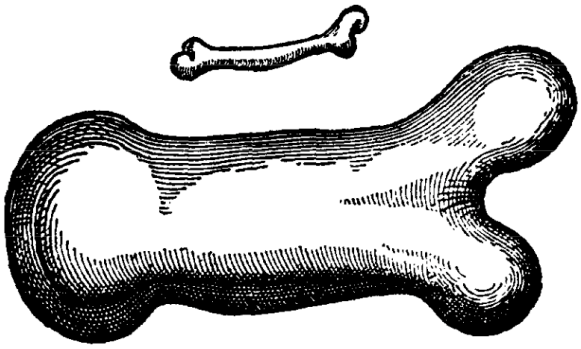

Figure 1.1: In 1638, Galileo Galilei was the first known to report a relation between tissue adaptation and mechanics [8]. He included this sketch to illustrate his theory that the form of bones from animals of different sizes is determined by their function and the animal's weight [75].

found to decrease in response to a decreased pressure, induced by cuffing the artery [13]. These observations motivated the hypothesis that arterial growth and remodeling via an increase in wall thickness (which decreases wall strain and tension) occurs as a compensatory mechanism for the increase in blood pressure (which initially increases arterial wall strain and tension) [79,80].

More recently, a similar relation was observed in the mitral valve of patients suffering from dilated cardiomyopathy. This pathology is characterized by a dilated left ventricle, which elevates stretch and stress of mitral valve leaflets through extension of the papillary muscles and chordae tendinae. Interestingly, the mitral leaflets of patients suffering from dilated cardiomyopathy were significantly larger than those of healthy persons [31,32], suggesting that leaflet growth occurred to negate the elevated leaflet stretch and stress that were induced by the dilated left ventricle [45]. Interestingly, leaflet growth also seemed beneficial for mitral valve functionality, as patients with enlarged leaflets suffered less from regurgitation than patients with normal leaflets [32].

The compensatory mechanism demonstrated for both arteries and heart valves suggest that growth and remodeling in cardiovascular tissues occur, from a biomechanical perspective, to maintain a certain preferred mechanical state. This concept has been defined as *mechanical homeostasis* and implies that growth and remodeling occur to maintain cardiovascular tissue function regardless of changes in their external mechanical environment [72,94,102,103]. Interestingly, this paradigm holds for many mammalian species ranging from mice to men, as for instance arterial tension per lamellar unit [242] and the arterial stiffness at mean blood pressure [202] were found to be remarkably constant across these species.

1.2.3 Maintaining mechanical homeostasis

Mechanical homeostasis in cardiovascular tissues is maintained by the residing cells, such as fibroblasts and valvular interstitial cells, as they are responsible for producing and degrading ECM and are known to be highly mechanosensitive [33,34,94,103,133,189]. For instance, ECM protein production rate

of smooth muscle cells is up-regulated when they are exposed to cyclic stretching[133]. This leads to a highly reciprocal relationship between cells and ECM: the cells establish the ECM and subsequently adapt it via growth and remodeling if changes occur in the cells' mechanical environment. Conversely, the ECM is one of the main determinants (the other being external loading) of the mechanical environment that the cell senses. Therefore, changes of the ECM will influence growth and remodeling. This reciprocal relationship makes it complicated to understand, and distinguish between, the causes and consequences of growth and remodeling. Moreover, it is unknown at which length scale(s) growth and remodeling are governed. In this thesis, we will primarily focus on the mechanical aspect of growth and remodeling at the tissue scale.

To date, no consensus has been reached regarding the constituent(s) that determine(s) mechanical homeostasis. As different tissues types are exposed to different types of external loads and harbor different cell types, it is not self-evident that mechanical homeostasis is determined by one single mechanical constituent across all tissues. Indeed, different mechanical quantities have been proposed to determine mechanical homeostasis within and across cardiovascular tissues, including strain[10,32,45,167], stress[66,104,214,224], strain energy density[40,232], and stiffness[14,66,202]. Note that all these mechanical constituents are related through constitutive laws, which makes it even more challenging to identify their independent effects on maintaining tissue homeostasis.

1.3 Cardiovascular tissue replacements

1.3.1 Valvular and arterial diseases

Growth and remodeling are pivotal for maintaining the function of cardiovascular tissues, regardless of changes in their mechanical environment. However, several pathologies can compromise the function of heart valves and arteries.

Chronic heart valves diseases can be either congenital or acquired. 75 per 1000 newborns have congenital heart valve diseases (such as bicuspid valves or a complete lack of valves), of whom approximatively 25% require heart valve replacements[95]. Acquired valvular diseases are manifested later in life through either stenosis or regurgitation. Stenosis is typically caused by calcification of the leaflets, while regurgitation is associated with infections, such as endocarditis and rheumatic fever, or dilation of the valvular annulus[201].

Commonly acquired arterial diseases include atherosclerosis, plaque formation, and aneurysm development. Interestingly, aneurysm development has been considered as unstable growth and remodeling via wall stiffening and altered collagen production rates[42,176,235].

To date, the underlying causes and mechanisms of many valvular and arterial pathologies remain a topic of scientific studies, and are beyond the scope of this thesis. Most importantly, these diseased tissues need to be replaced if no other therapy is available to slow down the disease or alleviate patient suffering. Several options are currently available to replace heart valves and arteries.

1.3.2 Current valvular and arterial tissue replacements

Two types of heart valve replacements are currently available: mechanical and biological valves. Mechanical valves consist solely of non-biological materials, and come in various designs, from ball-in-cage to bileaflet valves[84]. These valves have excellent durability but create a suboptimal blood flow. Due to this, patients are at increased vulnerability for thrombus formation and thus, life-long treatment with anticoagulation medication[46]. Biological heart valves, on the other hand, are composed of animal (xenogenic), human donor (allogenic), or patient's own (autograft) tissue. In contrast to mechanical valves, they are less prone to thrombosis and therefore patients are not required to take lifelong blood thinning medication. However, their durability is limited[131,173]. As both valve types have specific pros and cons, the most suitable heart valve differs across patient, depending on their age, concomittant medical conditions, lifestyle, and personal preference.

Similar to heart valves, diseased arteries can be replaced by either biological or synthetic prostheses. For small artery replacements, autologous replacements are considered the gold standard, but are only scarcely available due to limited supply and concomitant vascular diseases. Large-diameter arteries cannot be replaced by autologous tissues, and are for this reason typically replaced by synthetic grafts. In contrast to autologous replacements, synthetic grafts are widely available, but often suffer from post-operative complications such as calcification, infection, thrombosis and aneurysm formation in the surrounding native arterial tissue[65,114,168,211].

Overall, the currently available replacement options for diseased heart valves and arteries are life-saving devices, albeit with specific pros and cons. Most importantly, the major limitation across replacement options is their lack of growth and remodeling potential. This is particularly problematic for young patients, who are still growing, or young adults that require lifelong solutions capable of remodeling to cope with changing physiological demands. They consequently have to undergo multiple re-operations to compensate for size mismatch[1], which results in a lower life expectancy[175].

1.3.3 Cardiovascular tissue engineering: prospects and challenges

The field of tissue engineering can potentially address the shortcomings of the current cardiovascular tissue replacements, in particular their lack of growth and remodeling potential. This is especially relevant for pediatric patients that are born with congenital diseases, as discussed in the previous two sections. First defined in the landmark paper by Langer & Vacanti[129], tissue engineering is "an interdisciplinary field that applies the principles of engineering and life sciences toward the development of biological substitutes that restore, maintain, or improve tissue function or a whole organ". Thus, tissue engineering aims to harness the body's intrinsic regenerative capacity to create a living tissue replacement that has the capability of growth and remodeling and lasts for a lifetime. Two main approaches have been pursued: the classical in vitro approach, and the recently emerging in situ approach.

Tissue engineering approaches

In the classical approach of in vitro tissue engineering, cells are isolated from the patient or a donor and then seeded on a scaffold material in order to produce native-like tissues in a laboratory. Tissue production is typically stimulated and guided in a bioreactor that applies biochemical and mechanical stimuli to the tissue-engineered constructs[155,166]. Meanwhile, the scaffold degrades until only the engineered tissue remains. To create off-the-shelve availability, engineered tissues can be decellularized, which allows for long-term storage[53]. Unfortunately, producing these valves is time-consuming, labour-intensive, and logistically challenging, leading to high costs.

The approach of in situ tissue engineering appears more straight-forward than the classical approach but is certainly not less challenging. In this approach, a bioresorbable scaffold material is directly implanted in the patient at the functional site, after which neo-tissue is formed in vivo[187]. In contrast to the classical approach, producing these prostheses does not require ex vivo culture, and is therefore less time-consuming and allows for off-the-shelve availability. However, it poses high demand on the scaffold material, which must immediately take over the function of the replaced native tissue, as well as recruit cells and subsequently stimulate autologous tissue formation[187,205]. Moreover, the balance between tissue formation and degradation should be meticulously tuned.

The importance of scaffold design

For both tissue engineering approaches, the scaffold is essential to balance, or even modulate, tissue formation. The material should be biocompatible and bioresorbable to enable newly formed tissue to eventually replace the scaffold. Ideally, the scaffold is porous in order to allow cell infiltration and provides structural and mechanical support for the cells and tissue[23,111,139]. To fulfill these requirements, both natural (e.g. collagen) and synthetic (e.g. supramolecular polymer) bioresorbable materials have been used as scaffold material[23]. Electrospinning is often used to produce scaffolds from these materials, as it provides control over a myriad of parameters, including scaffold thickness, porosity, fiber alignment, fiber diameter, compliance, degradation rate, and polymer composition[113]. All of these parameters determine the mechanical properties of scaffolds and can therefore influence tissue growth and remodeling.

Growth and remodeling in engineered tissues

Previous studies have successfully demonstrated that tissue-engineered arteries and heart valves have the potential for growth and remodeling in growing animal models. For instance, Hoerstrup et al. implanted cell-seeded tissue-engineered vascular grafts in the pulmonary artery of growing lambs[92]. The graft diameter (30%) and length (45%) increased significantly during a two-year follow-up period, in parallel to a twofold increase of the animals' weight. More recently, Syedain et al. [212] used a similar animal model to demonstrate that decellularized vascular grafts showed a similar trend, with

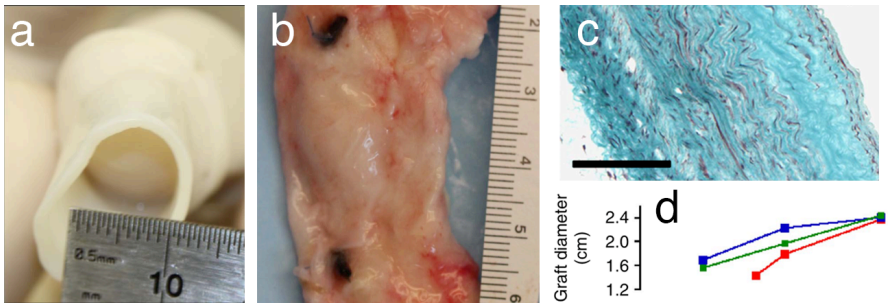

Figure 1.2: Decellularized tissue-engineered pulmonary arterial grafts **(a)** were implanted in three young lambs. Explant photos **(b)** and trichrome stainings **(c)** showed that neo-tissue had been formed in vivo. The diameter of the three grafts increased by 56% **(d)**. Figures reprinted from Syedain et al. [212] under Creative Commons Attribution 4.0 International License (CC BY 4.0, https://creativecommons.org/licenses/by/4.0/).

the diameter increasing by 56% upon a 366% increase in animal body weight (Fig. 1.2). Neo-tissue formation was found in all of the explanted grafts.

Interestingly, and in contrast to the native tissues they ought to replace, it appears that to date no mechanical homeostasis was established in tissue-engineered prostheses. On the contrary, despite promising early results of growth of engineered heart valves [92,212], adverse growth and remodeling have often led to aneurysm formation in tissue-engineered vascular grafts [118,134,147], while tissue-engineered heart valves have suffered from leaflet shortening that causes valvular insufficiency [57,85,183,200]. So, if engineered cardiovascular tissues are to be successful in the long term, further research on and, eventually, control of growth and remodeling in engineered cardiovascular tissues is required.

1.4 Model systems are required to study growth and remodeling in engineered tissues

Many valuable insights into the mechanical aspects of growth and remodeling in native tissues have been gained from studying their development during health and disease (Section 1.2.2). Today, cardiovascular tissue engineering is not widely available in the clinic, so we are unable to investigate long-term development of these novel prostheses. Model systems are therefore required to investigate the long-term functionality of engineered cardiovascular tissues. These models can be pivotal to improve our understanding of the mechanics of growth and remodeling in engineered cardiovascular tissues, in particular if a mechanical homeostasis can be established. To this end, several model approaches are available: in vivo, in vitro, or in silico, each with their specific pros and cons.

1.4.1 In vivo models

Animal models can provide vital insights into the effect of systemic processes, e.g. genetic and immunological factors, on growth and remodeling in engineered tissues. Ovine models are widely considered as ideal models for heart valve tissue engineering, as their high calcium metabolism makes

them a "worst-case-scenario" model[216], and they are easy to handle[5]. These models have been extensively used for proof-of-concept studies of heart valve tissue engineering[57,68,121,200,206].

Juvenile ovine modelsm in particular, can provide valuable insights into growth of engineered cardiovascular tissues, as their rapid somatic growth can simulate many years of human postnatal development in a relatively short time span[24,92,212]. This is especially useful for simulating growth and remodeling of engineered tissues in pediatric patients.

Aside from ovine models, small animals such as mice and rats have emerged as convenient models to study growth and remodeling in native and engineered arteries[15,118,222]. On top of rapid somatic growth, these models have relatively low costs, and the effect of pathologies on growth and remodeling can be studied in readily available knock-out animals[16,81,234].

Unfortunately, in vivo models involve animal suffering and sacrifices. Moreover, experiments are complicated by systemic processes, which all need to be taken into account when interpreting the results of in vivo studies. Although these processes make animal models the most representative model of the clinical situation, they also make it hard to isolate the effect of mechanics on growth and remodeling.

1.4.2 In vitro models

In contrast to animal models, important in vivo processes might be missing in in vitro models. Yet, well-designed in vitro models provide meticulous control over individual experimental parameters and therefore allow for a more systematic study of cardiovascular tissue growth and remodeling.

Strain-driven bioreactors

In vitro studies of cardiovascular tissue growth and remodeling in engineered tissues often involve bioreactor platforms. In these devices, engineered tissues can be cultured while being subjected to native-like biochemical and mechanical stimuli. Here, we will focus only on the later, as biochemical stimuli are outside the realm of this thesis. In their most elemental form, bioreactors were developed to study the effects of static strains on tissue growth and remodeling[64,98,132,229]. However, the cardiac cycle exposes cardiovascular tissues to dynamic loads, so other bioreactors have applied dynamic strains to engineered cardiovascular tissues[61,86,98,107,123,124,152,190,191]. An overview of previously developed static and dynamic strain-driven bioreactors is given in Table 1.1. Overall, either hydrogels or electrospun scaffolds are used as cell and/or tissue carriers, and the in vitro culture times range from several days up to 5 weeks, considerably less than in vivo growth times.

The need for pressure-driven bioreactors

Despite the insights that strain-based bioreactors have provided in cardiovascular growth and remodeling, the in vivo dynamic mechanical loading of cardiovascular tissues is governed by hemodynamics. Hence, tissue deformation is induced by hemodynamic pressure, not by external strains,

Table 1.1: Previously developed bioreactors to study growth and remodeling in cardiovascular tissues

Stimulus	Cell substrate	Culture time	Read-outs during culture	Ref.
Static strain	Collagen hydrogel	3 d	Tissue tension, cell and ECM (re)organisation	132
	Collagen hydrogel	14 d	Tissue tension	64
	Electrospun scaffold	21 d	Tissue tension and retraction	229
Static or dynamic strain	Collagen hydrogel	6 d	ECM (re)organisation	98,107
Dynamic strain	Collagen hydrogel	2 d	Protease activity	174
	Collagen hydrogel	4 d	Local tissue strain, cell and ECM (re)organisation	86
	Electrospun scaffold	28 d	ECM (re)organization	190,191
	Electrospun scaffold	28 d	Local tissue strain, mechanical properties	123,124
	Electrospun scaffold	35 d	Tissue stiffness	61
	Porcine heart valve leaflets	14 d	Tissue stiffness	152,10
Dynamic pressure	Electrospun scaffold or decellularized tissue	3 d	-	58
	Electrospun scaffold	56 d	ECM (re)organization and production	43,165,166
	Fibrin gel	63 d	Arterial distension, burst pressure, and compliance	213

which can lead to different growth and remodeling outcomes. For instance, in diseased hearts a volume overload leads to ventricular dilation (dilated cardiomyopathy), whereas a pressure overload leads to cardiac wall thickening (hypertrophic cardiomyopathy) [82].

To the best of our knowledge, only a limited number of bioreactors have been developed that apply dynamic pressures to engineered cardiovascular tissues [43,58,165,166,213] (Table 1.1). Still, most crucial for studying the mechanical aspects of growth and remodeling in engineering tissues, the currently available bioreactors mostly miss the possibility to measure changes in tissue mechanics during culture. In this thesis, we will attempt to address this need by presenting a novel bioreactor with an integrated nondestructive mechanical characterization method, in which engineered cardiovascular tissues can be cultured under dynamic pressure conditions for a prolonged time period.

1.4.3 In silico models

As briefly described in Section 1.2.3, there are many mechanical factors that may contribute to cardiovascular growth and remodeling. Due to the complex interplay between the mechanical aspects of growth and remodeling, it is hard to derive the exact contributions and consequences of each of them. Even growth and remodeling themselves, although typically expressed as inseparable terms, are two distinctly different phenomena (Section 1.2) that can occur simultaneously during e.g. postnatal development. Computational models are therefore indispensible tools to elucidate the individual roles of cardiovascular growth and remodeling and their underlying factors. Ultimately, these models could also predict growth and remodeling in both native and engineered cardiovascular tissues.

Here, we will focus on continuum mechanics models, which have been widely used to model the mechanics of biological tissues. They are particularly powerful tools when combined with both in vivo and in vitro experiments that can provide model hypotheses and parameters. Moreover, computational models can unlock access to mechanical constituents, such as stress and strain energy density, which cannot be directly measured experimentally [9,176]. The past two decades have seen the development of several cardiovascular growth and remodeling models within the context of continuum mechanics. Although various numerical approaches have been developed [41], two classes of growth and remodeling models have become particularly wide-used: kinematic growth models (for growth only), and constrained mixture models (for growth and remodeling).

Kinematic growth models

Arising from concepts by Richard Skalak [221] and first formally posed by Rodriguez et al. [186], kinematic growth models consider growth as stress-free changes of unloaded tissue volume, typically governed by mechanical stimuli to reach a homeostatic target [6,127]. In addition, when experimental data are available, kinematic growth can be defined in terms of known geometrical changes, rather than being driven by a mechanical stimulus. Kinematic growth models are relatively simple to implement and have relatively low computational costs. However, their value remains limited to the

whole-tissue level, as the tissue is treated as a single unit and the direction of growth (e.g. isotropic, uniaxial, or transversely isotropic) has to be chosen beforehand. To the best of our knowledge, kinematic growth models have only been used to model native, and not engineered, tissues, including arteries[196] and mitral valves[181], and are the model of choice when it comes to cardiac growth[83,117,239].

Constrained mixture models

In contrast to kinematic growth models, constrained mixture models, first proposed by Humphrey & Rajagopal[105], consider a material as a mixture of constituents, e.g. different collagen and elastin volume fractions. Each constituent can be deposited and degraded within the tissue at a certain time point, governed by mechanically-driven turn-over rates. The constituents that are deposited at each time point all have their own stress-free configuration, yet deform together with the overall tissue. Thus, constrained mixture models can provide insights into the relative contributions of different tissue constituents to tissue growth and remodeling. However, the model parameters are hard to derive from experimental data. Additionally, the computational costs and implementation efforts are much higher than for kinematic models, although efforts are ongoing to address these issues[39]. Constrained mixture models have been used primarily to study growth and remodeling in arteries in response to physiological and pathological changes in hemodynamic loading[42,115,145,179,184,225,235]. Recently, a constrained mixture model was used to assess the effect of scaffold design parameters (as discussed in Section 1.3.3) on growth and remodeling of tissue-engineered vascular grafts[154].

1.5 Thesis rationale and outline

Over the past four centuries, the field of growth and remodeling has come a long way. From a biomechanical perspective, it is now well accepted that growth and remodeling occur in response to changes in the tissue's mechanical environment, in order to maintain a certain mechanical homeostasis. To date, no consensus has been reached on which mechanical constituent(s) determine(s) mechanical homeostasis across different native tissue types. Moreover, recent studies indicate that no mechanical homeostasis may have been established in engineered cardiovascular tissues. On the contrary, adverse growth and remodeling have led to geometrical and mechanical instabilities of these novel prostheses, ultimately leading to failure. The overall aims of this thesis are, therefore, (1) to identify what mechanical quantity determines mechanical homeostasis in native cardiovascular tissues, in this case heart valves, and (2) to investigate if a mechanical homeostasis can also be established in engineered cardiovascular tissues.

To address the first aim, in *Chapter 2* we use a numerical-experimental approach to assess age-related changes in human native heart valves to unravel which mechanical quantity determines mechanical homeostasis in native valvular tissue during postnatal development.

We furthermore hypothesize that growth and remodeling may play different roles in maintaining mechanical homeostasis during the lifetime of native heart valves. As growth and remodeling

may occur simultaneously during postnatal valvular development, their relative contributions to maintaining mechanical homeostasis are hard to deduce from experimental findings. Therefore, a computational model, informed by the results acquired in the previous chapter, is used in *Chapter 3* to elucidate the relative influences of growth and remodeling on preserving mechanical homeostasis in native heart valves.

We then switch from native to engineered cardiovascular tissues to address the second aim of this thesis. We hypothesize that the scaffold design is crucial to guide growth and remodeling into establishing a mechanical and geometrical homeostasis, as it is the scaffold (alongside with hemodynamic loading) that primarily determines the engineered tissue's mechanical environment directly after implantation.

To test this hypothesis, in *Chapter 4* we present and validate a novel pressure-driven bioreactor system to study growth and remodeling in engineered cardiovascular tissues. In *Chapter 5*, we complement this bioreactor platform with an integrated nondestructive mechanical characterization method and inverse analysis.

Using this in vitro platform, we investigate in *Chapter 6* if a geometrical and mechanical homeostasis can be established in engineered cardiovascular tissues, and how it is influenced by the scaffold design – in this case scaffold thickness.

Finally, *Chapter 7* provides a general discussion on the presented results, their impact, and potential limitations.

CHAPTER 2

I have no special talents. I am only passionately curious.

Albert Einstein – Letter to Carl Seelig, 11 March 1952

Age-dependent changes of stress and strain in the human heart valve and their relation with collagen remodeling

The contents of this chapter are based on:

Oomen, P. J. A. ,Loerakker, S., van Geemen, D., Neggers, J., Goumans, M.-J. T. H., van den Bogaerdt, A. J., Bogers, A. J. J. C., Bouten, C. V. C., & Baaijens, F. P. T. (2016). Age-dependent changes of stress and strain in the human heart valve and their relation with collagen remodeling. *Acta Biomaterialia*, 29, 161–169.

2.1 Introduction

It has been known for many years that the form and function of many biological tissues are strongly influenced by mechanical stimuli [6,102,103]. Numerous cell types remodel their surrounding extracellular matrix in response to changes in mechanical loading [99,133,174,193], which has been hypothesized to occur to maintain a certain mechanical homeostasis [102,103]. Yet, there is no consensus as to which mechanical quantity is the driving factor behind the remodeling process.

Collagen fibers are one of the key players in the remodeling process, since these proteins are the main load-bearing component of many soft tissues. In particular, collagen fiber orientation and bundle formation through cross-linking [4,11] play a significant role in valvular tissue mechanics. As a consequence, the architecture of the collagen network has a major influence on the mechanical functionality of soft tissues, as well as on mechanically induced growth and remodeling processes. Therefore, a deeper knowledge of collagen remodeling will greatly benefit our understanding of healthy tissue development as well as pathological adapatations such as those seen during fibrosis, aneurysm formation [145] and wound healing [150,153]. Moreover, it is of great interest to the rapidly growing field of tissue engineering, which aims to provide patients with living autologous tissue replacements that have the potential to grow and remodel in response to changes in functional demand [129].

One of the endeavors of this field is the development of tissue-engineered heart valves (TEHVs). Despite promising early results, short-term remodeling often leads to tissue crimp that causes leaflet shortening and, ultimately, valve malfunctioning [57,85,93,200]. In order to ensure long-term functionality of TEHVs, understanding and subsequently controlling the collagen remodeling process is of the greatest importance. However, this is impeded by the lack of long-term data due to the early failure of TEHVs.

We aim to identify the driving factor of collagen remodeling in heart valves and have investigated age-dependent changes in human semilunar heart valves. During their lifetime, the geometry and collagen architecture of heart valves change [3,130,142,220], which is likely due to temporal changes in hemodynamical conditions [3,102,177]. Still, it remains unknown how these temporal changes are related to valve mechanics, including tissue stress and strain.

Knowledge of the evolutionary changes with age in stress and strain status of human heart valves might explain which of these factors, if any, determines mechanical homeostasis. Therefore, we determined the collagen architecture as well as the geometric and mechanical properties of human semilunar heart valves of fetal to adult age using confocal microscopy, micro-indentation and inverse finite element analysis. The collagen architecture and geometric and mechanical properties were used to predict age-dependent changes in stress and stretch in the heart valves via finite element modeling.

2.2 Materials and methods

2.2.1 Tissue preparation

Sixteen sets of paired cryopreserved healthy human aortic and pulmonary valves of different ages were obtained from Dutch postmortem donors, given permission for research according to national ethical and regulatory guidelines with written informed consent. These valves were assessed to be unfit for implantation and provided by the Heart Valve Bank Rotterdam (Erasmus University Medical Centre, Rotterdam), with ages ranging from 2 months to 53 years old. Of these valves, thirteen pairs were previously studied by Van Geemen [226] and three pairs (2 months, 2 years and 49 (for microscopy only) years old) were analyzed for the first time in this study. The valves were deemed unfit for implantation due to findings that contra-indicated implantation, consisting amongst others of positive bacteriological sampling, serological findings in the donor and other procedural nonconformities that caused rejection of the donor (e.g. sexual risk behavior and/or risks in drug abuse). Additionally, one cryopreserved fetal heart (19 weeks old) was obtained from the department of Molecular Cell Biology, Leiden University Medical Center, Leiden, after approval of the by the medical ethical committee of the Leiden University Medical Center and written informed consent.

All valves were structurally and mechanically unaffected, and the cause of death was not related to valvular disease or conditions known to precede valvular disease. The cryopreserved valves were stored at -80 °C and thawed and prepared just prior to testing, as described previously [226]. Previous studies showed that the applied cryopreservation protocol did not affect structural integrity [78] and mechanical properties [51]. The valves were stained overnight with CNA35 [22] to enable collagen visualization.

2.2.2 Collagen architecture visualization and quantification

The collagen architecture of a single leaflet of the fetal valve and 2-month, 2-year and 43-year-old valve pairs was visualized using a confocal laser scanning microscope (TCS SP5X, Leica Microsystems, Wetzlar, Germany) with complimentary software (Leica Application Suite Advanced Fluorescence, Leica Microsystems, Wetzlar, Germany). The valves were placed on the microscope such that the fibrosa faced the camera. A tile scan (magnification 10x, excitation 488 nm, emission 520 nm) was made to capture the collagen architecture of the entire leaflet in one single image. Collagen fiber orientation and dispersity were determined by analyzing the individual images of each tile scan, using a custom Mathematica (Wolfram, Champaign, IL, USA) script, based on the work of Frangi et al. [70], which has been used previously to measure collagen orientation [49,69]. In brief, the orientation of collagen fibers was determined via a multi-scale approach in which the principle curvature directions were calculated from the eigenvalues and the eigenvectors of the Hessian matrix of the image (second order derivative). For each tile scan, a histogram containing the fiber fraction per angle was obtained, from which the fiber main orientation and dispersity could be derived using a least-squares fitting method.

2.2.3 Mechanical testing

One leaflet of each valve was used for mechanical testing using micro-indentation, as described previously[37,223]. A spherical sapphire indenter with a diameter of 2 mm was used. The whole setup was mounted on an Axiovert 200M confocal laser scanning microscope (Carl Zeiss, Oberkochen, Germany) with iXon+ camera and complimentary Andor IQ software (Andor, Belfast, Northern Ireland). This setup enabled tracking of the deformation in the bottom plane of the samples during deformation by making images of the collagen fibers (magnification 10x, excitation 520 nm, emission 488 nm) during indentation. Each leaflet was indented at ∼7 locations across the belly region, with 3 indentation cycles performed at each location. During each cycle, the leaflet was indented up to 50% of the local leaflet thickness with a constant indentation speed of 0.01 mm/s. The vertical indentation force, planar valve deformation, and thickness were obtained for each cycle, which were averaged to one single data set per leaflet for further analysis. The first cycle was used as preconditioning cycle and excluded from further analysis. Mechanical testing of an 11-year-old pediatric pulmonary valve failed due to hardware failure.

2.2.4 Digital image correlation

A global digital image correlation (GDIC) algorithm was used to quantify deformation in the confocal microscopy images made during indentation. This algorithm was adapted from Neggers et al. in MATLAB (MathWorks, Natick, MA, USA)[17,163]. In brief, the algorithm considers each image as a scalar function of spatial coordinates that gives the gray level at each pixel. The displacement field relating two subsequent images was decomposed onto a basis of continuous functions. The parametrized displacement field was found by incrementally minimizing the squared difference between the two images using a multi-scale approach. For a full scope on the GDIC algorithm and implementation, please be referred to Neggers et al.[163].

2.2.5 Inverse finite element analysis

With force and strain data available, the material parameters for the constitutive model described in the next section were computed by inverse finite element analysis. Since the indenter was centered directly above the indentation site, quarter-symmetry could be assumed. Therefore, a small block of tissue surrounding the indenter was modeled in the commercial finite element package Abaqus (Dassault Systèmes, Simulia Corp., Providence, RI), using ∼100 quadratic brick elements with reduced integration (C3D20R). Mesh dimensions were sample-dependent due to differences in sample thickness. Material parameters were estimated by minimizing the difference between the experimental and numerical data, using a quadratic objective function to define the goodness of fit, as described previously[38]. The resulting parameters were used for numerical simulations and are displayed in Table 2.1.

2.2.6 Constitutive model

The finite element model is based on the work of Driessen et al. and Loerakker et al.[56,135]. The model was implemented in Abaqus using the user-defined subroutine UMAT. The heart valve leaflet is modeled as a fiber-reinforced composite material, consisting of an anisotropic fiber part (f) with volume fraction (ϕ_f) and an isotropic matrix part (m) with volume fraction ($1 - \phi_f$). The fiber volume fraction ϕ_f was set to 0.5, similar to Driessen et al.[56]. The total Cauchy stress hence consists of two components:

$$\boldsymbol{\sigma} = \boldsymbol{\sigma}_m + \boldsymbol{\sigma}_f \tag{2.1}$$

The isotropic part, describing the contribution of the cells and all extracellular matrix components except collagen, is modeled as a Neo-Hookean material:

$$\boldsymbol{\sigma}_m = (1 - \phi_f)\left(\kappa\frac{\ln(J)}{J}\mathbf{I} + \frac{G}{J}(\mathbf{B} - J^{2/3}\mathbf{I})\right) \tag{2.2}$$

with $\mathbf{F}$ the deformation gradient tensor, $J = \det(\mathbf{F})$, $\mathbf{B} = \mathbf{F}\cdot\mathbf{F}^{\mathrm{T}}$, and G and κ the shear and compression modulus, respectively. The anisotropic fiber part is modeled using an angular distribution with a discrete number of fiber directions. The fiber directions $\mathbf{e}^i_{f0}$ in the undeformed configuration are positioned within a plane spanned by two orthogonal vectors in the circumferential ($\mathbf{v}_1$) and radial ($\mathbf{v}_2$) direction at angles γ^i with respect to $\mathbf{v}_1$:

$$\mathbf{e}^i_{f,0} = \cos(\gamma^i)\mathbf{v}_1 + \sin(\gamma^i)\mathbf{v}_2 \tag{2.3}$$

The fiber volume fraction in each direction was described using a periodic version of the normal probability distribution function[56,76]:

$$\varphi^i_f = A\exp\left[\frac{\cos[2(\gamma_i - \alpha)] + 1}{\beta}\right] \tag{2.4}$$

where α is the main fiber angle with respect to $\vec{v}_1$ and β the dispersity of the fiber distribution. The scaling factor A is defined such that the total fiber content equals ϕ_f. An angular resolution of 3° was used to model the collagen distribution. The total collagen fiber stress depends on the orientation of the collagen fibers in the current configuration ($\mathbf{e}^i_f$) and the collagen stress and volume fraction φ^i_f in each direction:

$$\boldsymbol{\sigma}_f = \sum_{i=1}^{N} \varphi^i_f \sigma^i_f : (\mathbf{e}^i_f \otimes \mathbf{e}^i_f) \tag{2.5}$$

with σ^i_f the magnitude of the fiber stress depending on the fiber stretch λ_f. An exponential stress-stretch law with stiffness parameters k_1 and k_2 was used for the fiber stress when the collagen fibers are extended ($\lambda^i_f \geq 1$)[56]. It is assumed that collagen fibers can only bear stress in extension, with a

small compressive stress when $\lambda_f^i < 1$ to prevent numerical convergence issues due to discontinuities in fiber stress derivatives:

$$\sigma_f^i = \begin{cases} k_1(\lambda_f^i)^2 \left(\exp[k_2((\lambda_f^i)^2 - 1)] - 1\right) & , \lambda_f^i \geq 1 \\ \frac{k_1 k_2}{k_3} \left(\exp[k_3((\lambda_f^i)^2 - 1)] - 1\right) & , \lambda_f^i < 1 \end{cases} \tag{2.6}$$

where $(\lambda_f^i)^2 = \mathbf{C} : (\mathbf{e}_{f,0}^i \otimes \mathbf{e}_{f,0}^i)$ is the squared stretch in fiber direction $\mathbf{e}_i$.

2.2.7 Finite element meshes

Each valve was shaped by creating spherical leaflets using age-related geometrical properties (Table 2.1). Only half of one leaflet was modelled due to symmetry and divided into ∼500 quadratic brick elements with reduced integration (C3D20R). Mesh refinement was applied such that the mesh density was higher in the belly region. For every element, the radial direction was defined as the vector perpendicular to the outer normal of the element $\mathbf{n}$ and a unit vector in $\mathbf{x}$-direction $\mathbf{e}_x : \mathbf{v}_2 = (\mathbf{e}_x \times \mathbf{n})/||\mathbf{e}_x \times \mathbf{n}||$. Subsequently, the circumferential direction was calculated as $\mathbf{v}_1 = \mathbf{n} \times \mathbf{v}_2$ [135].

2.2.8 Analyses

Simulations were performed using the age-related geometric, hemodynamic and material properties measured in fetal, pediatric, adolescent and adult valves (Table 2.1). The age-related diastolic blood pressure was gradually applied. Circumferential and radial stretch and Cauchy stress were computed in the belly region.

2.3 Results

2.3.1 Collagen architecture evolution is a multi-scale process

High-resolution confocal microscopy images were obtained from the fibrosa side of one pulmonary fetal leaflet and paired aortic and pulmonary leaflets aged 2 months, 2 years and 49 years (Fig. 1). At the microscopic scale, quantification of the individual collagen fiber orientation revealed a circumferential main orientation in all valves, including the fetal valve. Across all ages, the fiber dispersity of the aortic valves was lower than their complementing pulmonary valves (Fig. 2). However, due to relatively large inter-patient variation in dispersity, particularly for the pulmonary valve, no temporal trends in fiber dispersity could be observed in both valve types.

On the macroscopic level, the postnatal architecture of the fibrosa of both the aortic and pulmonary leaflets was characterized by bundles of densely packed circumferentially oriented collagen fibers. No fiber bundles were visible in the fetal valve; bundles of limited size were observed in the 2-month-old and 2-year-old valves and larger bundles in the adult heart valve, in particular in the aortic valve. These observations suggest that the fiber bundles develop with time.

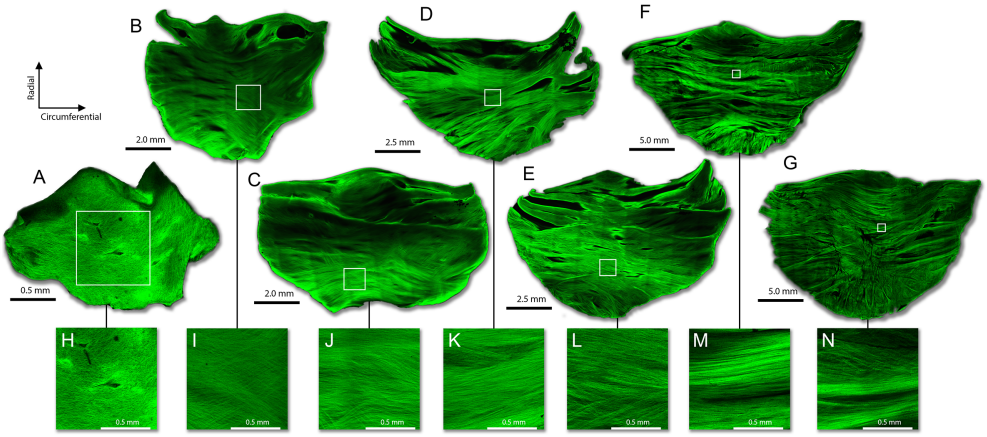

Figure 2.1: Collagen fiber architectures of human native heart valve leaflets' fibrosa side of a fetal pulmonary valve **(a)** and three valve pairs: 2-month-old aortic **(b)** and pulmonary **(c)**, 2-year-old aortic **(d)** and pulmonary **(e)** and 49-year-old aortic **(f)** and pulmonary valves **(g)**. Bundles of densely packed collagen fibers are visible postnatally and appear to arise with age, with individual fibers depicted in the insets (H-N). A mainly circumferentially oriented collagen architecture was found in all valves.

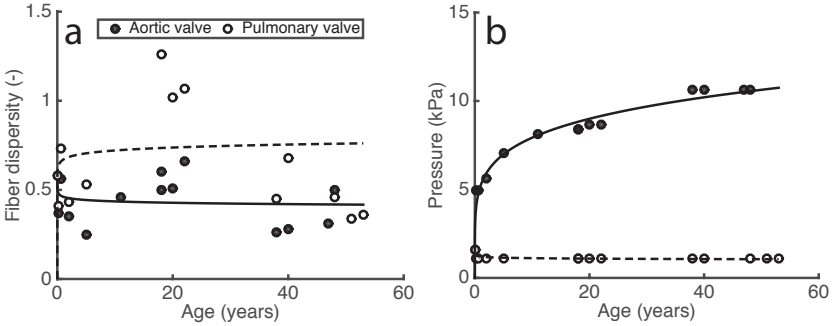

Figure 2.2: Age-related changes in fiber dispersity **(a)** and diastolic blood pressure **(b)** in the aortic, and pulmonary valve. Fiber dispersity was lower in the aortic valve than in the pulmonary valve and power law trend lines indicate the temporal evolution of both pressure and fiber dispersity. Fiber dispersity remains approximately constant as a function of age, however, a large spread in the data was observed. Diastolic blood pressure in the aortic valve increases rapidly postnatally [210,164], whereas in the pulmonary circulation a slight drop in pressure occurs [204].

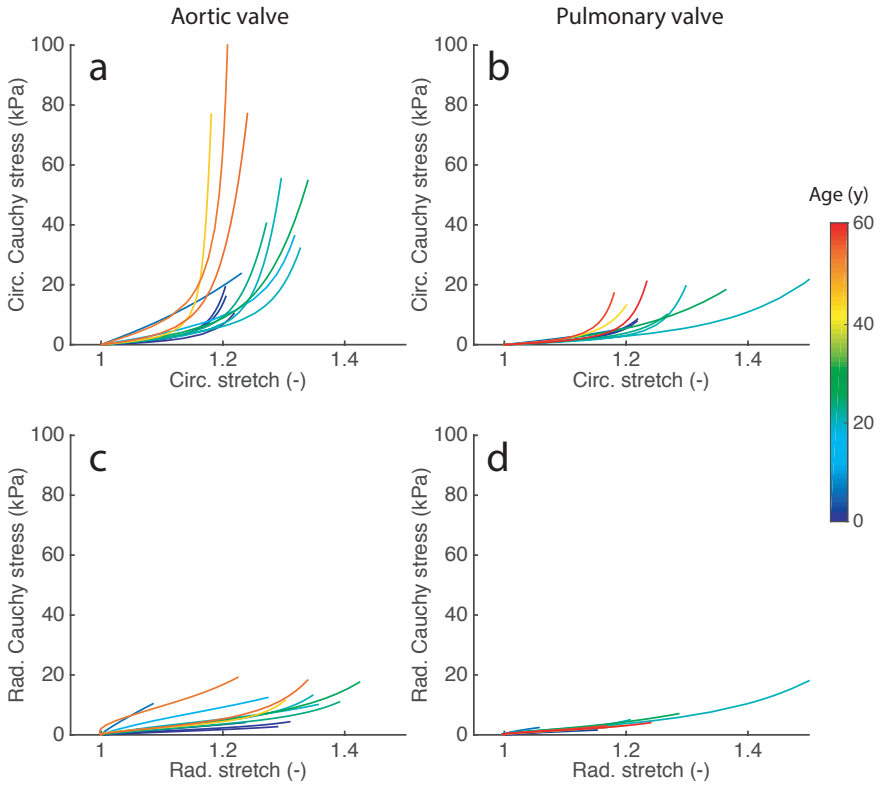

Figure 2.3: Stress-stretch curves in the circumferential **(a,b)** and radial **(c,d)** direction in the belly region of the aortic and pulmonary valve simulations. Valve stiffness in the circumferential direction increased as a function of age for both aortic and pulmonary valve.

2.3.2 Valve stiffness increases as a function of age

The mechanical properties of the valvular tissue were quantified using a combination of micro-indentation[37], digital image correlation[163], and inverse finite element analysis[38]. The resulting parameters for each individual valve can be found in Table 2.1. Unfortunately, the parameter estimation algorithm did not converge for three adult aortic valves.

One should be careful in directly comparing the material parameters from different valves, as different combinations of parameters could give a similar result. To compare the mechanical properties of the different valves, it is better to focus on the stress-stretch curves for each valve simulation. These curves (Fig. 3) show that the aortic valves were stiffer than the pulmonary valves in the circumferential direction. Moreover, a temporal increase of circumferential stiffness was observed in both valves, whereas no such trend could be observed for the radial direction.

Table 2.1: Geometrical, hemodynamic and material parameter values used in all simulations.

						Material parameters			
Age group	Age	Site	Radius (mm)	Thickness (mm)	Pressure[a](kPa)	G (kPa)	k_1 (kPa)	k_2 (-)	β (-)
Fetal	19w	Pulmonary	1.5	0.21±0.10	1.6	11.1	8.9	0.92	0.58
Pediatric	2m	Aortic	4.0	0.32±0.05	4.9	5.2	0.30	6.16	0.37
	2m	Pulmonary	5.0	0.29±0.04	1.1	6.3	0.14	6.92	0.41
	8m	Aortic	5.0	0.50±0.16	4.9	6.8	0.28	7.54	0.56
	8m	Pulmonary	5.5	0.28±0.09	1.1	5.0	0.43	5.70	0.73
	2y	Aortic	5.5	0.68±0.02	5.6	11.4	0.10	8.93	0.35
	2y	Pulmonary	6.5	0.52±0.04	1.1	5.0	0.55	4.82	0.43
	5y	Aortic	7.0	0.68±0.11	7.1	53.4	0.10	8.77	0.25
	5y	Pulmonary	9.0	0.60±0.17	1.1	12.8	0.48	3.52	0.53
	11y	Aortic	8.5	0.82±0.27	8.1	24.1	0.26	5.22	0.46
	11y[d]	Pulmonary	8.5	-	1.1	-	-	-	-
Adolescent	18y[b]	Aortic	10.5	1.0±0.44	8.4	13.7	0.28	4.75	0.50
	18y[b]	Pulmonary	11.0	0.32±0.09	1.1	5.0	0.10	7.20	1.67
	18y[c]	Aortic	9.5	0.73±0.24	8.4	10.2	0.21	6.70	0.60
	18y[c]	Pulmonary	13.0	0.28±0.15	1.1	5.0	1.50	2.02	1.26
	20y	Aortic	10.0	0.93±0.16	8.7	9.4	0.66	5.10	0.51
	20y	Pulmonary	10.0	0.48±0.13	1.1	5.0	0.43	4.85	1.02
	22y	Aortic	9.5	0.80±0.25	8.7	10.7	2.01	3.36	0.66
	22y	Pulmonary	9.5	0.34±0.13	1.1	5.0	8.92	1.32	1.07
Adult	38y	Aortic	10.5	0.48±0.38	10.6	15.1	0.10	11.3	0.26
	38y	Pulmonary	10.5	0.27±0.14	1.1	5.0	0.91	5.51	0.45
	40y	Aortic	11.0	0.64±0.20	10.6	11.1	0.10	12.6	0.28
	40y	Pulmonary	12.5	0.25±0.02	1.1	5.0	1.69	4.58	0.68
	47y	Aortic	13.0	0.54±0.17	10.6	35.8	0.20	10.8	0.31
	48y	Aortic	11.0	0.69±0.14	10.6	9.7	1.64	5.93	0.50
	48y	Pulmonary	13.5	0.27±0.07	1.1	5.0	1.63	4.23	0.46
	51y[e]	Aortic	11.0	0.67±0.31	10.6	-	-	-	0.27
	51y	Pulmonary	11.0	0.36±0.16	1.1	6.1	0.25	9.36	0.34
	53y[e]	Aortic	11.5	0.68±0.32	10.6	-	-	-	0.22
	53y	Pulmonary	13.0	0.38±0.18	1.1	5.0	0.18	7.47	0.36

[a] References for diastolic pressure magnitudes: fetal [210], pediatric aortic [164], adolescent aortic [243], adult aortic [204] and pulmonary [204].
[b,c] Paired 18-year-old valves.
[d] Hardware failure occurred during mechanical testing.
[e] No convergence was reached in the inverse analysis.

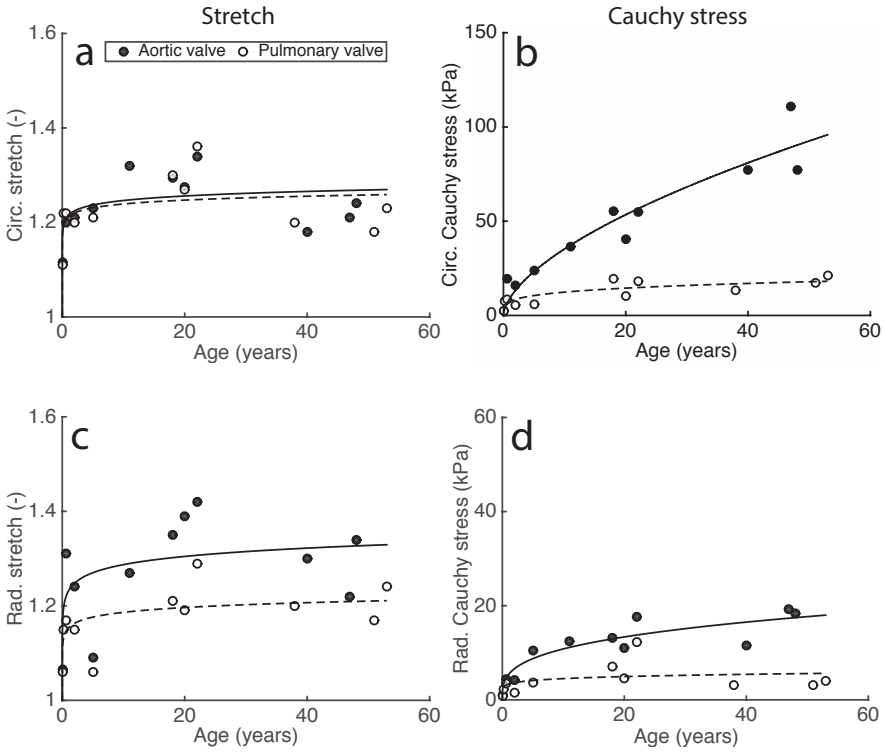

Figure 2.4: Circumferential **(a,b)** and radial **(c,d)** stretch ratios and stresses in the belly region for aortic and pulmonary heart valves after full coaptation. Power law trend lines were fitted using least squares to indicate the temporal trends for both valves. Circumferential stretch was similar in the aortic and pulmonary valves, whereas the radial stretch and circumferential and radial stress were larger in the aortic valve. The simulations for the 2-month, 18-year and 38-year-old aortic valves and 18-year and 40-year-old pulmonary valves failed to converge.

2.3.3 Age-related simulations point to stretch homeostasis and not stress homeostasis

The mechanical state of the different valves was simulated using finite element modeling[56,135] incorporating the experimentally obtained data (Table 2.1). The diastolic pressure corresponding with each age and location (Fig. 2) was applied to the arterial side of the valve, and the stretch ratio and Cauchy stress were computed in the circumferential and radial direction. Unfortunately, no convergence was reached for five valves (three aortic, two pulmonary), which were excluded from further analysis. Significant changes in leaflet stretch were predicted in the belly region at young age (<4 years), followed by a stretch homeostasis in both the aortic and pulmonary valve (Fig. 4a,c). Strikingly, this circumferential stretch homeostasis was similar for the aortic and pulmonary valves. On the other hand, the radial stretch in the aortic valves was higher than in their pulmonary counterparts, which can be explained by the higher aortic blood pressure in combination with the limited amount of radially oriented collagen fibers.

The circumferential stretch field is shown for selected valves of different ages in Fig. 5. Slight

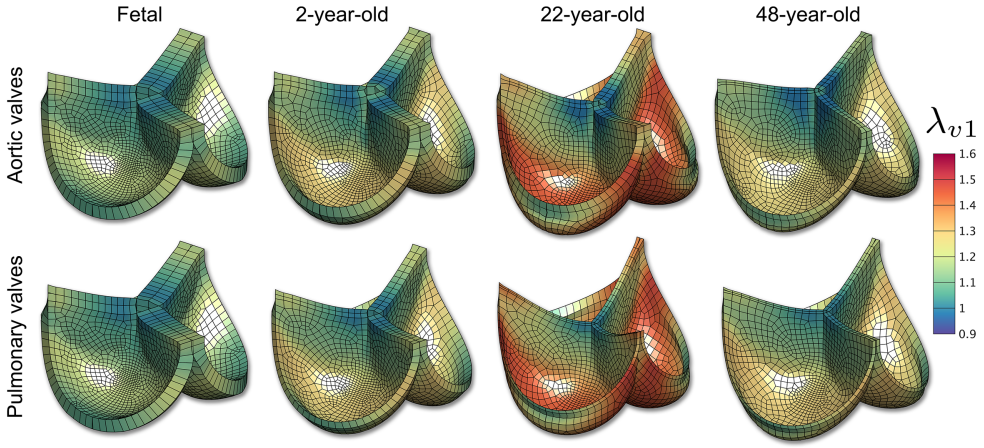

Figure 2.5: Circumferential stretch (λ_{v_1}) distributions estimated by the numerical models of four selected valve pairs (fetal, 2-year-old, 22-year old and 48-year-old) after full coaptation. The stretches were similar between the aortic and pulmonary valves across all ages. In this Fig., the valve radii were normalized to enable comparison between valves of different ages.

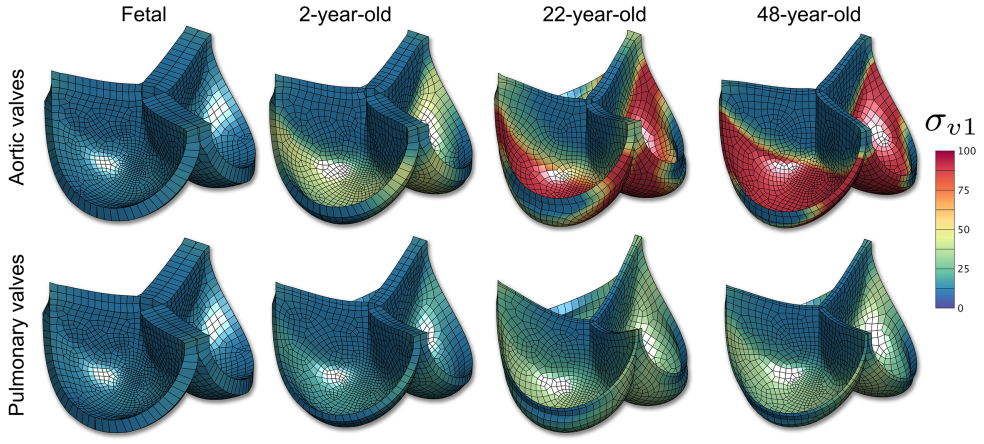

Figure 2.6: Circumferential stress (σ_{v_1}) distributions estimated by the numerical models of four selected valve pairs (fetal, 2-year-old, 22-year old and 48-year-old) after full coaptation. The circumferential stress in the aortic valves increased with age, whereas in the pulmonary valve no significant changes were observed. In this figure, the valve radii were normalized to enable comparison between valves of different ages.

differences can be observed between valves of different donors, for example a higher stretch in the 22-year-old valves compared to valves from other donors. Yet, aortic and pulmonary valves of the same donor feature a similar stretch field.

In contrast to the circumferential leaflet stretch, no homeostasis was predicted for the circumferential Cauchy stress in the aortic valve, with stress continuously increasing with age (Fig. 4b). The values and changes in stress in the pulmonary valve were relatively small compared to the aortic valve, which may be due to the low pulmonary blood pressure that hardly changes with age. The circumferential stress field is shown for selected valves of different ages in Fig. 6. The radial stress in both valve types was smaller than the circumferential stress (Fig. 4d), which can be explained by the circumferential alignment of the collagen fibers.

Due to the circumferential alignment of the collagen fibers, these results suggest that collagen remodeling ensures that the stretches in the collagen fibers are similar in the aortic and pulmonary valve across all ages. In contrast, the circumferential stress is different between the two valves and increases with time in the aortic valve. Therefore, these data suggest that collagen remodeling aims to maintain a constant collagen stretch.

2.4 Discussion

For the first time, human heart valves of different ages were used to reveal age-related changes in valve stress and stretch status, as well as geometry and collagen architecture. The data suggests that these changes may be related to collagen remodeling in response to changes in hemodynamics, in order to maintain a stretch-driven mechanical homeostasis.

2.4.1 Collagen remodeling is a stretch-driven phenomenon

Age-dependent finite element simulations predicted small differences in stretch with age and between the aortic and pulmonary valve leaflets, especially in the circumferential direction (Fig. 4a,c). As the collagen fibers are mainly oriented in this direction, this suggests that collagen remodeling aligns collagen fibers to prevent excessive tissue stretch that occurs due to the increasing diastolic blood pressure (Fig. 2b).

In contrast, no stress homeostasis was found in the circumferential direction, with the stress continuously increasing with age (Fig. 2b). This increase in circumferential stress as a consequence of rising blood pressure was apparently not counteracted by remodeling. A stress homeostasis could for instance have been maintained by tissue thickening. However, the increase in thickness in the aortic valve with time and in comparison with the pulmonary valve appears to be insufficient to prevent the increase in stress with age, thus making it less likely that collagen remodeling is stress-driven.

In the present study, we studied collagen remodeling at the tissue level. In order to fully unravel the underlying mechanisms of collagen remodeling, one needs to study how the cells sense and

respond to mechanical changes in their environment[103]. Recently, computational models were proposed that describe the interaction between cellular traction forces and collagen remodeling which may shed light on these mechanisms[52,136]. The findings of the present study can be valuable for developing these kind of models, in order to eventually develop a full understanding of the collagen remodeling mechanism.

2.4.2 Collagen remodeling can be attributed to changes in hemodynamics

The high spatial resolution of the confocal images in this study allowed for fiber architecture analysis and quantification on multiple scales: from dense fiber bundles on the macroscopic level up to individual fiber distributions on the microscale (Fig. 1). All valves that were measured featured a mainly circumferential fiber orientation, which is consistent with previous findings[89,185,195,199]. Most interestingly, the temporal evolution of the collagen architecture appears to feature different phenomena across the scales. This evolution can be related to temporal changes in hemodynamics, as well as differences in blood pressure between the aortic and pulmonary circulation.

At the microscale, the collagen alignment was higher in the aortic valve than in the pulmonary valve, which can be explained by remodeling in response to changes in hemodynamics. The postnatal rise in aortic blood pressure primarily leads to an increase in circumferential stretch (in case of isotropic collagen networks)[62,135]. Consequently, tissue remodeling in the aortic valve leads to a stronger alignment of the collagen network in the circumferential direction in order to decrease the circumferential stretch and maintain the stretch homeostasis.

Hemodynamics can also explain the large inter-patient variability in fiber dispersity that was observed in the pulmonary valve. Due to the highly nonlinear stress-stretch behavior of collagen fibers, the fibers will not be fully stretched at a low pressure. This implies that the collagen alignment is less crucial to maintain the stretch homeostasis in the pulmonary valve, as the blood pressure is much lower than in the aortic valve. Therefore, the collagen fiber dispersity in the pulmonary valves is higher and more diverse than in the aortic valves.

In contrast to the microscopic scale, the collagen architecture at the macroscopic scale evolves with time. Bundles of densely packed collagen fibers are visible in postnatal valves and become more pronounced in the older valves, which concurs with previous findings[3]. Since these bundles were found in both the aortic and pulmonary valve, their formation does not only appear to be induced by changes in leaflet stretch but may also be an effect of aging.

2.4.3 Valve stiffness is adapted by collagen remodeling to prevent excessive stretching

Several studies have characterized the mechanical behavior of heart valves[19,20,90,116,144,209]. Yet, to the best of the authors' knowledge, this is the first time that the mechanical properties of human semilunar heart valves of life-spanning age groups were quantified. The micro-indentation technique combined with inverse finite element analysis that was employed in this study has previously been used for characterizing anisotropic biological tissues[30,37,38]. The main advantage of micro-indentation

compared to for example biaxial tensile testing is that it can measure even the smallest samples, thus enabling mechanical characterization of the fetal and pediatric valves included in this study.

As collagen is the main load-bearing component of heart valves, changes in valve stiffness can be related to changes of the collagen architecture with age and between the aortic and pulmonary valve. The higher stiffness in the aortic compared to the pulmonary valve (Fig. 3) can be explained by the lower fiber dispersity in the aortic valve. On the other hand, the fiber dispersity remains constant with time, and the total collagen content is known to remain unchanged after childhood[3]. Therefore, the temporal increase in circumferential stiffness and nonlinearity can only be due to fiber bundle formation. Hence, fiber bundle formation influences valve mechanics by providing additional tissue stiffness, even though it may not be merely modulated by changes in mechanical loading.

2.4.4 Limitations

The use of unique human data to gain novel insights in valve tissue remodeling yields two main limitations. First, due to the limited availability the sample number was low. This can for example explain the stretch variations between valves from different donors (Fig. 5) and the spread in fiber dispersity (Fig. 2). These variations can amongst others be caused by deviating hemodynamics. For example, the high stretch that was predicted in the 22-year-old valve (Fig. 4A,C and 5) could be due to the donor being hypotensive, leading to a lower stiffness due to decreased mechanical demand and hence a higher stretch when normotensive conditions are assumed in the model.

Second, the stresses and stretches that were found in this study (Figs. 4–6) may be underestimated due to in vivo pre-stretches and residual stresses that are present in many biological tissues[35,50,73,180]. In aortic and pulmonary heart valve leaflets, they can be attributed to the cell tension in the leaflets themselves and pre-stretch and residual stresses in the aortic root. After dissection of the leaflets from the aortic root and cell death, these residual stresses were eliminated. Hence, mechanical characterization took place in a stress-free state. Yet, in our numerical simulations, the unloaded reference state was regarded as stress-free because the in vivo residual stresses could not be measured.

2.4.5 Implications for tissue engineering

In order to ensure long-term functionality of TEHVs, understanding and controlling the collagen remodeling process is of the greatest importance. However, long-term data is currently unavailable. In the current study, we aimed to identify the driving force of collagen remodeling by studying the evolution of stress and strain status in the human semilunar heart valves. By using heart valves of wide-ranging ages, different time points were obtained in the evolution of the human heart valve, which provided insight in the remodeling process. Additionally, the unique human data set created in this study is a valuable tool for developing future numerical collagen remodeling models that can predict the temporal changes observed in the present study.

Our results indicated that the circumferential stresses are different between the aortic and pulmonary valve, and, moreover, that the stress increases considerably over time in the aortic valve. In contrast, we found relatively small differences in valvular stretch with age and between the aortic and pulmonary valve, particularly in the circumferential direction, which is the main determinant of the stretch experienced by the collagen fibers. Therefore, we suggest that collagen remodeling in the human heart valve maintains a stretch-driven homeostasis.

Tissue engineers can take these findings into account in the design of TEHVs, for instance by adapting scaffold material, geometry and fiber alignment [135] to ensure that a developing tissue will be continuously exposed to a homeostatic stretch. This can direct the cells into functional regeneration of heart valve tissue while simultaneously preventing leaflet fibrosis. Once the collagen remodeling process can be predicted and controlled, long-term functionality of tissue-engineered heart valves can be ensured, thus providing patients with a heart valve that will last a lifetime.

CHAPTER 3

Ah, music, a magic beyond all we do here.

Albus Dumbledore – Hogwarts 1991 Start-of-Term speech

Mechanical models suggest that growth and remodeling play opposing roles during the development of human heart valves throughout life

The contents of this chapter are based on:

Oomen, P. J. A., Holland, M. A., Bouten, C. V. C., Kuhl, E. & Loerakker, S. (2018). Growth and remodeling play opposing roles during postnatal human heart valve development. *Scientific Reports* 8, 1–13.

3.1 Introduction

Scientists have been intrigued for many centuries by the intrinsic capability of biological tissues to actively change their form and properties. While these changes are most prominent during embryonic development, most living tissues are in a continuous state of adaptation. Since the time of Galileo Galilei, it has been believed that these changes are strongly influenced by mechanical factors[8]. Now, almost four centuries later, functional tissue adaptation, and its relation with mechanics, is still only partially understood. From a biomechanical perspective, it is well accepted that growth (here defined as mass or volume change) and remodeling (here defined as property change) occur at least partly in response to changes in the tissue's mechanical environment, in order to maintain a homeostasis[72,102,94,6,103]. Different mechanical constituents have been proposed to determine mechanical homeostasis across different tissue types, including stress[214,104,224,83], strain[32,182,167] (Chapter 2) and strain energy density[126,40,232].

By investigating the postnatal development of native heart valves, we can increase our understanding of how growth and remodeling maintain mechanical homeostasis in heart valves throughout life. During physiological development, the environment of the aortic and pulmonary heart valves, i.e. the annulus radius[226] and blood pressure[164,204,243], changes significantly (Table 2.1). As hypothesized by Aikawa et al.[3] and demonstrated in the previous chapter, tissue growth and remodeling occur in response to these changes in order to maintain mechanical homeostasis. Tissue growth occurs through production of new extra-cellular matrix (ECM), which leads to changes in leaflet length, area, and thickness[226,148]. Tissue remodeling, on the other hand, has been observed through a change in ECM structure and composition[3,226,12,207,116]. The most interesting changes in the ECM properties, from a biomechanical perspective, occur in the leaflets' collagen architecture, which is the main determinant of the mechanical behavior of heart valves. The collagen network matures with age, represented by thicker collagen fiber bundles[3,116] (Fig. 2.1) and increasing cross-link density[226]. As a result of the remodeling of the collagen network, the stiffness of the leaflets generally increases with age[226,11,207,116,209] (Fig. 2.3).

Recent research from our group on postnatal human native heart valves has shown relatively small differences in tissue stretch during development, and between aortic and pulmonary valves, thereby suggesting that tissue adaptation in this particular tissue occurs to maintain a stretch-driven homeostasis(Chapter 2). However, the relative roles of growth and remodeling in maintaining stretch homeostasis are still unclear. An improved knowledge of these roles is pivotal to understand the functioning of heart valves during health and disease, as adverse growth and remodeling can lead to valvular pathologies[87,32,31,182]. Moreover, growth and remodeling are of key importance for the emerging field of heart valve tissue engineering, which aims to create living heart valves that have the capability to grow and and remodel after implantation[92,68,85,57,212,121].

During postnatal valvular development, growth and remodeling occur simultaneously[226], which makes it challenging to experimentally deduce their relative contributions to maintaining mechan-

ical stretch homeostasis. Therefore, numerical models can be particularly useful to study their relative roles. The past two decades, two major approaches have been used to model growth and remodeling in collagenous tissues: constrained mixture models[105] and kinematic growth models[6,186,127]. Constrained mixture models may provide the more physiological representation of growth and remodeling. However, their parameters are hard to derive from experimental data, as they are based on the turnover of ECM components. Kinematic growth models, on the other hand, consider growth as isotropic or anisotropic volumetric changes, typically driven by a certain mechanical stimulus to reach a homeostatic target. In addition, when experimental data is available, kinematic growth could be defined in terms of known geometrical changes, rather than being driven by a mechanical stimulus. This approach only allows for prescribing homogeneous growth, as it is based on the overall geometrical changes, and is therefore not capable of releasing local stress concentrations.

The goal of the current study was to use a numerical model fueled by experimental data to elucidate the relative roles of tissue growth and remodeling in preserving the mechanical stretch homeostasis during physiological valvular development. In these mechanical models, growth was implemented prescribed via changes in leaflet area and thickness according to finite growth theory, and microstructural remodeling via prescribing changes in the material properties. Our mechanical model was informed by hemodynamic, geometric, mechanical, and structural data of paired aortic and pulmonary human native heart valves from infant to adult origin[226,164,204,243], as presented in Table 2.1 in the previous. We used a generic approach to divide age-dependent hemodynamic, geometric, and structural data for aortic and pulmonary valves to three groups: infant, adolescent and adult (Fig. 3.4a). Between these three groups, two developmental stages were addressed: early-stage development, from infant to adolescent, and late-stage development, from adolescent to adult. During these stages, the independent influences of growth and remodeling on leaflet stretch and valve function were studied. Moreover, we systematically studied the effects of growth and remodeling on the temporal evolution of the elastic stretches during development. To this end, we varied the initial rates of growth and remodeling relative to the environmental changes and each other and studied their influences on the temporal evolution of the elastic stretch. With this framework we show that growth and remodeling appear to play opposing roles in terms of preserving stretch homeostasis during the development of heart valves.

3.2 Methods

3.2.1 Age-dependent data from human native heart valves

The mechanical models were informed by age-related properties that were obtained from healthy paired aortic and pulmonary native human heart valves (n=24) that we analyzed in Chapter 2. The valves were obtained from postmortem donors from mixed gender, whose cause of death was not related to valvular disease or conditions known to precede valvular disease. These valves were mechanically and structurally uneffected, but were deemed unfit for implantations due to findings that

contra-indicated implantation, for instance: positive bacteriological sampling, serological findings in the donor, or other procedural non-conformities that caused rejection of the donor (e.g. sexual risk behavior and/or risks in drug abuse).

To accommodate the biological variability between individual valves, the valves were assigned to three generic age groups: infant (n=6, average age 0.9 $\pm$ 0.6 yr), adolescent (n=8, average age 19.5 $\pm$ 1.4 yr), and adult (n=10, average age 46 $\pm$ 3.0 yr). In between these groups two developmental stages were considered for both the aortic and pulmonary valve: early-stage development, from infant to adolescent, and late-stage development, from adolescent to adult (Fig. 3.4a). For each group, the average and standard deviation of the circumferential leaflet length L_c, radial leaflet length L_r, leaflet thickness t, and diastolic blood pressure (obtained from the literature[164,204,243]) were determined.

The data are presented as mean $\pm$ the standard error of the mean. Statistical differences between age groups and aortic and pulmonary valves were tested with two-way ANOVA, followed by Bonferroni post-hoc testing. GraphPad Prism (GraphPad Software, Inc., USA) was used for the analysis.

3.2.2 Mechanical model of physiological heart valve development

Finite element models were generated for each age group and valve type based on the age-dependent leaflet dimensions in Abaqus FEA (Dassault Systèmes, Simulia Corp., Providence, RI). Only one leaflet was modeled due to symmetry. The contact between the leaflets was modeled by adding two contact surfaces directly adjacent to the ventricular side of the leaflet, parallel to the two free edges (Fig. 8). As all leaflets were assumed to deform similarly, there cannot be any slip between adjacent leaflets. Therefore, the contact was set to be frictionless.

Although we previously generated leaflet geometries based on the lower half of a spherical surface[137] (Section 2.2.7), in the current study a spheroid surface with age-dependent thickness t was used to ensure an appropriate circumferential-radial length ratio L_c/L_r. The ratio $L_c/L_r \approx 2.0$ that we found for all valves (Fig. 3.4e–g) was measured *ex vivo* in excised leaflets, while it has recently been found in elderly patients who underwent heart transplantation that aortic heart valve leaflets are radially prestretched by 1.31 *in vivo*, with no evidence of circumferential prestretch[2]. Therefore, the *in vivo* leaflet length ratio should be $L_c/L_r \approx 2.0/1.31 \approx 1.53$. To ensure this, the major axis of the spheroid coincided with the annular radius and was equal to half the leaflet circumferential length, and the minor principal axis length was set such that the resulting radial leaflet length (equal to a quarter of the ellipsoid minor circumference) was 1/1.53 times the circumferential length (Fig. 3.1).

Valvular development was simulated by first of all changing the environmental properties, i.e. annular radius and diastolic blood pressure. The former was implemented via displacement boundary conditions on the leaflet nodes at the annulus, and the latter via a change in the hydrostatic pressure that was applied to the arterial side of the leaflets (Fig. 3.1). Growth and remodeling were implemented and applied either combined or separately during the developmental changes, in order to assess their relative effects on preserving the leaflet stretch.

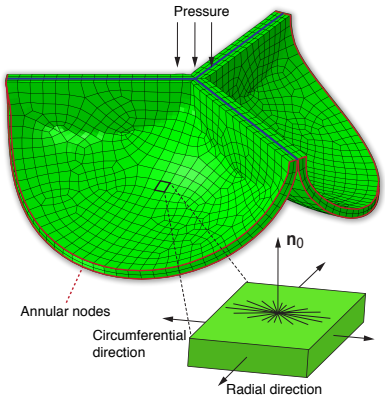

Figure 3.1: Mechanical model of heart valve development. A finite element model of a heart valve was generated for every age group based on the lower half of a spheroid. Due to symmetry, only one leaflet was modeled, and frictionless contact was modeled by adding a contact surface with friction coefficient 0 between adjacent leaflets, parallel to the free edges (blue lines). Somatic changes were applied by adjusting the diastolic blood pressure and prescribing displacement boundary conditions on the annular nodes (red lines). Leaflet stretch and stress were investigated in the highlighted element in the center of the belly region. Volumetric growth was applied in the plane spanned by the circumferential and radial direction, and in the thickness direction, given by plane normal $\mathbf{n}_0$. A collagen fiber network was implemented in the model which was mainly oriented in the circumferential direction.

3.2.3 Growth via geometrical changes

Growth was modeled as a change in volume. This was achieved kinematically according to the theory of finite growth, where the total deformation gradient tensor $\mathbf{F}$ was decomposed into an elastic contribution $\mathbf{F}_e$ and a growth contribution $\mathbf{F}_g$[186],

$$\mathbf{F} = \mathbf{F}_e \cdot \mathbf{F}_g \tag{3.1}$$

Similarly, the overall volume change $J = \det(\mathbf{F}) = J_e J_g$ was decomposed into a growth $J_g = \det(\mathbf{F}_g)$ and elastic change $J_e = \det(\mathbf{F}_e)$. The so-called growth tensor $\mathbf{F}_g$ was defined in terms of changes in circumferential leaflet length L_c, radial leaflet length L_r, and leaflet thickness t. Since the ratio between *ex vivo* circumferential and radial leaflet length remained constant during development (Fig. 3.4g), the relative change in circumferential $(L_c + \Delta L_c)/L_c$ and radial leaflet length $(L_r + \Delta L_r)/L_r$ were similar, thus defining an isotropic leaflet area change[27] $\vartheta = (L_c + \Delta L_c)(L_r + \Delta L_r)/(L_c L_r)$. Additionally, a relative thickness change $\eta = (t + \Delta t)/t$ was prescribed as a uniaxial change in the direction of plane normal $\mathbf{n}_0$ in the reference configuration[83]. Thus, we arrive at the definition of a transversely isotropic growth tensor that describes growth-induced volumetric changes in terms of area change ϑ and thickness change η,

$$\mathbf{F}_g = \sqrt{\vartheta}\mathbf{I} + \left(\eta - \sqrt{\vartheta}\right) \mathbf{n}_0 \otimes \mathbf{n}_0 \tag{3.2}$$

3.2.4 Remodeling via changes of material properties

Remodeling, e.g. stiffening due to cross-link formation or different degrees of anisotropy due to collagen fiber reorientation, leads to changes in the microstructure of valvular tissue. These microstructural changes lead to a different material response. In our model, we phenomenologically implemented microstructural remodeling by this change in material response. The (change in) material response was governed by (changes in) the material parameters of the constitutive model. These material parameters were interpolated between two developmental stages, by parameterizing them as a function of a weight factor w using polynomials (Fig. 3.2). The polynomials were fitted on the linear transition of the circumferential (d=circ.) and radial (d=rad.) Cauchy stress response:

$$\sigma^d(w) = (1-w)\sigma_0^d + w\sigma_{\text{end}}^d \qquad (0 \leqslant w \leqslant 1) \tag{3.3}$$

such that when $w = 0$ the Cauchy stress before remodeling σ_0^d was obtained, and when $w = 1$ the stress-stretch response after remodeling σ_{end}^d was obtained (Fig. 3.6).

The material behavior of the individual valves was previously estimated (Table 2.1, Fig. 2.3) using micro-indentation testing on a confocal microscope, in combination with inverse finite element modeling, as described before[38,37] (Section 2.2.3). This method allowed for anisotropic mechanical characterization in a strain range that is physiological for heart valve leaflets. For each age group (for both aortic and pulmonary valves) the average stress-stretch response in the circumferential and radial direction was determined. The material parameters for each group were then fitted to these average stress-stretch responses (Fig. 3.5).

The material behavior was modeled by a hyperelastic constitutive model, where the Cauchy stress $\boldsymbol{\sigma}$ was obtained from a strain energy density function Ψ. Since growth occurs stress-free, the strain energy density function is only dependent on elastic deformation $\Psi = \Psi(\mathbf{F}_e)$[186], and is therefore defined per amount of grown volume,

$$\boldsymbol{\sigma} = \frac{2}{J_e}\mathbf{F}_e \cdot \frac{\partial \Psi}{\partial \mathbf{C}_e} \cdot \mathbf{F}_e^T \tag{3.4}$$

with $\mathbf{C}_e = \mathbf{F}_e^T \cdot \mathbf{F}_e$ the elastic right Cauchy-Green deformation tensor. A fiber-reinforced material was used to model the valvular constitutive behavior, where the strain energy density function consists of an isotropic matrix part m and anisotropic fibrous part f with fiber volume fraction Φ_f, arbitrarily chosen to be 0.5[56],

$$\Psi = (1-\Phi_f)\Psi_m + \Phi_f\Psi_f \tag{3.5}$$

The constitutive behavior of the isotropic matrix part was described by a Neo-Hookean constitutive model,

$$\Psi_m = \frac{\kappa}{2}\ln^2(J_e) + \frac{\mu}{2}\left(I_{1,e} - 3 - 2\ln(J_e)\right) \tag{3.6}$$

where $\kappa = \frac{2\mu(1+\nu)}{3(1-2\nu)}$ is the bulk modulus, μ the shear modulus, and $I_{1,e} = \mathbf{C}_e : \mathbf{I}$ the first invariant

of the elastic right Cauchy-Green deformation tensor. Quasi-incompressibility was enforced by setting the Poisson ratio at $\nu = 0.498$. The fibrous part was modeled by an angular fiber distribution given by a periodic version of the normal probability distribution function[76,55], with a main circumferential orientation[135] and age-dependent dispersity β (Fig. 3.1). The direction of each fiber i was given by the unit vector $\mathbf{e}_0^i$ in the reference configuration and $\mathbf{e}_g^i$ in the configuration after growth. Each fiber additively contributed to the total fiber strain energy density function[56], where the strain energy density function Ψ_f^i for each individual fiber i was given by an exponential model[135,137,56],

$$\Psi_f^i = \frac{k_1}{2k_2}\left(\exp\left[k_2\left\langle(\lambda_e^i)^2 - 1\right\rangle\right] - k_2\langle(\lambda_e^i)^2 - 1\rangle - 1\right) \tag{3.7}$$

with k_1 and k_2 material parameters, $(\lambda_e^i)^2 = \mathbf{C}_e : \left(\mathbf{e}_g^i \otimes \mathbf{e}_g^i\right)$ the squared elastic fiber stretch, and $\langle\circ\rangle$ the Macaulay brackets to enforce that the fibers only resist tension.

3.2.5 Kinetics of growth and remodeling

The environmental changes were applied as a linear function of developmental time τ ($0 \leqslant \tau \leqslant 1$). The importance of the kinetics of growth and remodeling were investigated by defining the growth (ϑ and η) and remodeling (w) parameters as a function of τ and adjusting their rate change in an exponential fashion relative to the environmental changes, governed by rate change parameters k_g (growth rate) and k_r (remodeling rate),

$$\vartheta(\tau) = (\vartheta_{end} - 1)\frac{e^{k_g\tau} - 1}{e^{k_g} - 1} + 1 \tag{3.8}$$

$$\eta(\tau) = (\eta_{end} - 1)\frac{e^{k_g\tau} - 1}{e^{k_g} - 1} + 1 \tag{3.9}$$

$$w(\tau) = w_{end}\frac{e^{k_r\tau} - 1}{e^{k_r} - 1} \tag{3.10}$$

where ϑ_{end}, η_{end}, and w_{end} were the parameter values at the end of the developmental stage. Note that if $k_g \to 0$ and $k_r \to 0$ growth and remodeling occur linearly with time (and at an equal rate to the environmental changes), if $k_g < 0$ and $k_r < 0$ growth and remodeling initially occur faster, and if $k_g > 0$ and $k_r > 0$ growth and remodeling initially occur slower compared to the environmental changes (Fig. 3.3).

3.2.6 The relative influences of growth and remodeling

A total of six models (aortic and pulmonary infant, adolescent, and adult) were prepared to study the homeostatic stretches and stress. Subsequently, early development was simulated by applying environmental changes to the aortic and pulmonary infant valves, whereas for late development

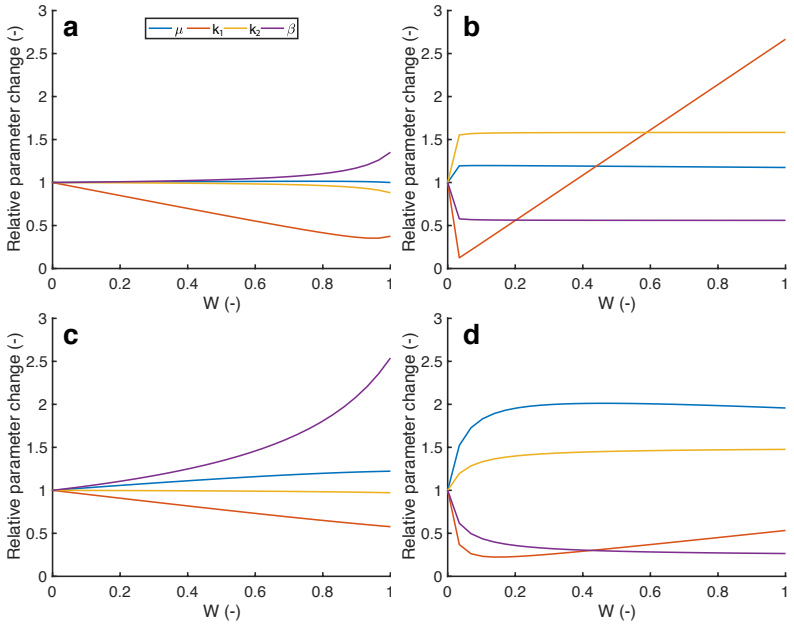

Figure 3.2: Remodeling was implemented by prescribing changes of the material properties. The four material parameters were fitted as function of a weighting factor w (with $w = 0$ returning the stress-stretch response before remodeling and $w = 1$ after remodeling) for aortic early **(a)** and late-stage **(b)** development, and pulmonary early **(c)** and late-stage **(d)** development.

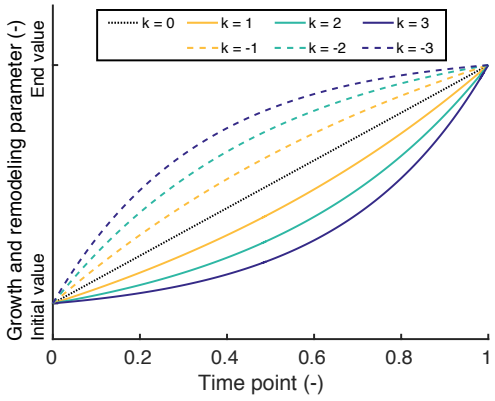

Figure 3.3: Variations in the kinetics of growth remodeling. The rate change of growth and remodeling relative to the environmental changes was investigated via a time-dependent exponential evolution of the growth and remodeling parameters. The exponential behavior was governed by rate parameter k (k_g for growth, k_r for remodeling), where if $k < 0$ growth and remodeling initially occurred faster, and $k > 0$ initially occurred slower compared to the environmental changes.

these changes were applied to the adolescent valves. The relative influence of growth and remodeling on leaflet stretch was investigated by applying growth and remodeling combined, only growth, only remodeling, and no growth and remodeling. For all simulations, leaflet stretch in the middle of the belly region (Fig. 3.1) was investigated. The importance of the kinetics of growth and remodeling relative to the environmental changes were investigated by applying combined growth and remodeling with different rates, using three cases: changing only the growth rate ($k_g = \pm 1, \pm 2, \pm 3$ while $k_r = 0$), changing only the remodeling rate ($k_r = \pm 1, \pm 2, \pm 3$ while $k_g = 0$), and changing both rates simultaneously ($k_g = k_r = \pm 1, \pm 2, \pm 3$). For all cases, the temporal changes in valve coaptation and leaflet stretch were investigated.

3.3 Results

3.3.1 Temporal changes occur in and around the human native heart valve during development

The hemodynamic, geometric and structural properties of 24 previously analyzed paired aortic (n=12) and pulmonary (n=12) human native heart valves (Chapter 2) were assigned to three age groups: infant (n=6, average age 0.9 $\pm$ 0.6 yr), adolescent (n=8, average age 19.5 $\pm$ 1.4 yr), and adult (n=10, average age 46 $\pm$ 3.0 yr) (Fig. 3.4a). Several changes were considered between the age groups. In the valves' environment, the aortic diastolic pressure increased with age (Fig. 3.4b), and the annulus radius increased significantly during early development ($p < 0.01$ for aortic and p < 0.05 for pulmonary) and only slightly during late development (Fig. 3.4c). Within the valves themselves, aortic leaflet thickness increased significantly (p $<$ 0.01) during early-stage development, followed by a significant (p $<$ 0.05) decrease during late-stage development (Fig. 3.4d). The adolescent ($p < 0.001$) and adult ($p < 0.01$) aortic valves were thicker than their pulmonary counterparts. The circumferential and radial leaflet length increased with age ((Fig. 3.4e,f), while no significant differences were found between the aortic and pulmonary leaflet lengths. Finally, no significant differences were found in the circumferential-radial length ratio with age and between the two valve types (Fig. 3.4g).

To estimate the mechanical behavior of the different age groups, a set of material parameters was determined for each age group by fitting a fiber-reinforced hyperelastic constitutive model to the group's individual stress-stretch responses (Fig. 3.5). According to the stress-stretch curves, aortic leaflet stiffness decreased during early development (Fig. 3.6a), followed by an increase during late development (Fig. 3.6b). The pulmonary leaflets were more compliant than their aortic counterparts, but featured the same temporal evolution (Fig. 3.6c,d).

The mechanical properties, alongside the other age-dependent data (Fig. 3.4), were used to generate a finite element model of each valve group in order to simulate the average mechanical state of heart valves at valve closure during diastole. The elastic stretch in the center of the belly region in the circumferential direction, which coincides with the main collagen orientation, was similar between

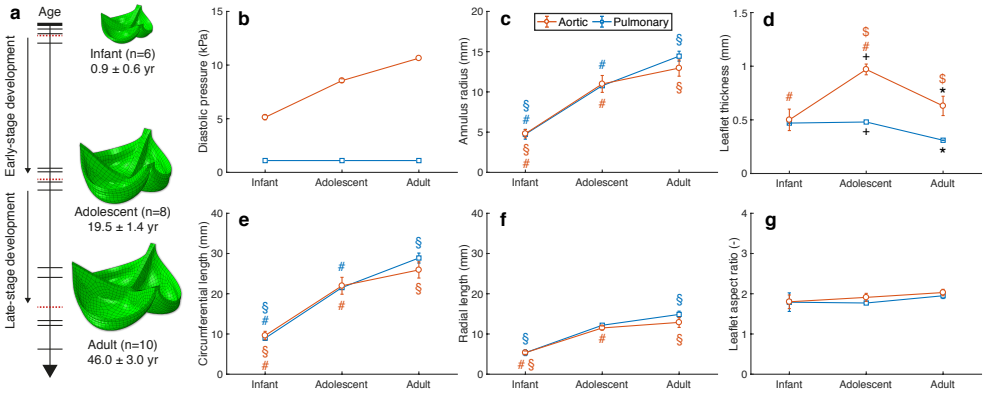

Figure 3.4: Age-dependent changes in human heart valves. **(a)** A timeline of experimental data of 24 paired human aortic and pulmonary heart valves (where each horizontal bar represents the age of one pair) were assigned to three age groups: infant, adolescent, and adult (where the red dashed bars indicate the average age of each group). The age-dependent data informed the generation of a finite element model for each group. Temporal changes were considered in diastolic blood pressure [164,204,243] **(b)**, annulus radius **(c)**, leaflet thickness **(d)**, circumferential **(e)**, and radial **(f)** leaflet length, and aspect ratio between the circumferential and radial length **(g)** [226]. Significant differences ($p < 0.05$) of geometrical measurements **(c–g)** between groups are indicated by paired symbols.

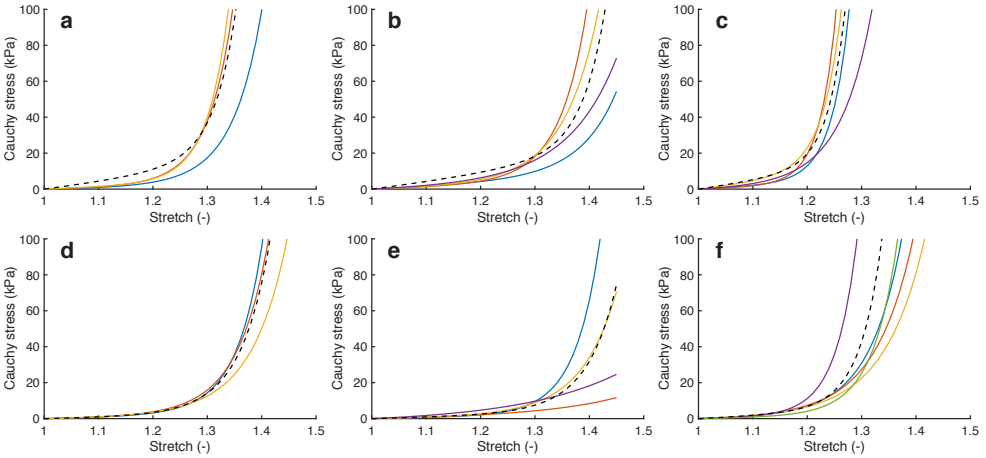

Figure 3.5: The material behavior of the aortic **(a–c)** and pulmonary **(d–f)** valves of infant **(a,d)**, adolescent **(b,e)**, and adult **(c,f)** origin was previously estimated (Section 2.3.2, Table 2.1). The material behavior for each age group was estimated by fitting a fiber-reinforced hyperelastic constitutive model (dashed line) to the group's average stress-stretch response in the circumferential (shown here) and radial direction.

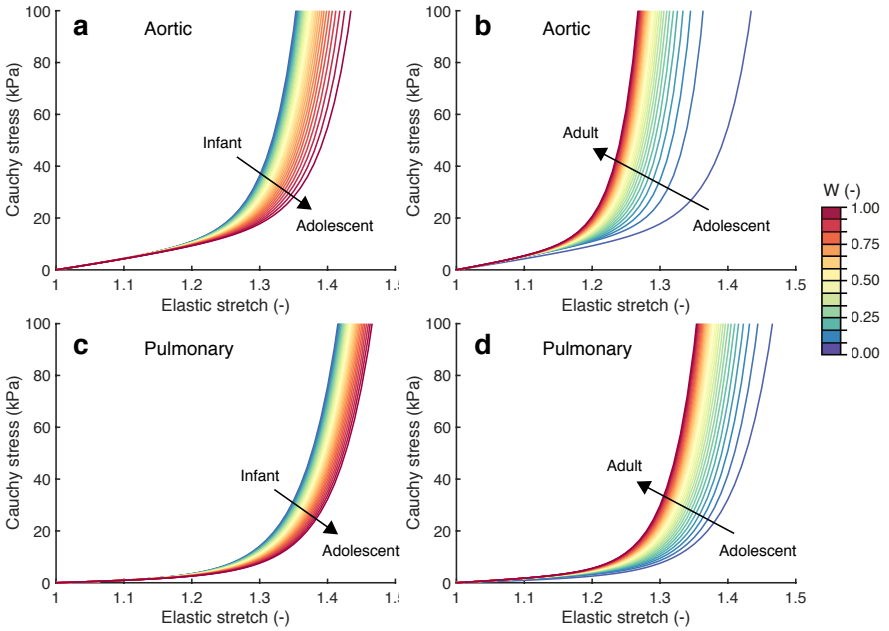

Figure 3.6: Remodeling was defined as changes in material behavior. The material properties of each age group were estimated by fitting a fiber-reinforced hyperelastic constitutive model to the group's average stress-stretch response. The changes in material behavior during early and late-stage development were modeled as a function of a weight factor W (color legend). The circumferential stress-stretch plots indicate that the aortic **(a)** and pulmonary **(c)** leaflets became more compliant during early-stage development and became stiffer during late-stage development **(b,d)**.

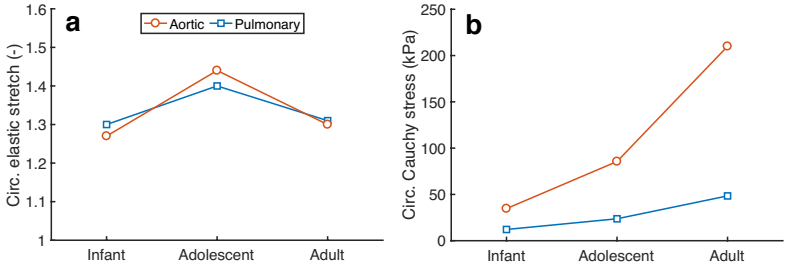

Figure 3.7: Evolution of stretch and stress with age. Age-dependent simulations indicated that the circumferential (circ.) stretch was similar with age and between the aortic and pulmonary valves **(a)**, whereas the circumferential Cauchy stress was higher in the aortic valve than in the pulmonary valve and increased continuously with age **(b)**.

the aortic and pulmonary valves for all age groups, and between infant and adult valves (Fig. 3.7a). Of note, stretch in the adolescent valves was slightly higher than in the other age groups. In contrast, the circumferential Cauchy stress in the belly region was considerably higher in the aortic valves than in the pulmonary valves, and continuously increased with age (Fig. 3.7b). These findings comply with our previous observations in individual valves (Fig. 2.4).

3.3.2 During early-stage development growth reduces stretch, whereas remodeling increases stretch

Physiological valve development from the infant to the adolescent and from the adolescent to the adult valve was simulated by applying environmental changes (annulus radius and diastolic blood pressure) to the infant and adolescent models. With these simulations, the combined and individual influences of growth (change in leaflet length and thickness according to Fig. 3.4d–f) and microstructural remodeling (change in mechanical properties according to Fig. 3.6) after development on leaflet stretch were estimated.

Growth and/or remodeling during early-stage development had a similar effect on tissue stretch in both the aortic and pulmonary valve, despite their different mechanical, geometric, and environmental properties (Fig. 3.8a,3.9). Tissue growth alone reduced circumferential stretch after early-stage development towards homeostatic values. In contrast, with remodeling alone, or without growth and remodeling altogether, the stretches after early-stage development were extremely high. Interestingly, the combination of growth and remodeling also prevented excessive stretches, although the stretches were larger compared to applying growth alone, and to the initial state. The latter result coincides with the elevated stretch that we found in the adolescent valve (Fig. 3.7a). Incomplete valve closure was observed without leaflet growth, while remodeling was not observed to significantly influence valve closure (Fig. 3.8a).

3.3.3 During late-stage development remodeling reduces stretch, whereas growth increases stretch

Similar to early-stage development, growth and/or remodeling during late-stage development had comparable effects on leaflet stretch between the aortic and pulmonary valve (Fig. 3.8b, 3.9). Interestingly, during this stage the effects of growth and remodeling on tissue stretch were opposite compared to early development: remodeling alone reduced the circumferential stretch, while growth alone increased tissue stretch. When growth and remodeling were combined, the stretch was reduced compared to the initial state, which coincides with the lower stretch that we found in the adult valve compared to the adolescent valve (Fig. 3.7a). Incomplete valve closure was only observed in this stage in the pulmonary valve when no growth was applied (Fig. 3.8b).

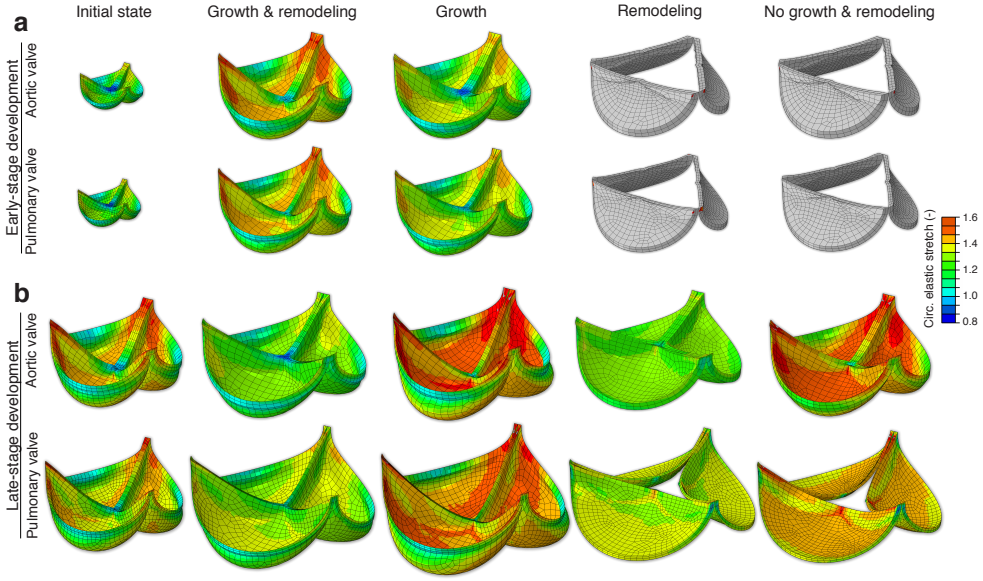

Figure 3.8: The influence of growth and/or remodeling on circumferential leaflet stretch and valve closure. Valve closure during diastole was simulated for early-stage **(a)** and late-stage **(b)** development of aortic and pulmonary heart valves and tissue stretch was assessed after applying growth and remodeling either combined or alone. Circumferential elastic leaflet stretches after growth and/or remodeling were similar in the aortic and pulmonary valves, with stretches in the early-stage valves without growth higher than 1.6. Insufficient valve closure was observed without growth after early-stage development of the aortic and pulmonary valves, and pulmonary late-stage development.

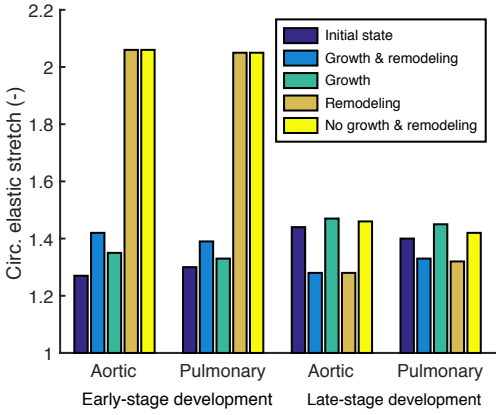

Figure 3.9: The influence of growth and/or remodeling on circumferential stretch in the belly region. For both the aortic and pulmonary valve, growth and remodeling appeared to play opposing roles on tissue stretch and with time. Growth decreased circumferential stretch during early-stage development while remodeling lead to and increase in stretch, and vice versa for late-stage development.

3.3.4 Leaflet volume changes primarily during early development

During both early and late-stage development, leaflet area was found to increase with age, while thickness increased during early-stage development and decreased during late development (Fig. 3.4d–f). As a consequence, the total leaflet volume of the models increased dramatically during early-stage development for both valves (Fig. 3.10), whereas stabilization of leaflet volume was observed during late-stage development. This suggests that changes in leaflet geometry during late-stage development are rather due to tissue dilation than to growth.

3.3.5 Importance of growth and remodeling kinetics

The model was used to systematically study the effects of growth and remodeling on the temporal evolution of the elastic stretches during development. To this end, we varied the initial rates of growth and remodeling relative to the environmental changes and each other, and studied their influences on the temporal evolution of the elastic stretch. Rate change parameters were introduced for both growth (k_{g}) and remodeling (k_{r}), which governed their initial rate change relative to the environmental changes. Overall, the aortic and pulmonary valves showed similar temporal trends in terms of stretch, so for the sake of brevity only the results for the aortic valve are shown (Fig. 3.11).

During early development, the stretch increased more or less linearly when growth and remodeling occurred at the same rate as the environmental changes (Fig. 3.11a–c). The changes in growth rate affected leaflet stretch most at the beginning of the developmental time, with a slower relative growth rate ($k_{\mathrm{g}} > 0$) leading to increased intermediate stretches, observed at the halfway point of early development (Fig. 3.11b). In contrast, the changes in remodeling rate had the largest effect at the end of the development, with a faster rate ($k_{\mathrm{r}} < 0$) leading to higher intermediate stretches (Fig. 3.11c). Accordingly, when both rates were changed simultaneously, growth was most most influential at the beginning and remodeling at the end of development (Fig. 3.11a), with a transition taking place halfway. When growth initially occurred slower than the environmental changes, no full valve closure was observed halfway the developmental time.

Interestingly, during late-stage development, the stretch decreased in an exponential decay fashion when growth and remodeling occurred with the same rate as the environmental changes (Fig. 3.11d–f). The effect of different growth rates on the temporal change in stretch was negligible (Fig. 3.11d–e), while a relatively fast remodeling rate ($k_{\mathrm{r}} < 0$) led to a fast decrease in intermediate stretches (Fig. 3.11d,f). Full valve closure was observed at all times.

3.4 Discussion

Growth and remodeling are widely believed to occur to maintain a certain mechanical homeostasis[72,102,94,6,103], with evidence in the previous chapter indicating that in native heart valves this homeostasis is determined by tissue stretch. In this study, we used mechanical models that were informed

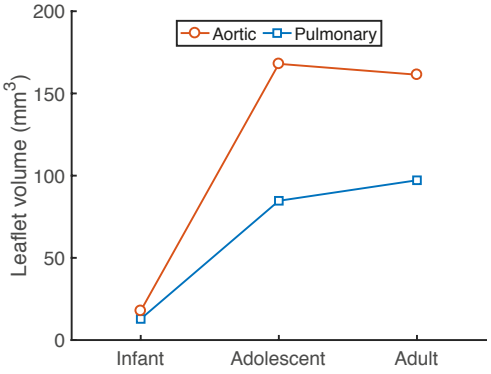

Figure 3.10: Changes in leaflet volume with age. Single leaflet volume in the models of both aortic and pulmonary valves increased dramatically during early-stage development due to tissue growth, whereas no clear change in volume was observed during late-stage development. The volume of the aortic valve was always higher than that of the pulmonary valve.

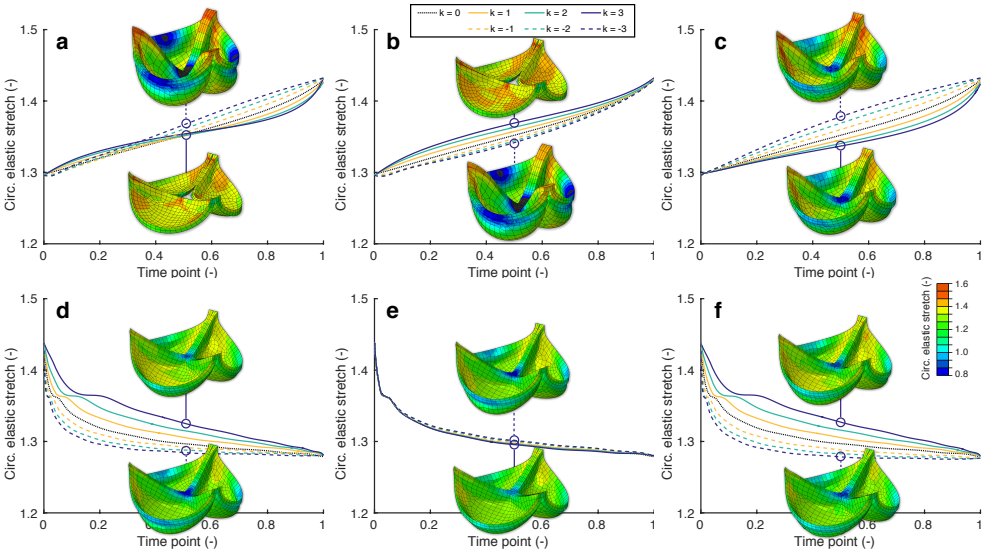

Figure 3.11: Importance of growth and remodeling kinetics. The relative rates k of growth ($k = k_g$) and remodeling ($k = k_r$) with respect to the environmental changes were altered to study their effects on the temporal stretch evolution. Three cases were investigated for early **(a–c)** and late-stage **(d–f)** development: **(a,d)** changing growth rate k_g and remodeling rate k_r simultaneously, **(b,e)** changing only the growth rate k_g while $k_r = 0$, and **(c,f)** changing only the remodeling rate k_r while $k_g = 0$. Growth and remodeling occurred with the same rate as the environmental changes if $k = 0$, initially slower if $k > 0$; and initially faster if $k < 0$. The three-dimensional circumferential stretch distributions are shown halfway the developmental steps at time point 0.5 for $k_g = \pm 3$ and/or $k_r = \pm 3$.

by experimental data to elucidate the relative roles of growth and remodeling on the preservation of tissue stretch in aortic and pulmonary human native heart valves during physiological development.

3.4.1 Growth and remodeling have opposing effects on valve tissue stretch and with age

Our results indicate that growth and remodeling play opposing roles in preserving tissue stretch and with time. During early-stage development, growth preserved tissue stretch, whereas remodeling led to an increase in stretch (Figs. 3.8a and 3.9). These effects occurred more rapidly when the initial growth and remodeling rates were increased (Figs. 3.11a,b). The decrease in tissue stretch via growth can be explained by the increase in both leaflet area and thickness (Figs. 3.4e,f). The increase in stretch via remodeling can be explained by the tissue softening that occurred during early-stage development (Figs. 3.6a,c). Changes in the material stiffness of heart valves by remodeling have previously been correlated with collagen cross-link formation [11,226]. Collagen cross-link formation is a much slower process than tissue growth, and cannot occur while ECM is being produced [11]. Therefore, we hypothesize that the tissue softening that was observed during early-stage development is a repercussion of growth, as an increase in tissue stiffness via remodeling may be impossible while ECM is still being produced.

In contrast to early-stage development, the influences of growth and remodeling on stretch appeared to be reversed during late-stage development. Our results indicate that during late-stage development, leaflet stretch is decreased by remodeling and increased via geometrical changes (Fig. 3.8b and 3.9). Interestingly, the geometric changes that occurred during this stage (Fig. 3.4d–f) did not result in a clear change in volume. Therefore, it can be concluded that valvular tissue growth, which we defined as change in volume, primarily occurs during early-stage development, with tissue dilation, rather than growth, occurring during late-stage development. Leaflet thinning due to dilation appears to be mostly responsible for the large deformations that were observed after late-stage development with only growth, in both the aortic and pulmonary valve. These deformations cannot be solely caused by the increase in pressure, since the diastolic pressure only increases for aortic valve, whereas it remains constant for the pulmonary valve throughout development.

Since no active growth took place during late-stage development, tissue remodeling is more likely to occur via cross-link formation. This could be responsible for tissue stiffening (Fig. 3.6b,d) and thus counteracts the increase in leaflet stretch that occurs via dilation, associated with the decrease in leaflet thickness. Aside from cross-link formation, leaflet calcification and collagen fiber alignment could have contributed to leaflet stiffening with ageing. Calcification occurs gradually with age in most valves and increases local stiffness during late-stage development [201]. Collagen fiber alignment was in the previous Chapter found to increase during late development (Fig. 2.2) for both aortic and pulmonary valves, which coincides with the increased circumferential stiffness that was found in the same valves.

3.4.2 Volumetric changes with age can be explained by mechanical stimuli

The presence of active growth during early-stage development, and its absence during late-stage development, can be explained by the influence of mechanical stimuli on valvular interstitial cells, which are responsible for leaflet growth and remodeling. In previous in vitro studies, it was shown that valvular interstitial cells become activated upon mechanical stimulation [86,128], resulting in a myofibroblast-like phenotype that is associated with ECM production [3,177]. Clearly, larger overall changes in mechanical stimuli are provided via environmental changes during early-stage in comparison with late-stage development (Fig. 3.4b,c). These changes in mechanical stimuli activate the valvular cells and thus explains why in our study leaflet growth was only observed during early development. Leaflet dilation during late-stage development would then be a passive process. During the latter stage, the cells remain quiescent due to less prominent changes in mechanical stimuli, since the environmental changes are much smaller compared to early development.

In a physiological situation, changes in mechanical stimuli are primarily present during early-stage development. At an older age, cells can still become activated when mechanically stimulated by pathologies, as observed in dilated cardiomyopathy, where the ventricle and mitral valve annular radius are enlarged and cause increased leaflet stretch [122,171,182]. It has been demonstrated in adult human patients [32] and animal models [31,182,45] that this pathology results in significantly enlarged mitral leaflets, and that interstitial cells are activated [45], which is in a physiological situation only the case during early development [3,226,177]. The occurrence of leaflet growth during cardiomyopathy suggests that growth can occur regardless of age, provided that the valvular interstitial cells are presented with changes in mechanical stimuli.

3.4.3 Growth and remodeling feature similar temporal trends but different magnitudes in the aortic and pulmonary valves

It is interesting to note that the aortic and pulmonary valve operate under completely different mechanic al circumstances, since the aortic diastolic pressure, leaflet thickness, and leaflet stiffness are much higher than the pulmonary pressure. Still, the same homeostatic stretches (Fig. 3.7) and temporal effects of growth and remodeling on preserving stretch (Fig. 3.8 and Fig. 3.9) were found for both valve types. Growth and remodeling appeared to occur proportionally to the environmental changes, with higher magnitudes in the aortic than in the pulmonary valves. More growth occurred in the aortic valve (Fig. 3.10), mainly characterized by a larger increase in thickness (Fig. 3.4d). The stiffness, modulated by remodeling, of the aortic valves was also higher than in their pulmonary counterparts (Fig. 3.6). This further supports the hypothesis that growth and remodeling occur to maintain a stretch homeostasis, for more growth and remodeling are required in the aortic valve to counteract the increasing aortic diastolic pressure, and thus to establish the same stretches as in the pulmonary valve.

3.4.4 Limitations of the mechanical model

The current model features three main limitations. First, although the experimental foundation of the model is a great advantage, we were limited by data availability. We could now only consider developmental stages of rather large time spans of at least 18 years. Particularly, the temporal step between the infant and adolescent groups was relatively large, since extensive somatic changes take place during this transition. An intermediate group of around 12 years old would have been desirable, but no experimental data were available around this age.

Second, we did not implement prestretch, which is known to significantly influence tissue mechanics[180]. To the best of our knowledge, the only data on aortic and pulmonary leaflet prestretch has recently been obtained from valves from elderly patients (average age 63 yr) who underwent heart transplantation[2]. We used these novel findings in the generation of the leaflet geometry to ensure an appropriate circumferential-radial leaflet length ratio of 2 according to Fig. 3.4g. Yet, since it is still unknown if and how prestretch evolves with age, no actual tissue prestretch was implemented in the age-dependent growth and remodeling simulations.

Third, the growth and remodeling that we applied in the numerical model was different to traditional approaches, where tissue growth not only occurs to reach a mechanical homeostasis, but also to release any local stress and/or strain concentrations. Due to the global manner in which growth and remodeling were applied in our model, local artifacts in the stress and strain fields may have arisen.

3.4.5 Conclusion

Our mechanical model, that was informed by experimental data from Chapter 2, indicates that growth and remodeling play opposing roles in preserving tissue stretch and with time. During early-stage development, growth preserves tissue stretch, while remodeling leads to an increase in stretch, which we hypothesize is caused by tissue softening as a repercussion of growth. In contrast, the influences of growth and remodeling on stretch appeared to be reversed during late-stage development. During this stage, leaflet stretch was decreased by remodeling, and increased by volume changes that we now identified as dilation, rather than growth. The obtained understanding of the distinct roles of valvular growth and remodeling is pivotal for improving the knowledge of the functioning of native heart valves during health and disease. This is highly relevant for understanding pathologies like valvular stenosis and dilated cardiomyopathy, but also for heart valve tissue engineering, which aims to create heart valves that have the capability to grow and remodel after implantation.

CHAPTER 4

To invent, you need a good imagination and a pile of junk.

Thomas Edison

A bioreactor to identify the driving mechanical stimuli of tissue growth and remodeling

The contents of this chapter are based on:

Van Kelle*, M. A. J., Oomen*, P. J. A., Bulsink, J. A., Janssen-van den Broek, M. W. J. T., Lopata, R. G. P., Rutten, M. C. M., Loerakker, S. & Bouten, C. V. C. (2017). A Bioreactor to Identify the Driving Mechanical Stimuli of Tissue Growth and Remodeling. *Tissue Engineering Part C: Methods* 23, 377–387.

*These authors contributed equally

4.1 Introduction

Cardiovascular tissues are known to adapt in response to changes in their environment through growth and remodeling. While the underlying mechanisms that govern growth and remodeling are not completely understood, it is well accepted that they are at least partly driven by mechanical cues. Cells residing in these tissues are capable of sensing mechanical cues, and as a response regulate their own behavior (e.g. proliferation) and the surrounding matrix by growth (increase in tissue mass) and remodeling (changes in tissue structure). It is believed that these processes occur to maintain a cell-mediated mechanical homeostasis[94,103]. Yet, the mechanisms through which this mechanical homeostasis is maintained remain largely unknown. An improved knowledge of these mechanisms is key to better understand pathologies where adverse growth and remodeling occur, such as dilated and hypertrophic cardiomyopathy[71], valvular disease[67,64], and aneurysm formation[145,106]. Moreover, a fundamental understanding of growth and remodeling is essential in the fields of regenerative medicine and tissue engineering.

In order to unravel the mechanisms of growth and remodeling, a systematic investigation of the underlying processes and associated mechanical parameters is required. To this end, bioreactor systems are valuable for studying the response of soft tissues to mechanical stimuli at the cellular and the tissue level. Initially, bioreactor systems were developed to study the effects of mechanical stimuli under static conditions[64,132,229,98]. As cardiovascular tissues are mainly exposed to dynamic loading conditions, other bioreactors applied dynamic deformation to the tissue engineered (TE) constructs[61,152,107,124,86,190]. For example, Rubbens et al. and Gould et al. applied cyclic strain to study the remodeling of 3D TE constructs[86,190]. Moreover, Engelmayer et al. tested different scaffold candidates for heart valve tissue engineering by designing a bioreactor capable of applying cyclic flexure and laminar flow[61]. In addition, several strain-driven bioreactors have been proposed applying physiological mechanical and electrical stimulation to cardiac tissues[208]. Finally, Kortsmit et al. introduced a bioreactor with a feedback system, to attain a constant maximal deformation while culturing TE heart valves in vitro[124]. Yet, for cardiovascular tissues in vivo deformation is mainly governed by hemodynamic flow and pressure, which are known to play an important role in tissue growth and remodeling[102]. To incorporate hemodynamic loading, Shaikh et al. and Hollweck et al. mimicked in vivo loading conditions, by using pulsatile bioreactors that applied physiological pressures to TE constructs[96,203].

The previously mentioned bioreactors lacked two main features to study mechanically-driven growth and remodeling over time. First, these systems were not capable of tissue culture and mechanical stimulation for a prolonged time period, while simultaneously performing mechanical testing. Consequently, changes in the mechanical state of tissues with time could not be assessed for individual samples. Moreover, these systems did not retain a (dynamic) pressure during culture, which resembles the physiological load of many, primarily cardiovascular, tissue types, and can lead to a different adaptation mechanism of these tissues compared to displacement-controlled mechanical stimulation. Particularly, when applying a constant pressure during culture, the strain will not

necessarily remain constant over time. Consequently, a strain-driven bioreactor may not capture the in vivo loading conditions and hence growth and remodeling phenomena.

The goal of the present study was to design and test a bioreactor that is capable of tissue culture and mechanical stimulation for a prolonged time period, while simultaneously performing mechanical testing. The bioreactor features a two-chamber design that allows easy and sterile handling of a TE construct, resembling thin cardiovascular tissues such as arteries and heart valves, in a dedicated culture chamber, while a second pressure chamber applies a physiologically relevant dynamic pressure regime, regulated by a custom-made feedback system.A novel non-destructive mechanical testing method is employed, involving a bulge test which can be performed inside the bioreactor, in which the construct's curvature is determined by ultrasound (US) imaging. This technique can be used to quantify temporal changes in tissue mechanical properties, without sacrificing the sample. Additional microscopy measurements of tissue thickness and prestretch serve to obtain the tissue geometry. Finally, confocal microscopy, histology and biochemical assays allow for determining tissue composition and architecture.

4.2 Methods

4.2.1 Vertigro bioreactor

The 'versatile tissue growth and remodeling' (Vertigro) bioreactor consists of two chambers: a pressure chamber (bottom) and a detachable culture chamber (top) (Fig. 4.1) in which a TE construct is cultured. This design was chosen in order to have a separate chamber for sterile tissue culture and medium changes, while the other chamber is dedicated to applying the dynamic pressure. Both chambers are made of polysulfone (PSU, Röchling, Mannheim, Germany) and have connection ports fitting standard luer-lock slip tips. After sealing both chambers with a silicone membrane, the culture chamber is secured on top of the pressure chamber by means of three metal clamps. In this configuration, the two silicone membranes form a double membrane connection between the two chambers to ensure the transmission of pressure from the pressure chamber to the culture chamber.

The pressure chamber is connected to a pump containing a flexible silicone tube, which can be compressed with pressurized air. A proportional pneumatic valve (Festo, Esslingen Berkheim, Germany) regulates the inflow of pressurized air, by opening in accordance to a programmable waveform function, supplied by a multi-IO-card using LabVIEW software (National Instruments, Austin, TX, USA).

The culture chamber consists of a lower and an upper part, separated by an insert that is clamping the tissue construct. Both parts of the culture chamber are filled with culture medium. The top chamber is closed with a lid that allows free air exchange with the external environment, required to buffer the pH of the medium. Upon an increase in pressure in the pressure chamber, the membranes bulge into the culture chamber, pressurizing the tissue construct. A pressure sen-

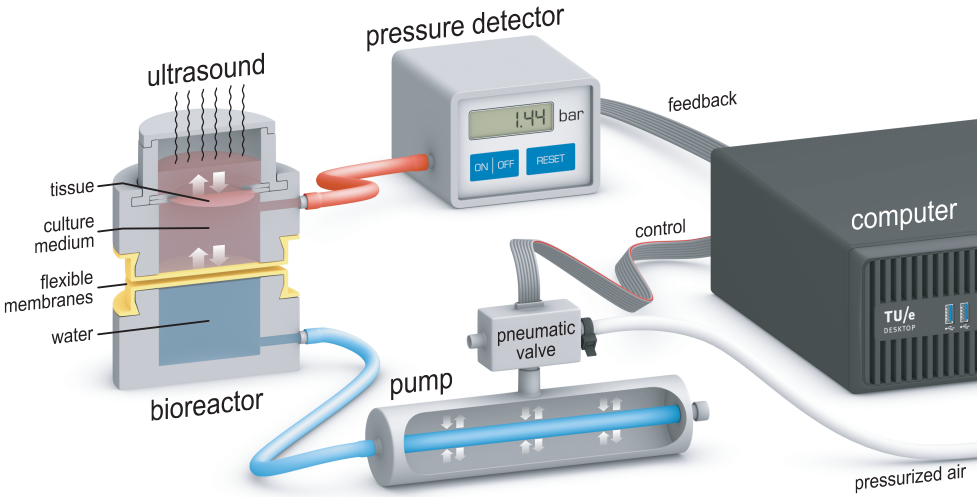

Figure 4.1: Schematic representation of the Vertigro bioreactor and pressure application system.

sor (P10EZ-1, BD|SENSORS, Thierstein, Germany) is connected to the lower part of the culture chamber to measure the pressure on the tissue in real-time.

A feedback system was implemented in the LabVIEW framework in order to keep the minimal and maximal pressures at preset levels. In case of deviations from this preset level (±5% tolerance), either the offset (minimal pressure) or the amplitude (maximal pressure) of a square waveform function are changed accordingly, therefore maintaining a constant peak pressure during culture. The Vertigros, pressure sensors and pumps can be placed in an incubator (37C°, 100% RH and 5% CO_2), while the proportional air valves, pressure modules, and other hardware remain outside.

4.2.2 Cell and tissue culture

Tissue constructs were engineered using vascular derived cells, previously characterized as contractile, matrix-producing myofibroblasts[158], harvested from the human vena saphena magna according to the Dutch guidelines for secondary use of materials. Cells were expanded until passage 7 using culture medium containing advanced Dulbecco's Modified Eagle Medium (DMEM, Invitrogen, Carlsbac, CA, USA), supplemented with 10% Fetal Bovine Serum (FBS, Greiner Bio One, Frinckenhausen, Germany), 1% Glutamax (Invitrogen) and 1% penicillin-streptomycin (Lonza, Basel, Switserland), with medium changes twice a week.

Prior to seeding, rapidly degrading non-woven polyglycolic acid (PGA) Biofelt (Biomedical Structures, Warwick, USA, 0.5 mm thickness, 70 mg/cm2 density) was cut to size to fit inside the inserts. To provide a slow-degrading fixation of the tissue on the edge of the insert, a polycaprolactone scaffold (PCL, electrospun in-house, thickness 0.25mm) was cut to the same diameter as the PGA

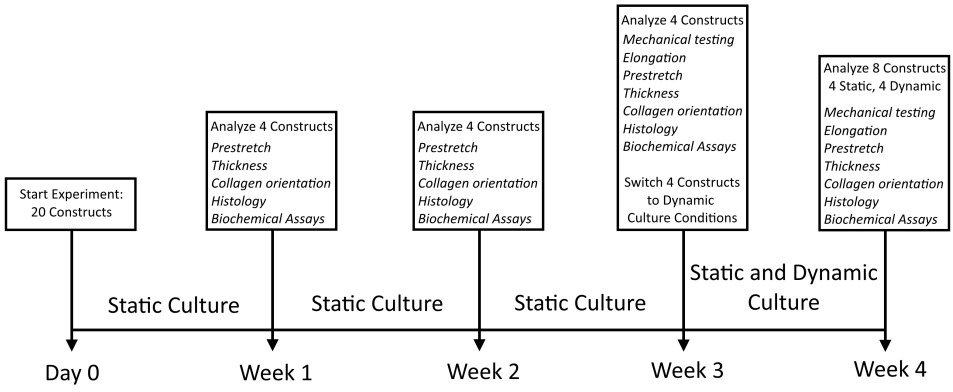

Figure 4.2: Timeline used for proof of concept experiment.

scaffolds, while a circular 13mm cutout was made in the center. Next, the PGA was coated with poly-4hydroxybutyrate (P4HB, Tepha, MA, USA) and mounted together with the PCL rings into the bioreactor inserts. The inserts were then immersed in 70% ethanol for 30 min. After sterilization, the inserts were washed with PBS and placed in 0.25 mg/ml L-ascorbic 2-phosphate acid (Sigma-Aldrich, St. Louis, MO, USA) supplemented standard culture medium (TE medium) overnight at 37 C° and 5% CO2. The next day, the cells were seeded onto the scaffolds (15x106 cells/cm3) using fibrin as a cell carrier[158]. Finally, the constructs were cultured statically for three weeks in 6-well plates in TE medium (which was changed three times a week). After this period, the constructs were strong enough to be cultured dynamically.

4.2.3 Experimental protocol

To assess bioreactor functionality and to evaluate the proposed analysis techniques, a proof-of-principle experiment was performed (Fig. 4.2). In this experiment, 20 tissue constructs were cultured: In the first three weeks these were cultured statically, taking out four samples at the end of each week. From the remaining eight constructs, four were cultured under static conditions for one additional week, whilst the other four samples were cultured under dynamic loading conditions (minimal pressure 0 kPa, maximal pressure 2 kPa, frequency 1 Hz).

4.2.4 Analysis techniques

Mechanical testing

The bioreactor system was designed to perform mechanical testing via classical mechanical bulge tests without removing the constructs. A syringe was connected to the pressure chamber and placed in a Harvard pump (PHD2000, Harvard Apparatus, Holliston, MA, USA) to apply a volume-controlled pressure to the samples. The volume was gradually increased until a pressure of 2 kPa was

reached in the culture chamber. Subsequently, three pressure cycles were performed, of which the first two served as preconditioning cycles. An US transducer was mounted on top of the bioreactor, perpendicular to the sample surface, in order to nondestructively measure construct displacement as a function of pressure. Two-dimensional US imaging was performed with a MyLab70 US system (ESAOTE, Maastricht, NL), equipped with a linear array (LA523, center frequency of 7.5 MHz). The data were exported in video format (AVI) at a frame rate of 20 Hz.

To quantify the mechanical behavior of the tissue, the in-plane stress was estimated as a function of stretch, assuming tissue isotropy. Tissue stretch was determined from the frames of the US movies (resolution 21.5 px/mm) using a custom MATLAB script (MathWorks, Natick, MA, USA). In particular, for each frame, the tissue profile was detected using MATLAB's built-in edge detection function, through which a circle was fitted in the center region. The constrained tissue length L_0 at zero pressure and current tissue length L in each consecutive frame were then obtained by calculating the circle's arc length. Additionally, tissue elongation, defined as the relative change of constrained length during culture time, was calculated as L_0 (at 0 pressure) divided by the initial construct diameter (15.0 mm). The in-plane stretch due to bulging $\lambda = L/L_0$ was then calculated as the change in length from the initial constrained sample length L_0 at zero pressure. Accounting for the presence of cell-induced tissue prestretch λ_p (see next Section), a multiplicative decomposition was used to calculate the total elastic in-plane tissue stretch λ_e:

$$\lambda_e = \lambda \lambda_p \tag{4.1}$$

To estimate the mechanical state of the tissue, the Tension T and Cauchy stress σ in the in-plane direction of the construct were calculated using Laplace's law for a thin-walled shell:

$$T = \frac{p}{2\kappa} \qquad \sigma = \frac{p}{2\kappa t} \tag{4.2}$$

with p the pressure, κ the curvature and t the deformed sample thickness. The curvature was calculated as the inverse of the fitted circle's radius. The deformed tissue's thickness was derived from the measured thickness t_0 and in-plane elastic stretch, assuming tissue isotropy and incompressibility:

$$t = \frac{t_0}{\lambda_e^2} \tag{4.3}$$

Prestretch

Tissue prestretch was measured by calculating the change in surface area upon releasing the tissue constraints. Nine circular markers were placed in a 3x3 rectangular grid on each construct and positions were tracked using a high-resolution digital microscope (VHX-500, Keyence, Itasca, IL, USA) at a resolution of 100 px/mm and 20x magnification. Subsequently, tissues were released from their constraints by dissecting them from the sample holder using a cork borer with a diameter of 13.0

mm and a second image was recorded immediately. The surface area spanned by the markers was calculated for both images using a semi-automatic custom MATLAB script. The amount of tissue prestretch was then calculated in terms of surface area change, defined as the unconstrained surface area divided by the constrained surface area. The surface area change equals the squared length change λ_p, used in the previous section.

Thickness

After the prestretch measurements, all constructs were cut in half. Three high-magnification (100x) images using the VHX-500 digital microscope were taken perpendicular to the cutting edge of one of the two halves, with the three positions coinciding with the three markers that were placed at the sample cutting edge for the prestretch measurements. Using the microscope's complimentary software, the thickness t_0 was manually determined at 5 positions in each image.

Collagen Orientation

The tissues were stained with CNA35[22] to enable collagen visualization. After a 1-hour incubation period, constructs were visualized using a confocal laser scanning microscope (TCS SP5X, Leica Microsystems, Wetzlar, Germany) with complimentary software (Leica Application Suite Advanced Fluorescence). A tile scan (magnification 10x, excitation 488 nm, emission 520 nm) was made to capture the gross collagen architecture of the entire tissue. Collagen fiber orientation was quantified by analyzing the individual images of each tile scan, using a custom MATLAB script, based on the work of Frangi et al.,[70] (Section 2.2.2). For each tile scan, a histogram containing the fiber fraction per angle was obtained.

Histology

Constructs were fixed in 3.7% formaldehyde overnight, and subsequently embedded in paraffin and sectioned into slices of 7 µm. The slices were stained for Glycosaminoglycans (GAGs) and collagen using Alcian blue (AB) and Picosirius red (PR), respectively. The stained sections were imaged using a brightfield microscope (Axio Observer Z1, Zeiss, Oberkoch, Germany) equipped with filters to provide polarized light illumination. Additionally, a fluorescent co-staining for collagen type 1, αSMA and cell nuclei was performed and visualized using an Axiovert 200M microscope (Zeiss).

Biochemical assays

Half of each construct was lyophilized overnight and subsequently digested using a papain digestion buffer at 60 C° for 16 hours. The total tissue dry weight was determined before and after digestion. Tissue GAGs were quantified using an adapted version of the protocol by Farndale et al.[63], together with a standard curve derived from chondroitin sulfate from shark cartilage (Sigma-Aldrich). Using the Hoechst dye method[29] and a standard curve of calf thymus DNA (Sigma-Aldrich), the total

DNA content was quantified. Finally, the total hydroxyproline content, a measure for the amount of collagen, was determined with a modification of the assay by Huszar et al.[109] and a standard curve derived from trans-4-hydroxyproline (Sigma-Aldrich). Protein amounts were normalized with respect to the total tissue dry weight before digestion.

4.3 Results

4.3.1 Tissue culture in the Vertigro bioreactor

All statically cultured tissues endured the entire culture period up to 4 weeks (Fig. 4.3). Throughout dynamic culture, the feedback system successfully applied and maintained the preset maximal and minimal pressures to the TE constructs (Fig. 4.4). However, 2 out of 4 constructs that were cultured under dynamic loading conditions ruptured.

4.3.2 Mechanical Testing

The tissue profile was successfully tracked via US imaging (Fig. 4.5). Also, the mechanical tests were performed for all four samples in week 3, showing similar tension-pressure relationships (Fig. 4.6A) and nonlinear stress-stretch behavior in all samples (Fig. 4.6C). During week 4, testing of two statically cultured constructs failed due to sample leakage and the presence of a fold in the tissue construct, respectively. The two successfully measured samples showed similar tension-pressure and stress-stretch behavior, featuring a higher extensibility and lower stiffness compared to week 3 (Fig. 4.6B,D). For 1 of the 2 dynamically cultured samples, the ultrasound signal was too weak to be processed, potentially due to the low thickness of this sample. A nonlinear stress-stretch curve was observed for the successfully measured sample (Fig. 4.6D).

4.3.3 Elongation

Comparing tissue elongation (constrained tissue length at 0 pressure divided by initial construct diameter), there was a clear difference between the statically and dynamically cultured samples. Where the static sample tissue length was similar to the initial construct diameter (1.01±0.01), the dynamic samples did show elongation (1.07±0.00) (Fig. 4.7A).

4.3.4 Prestretch

Tissue prestretch was hardly observed after one week of static culture (1.01±0.01) but increased with static culture time. At week 4, the area prestretch was slightly higher for the dynamically cultured samples (1.09±0.01), compared to the static samples (1.07±0.01) (Fig. 4.7B).

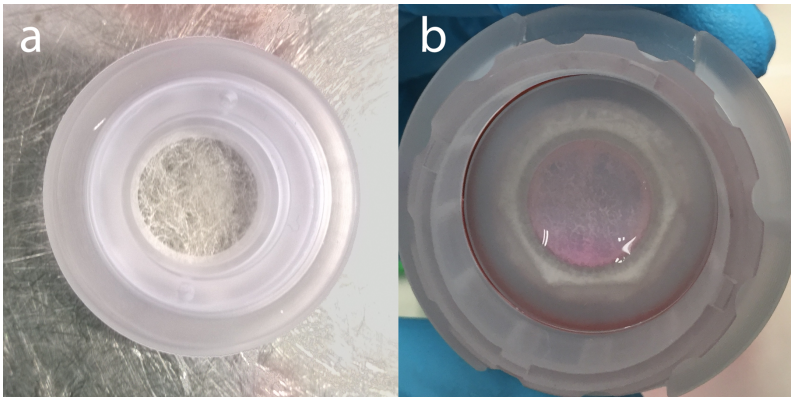

Figure 4.3: (a) Bioreactor insert with clamped scaffolds prior to seeding. (b) TE construct after 4 weeks of culture.

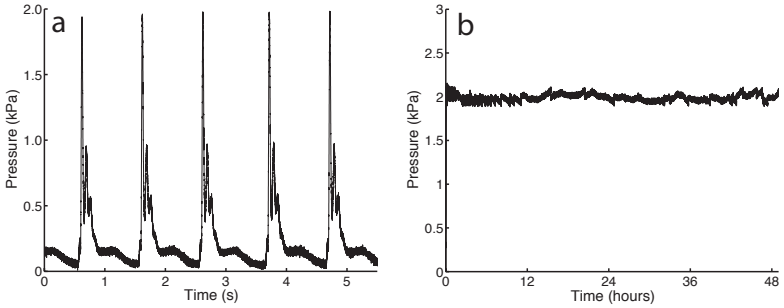

Figure 4.4: (a) 5 Loading cycles of the TE constructs for a preset pressure of 2 kPa and a frequency of 1Hz. **(b)** Peak pressures in between medium changes.

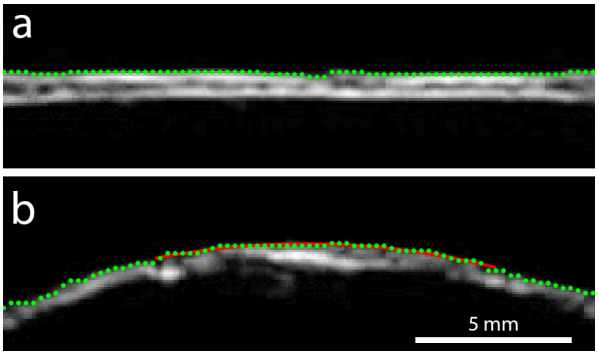

Figure 4.5: Ultrasound B-modes images of a 3-week-old sample in the **(a)** initial and **(b)** deformed configuration. The sample profile was tracked (green dots) and a circle was fitted to the center region (red) to estimate the curvature.

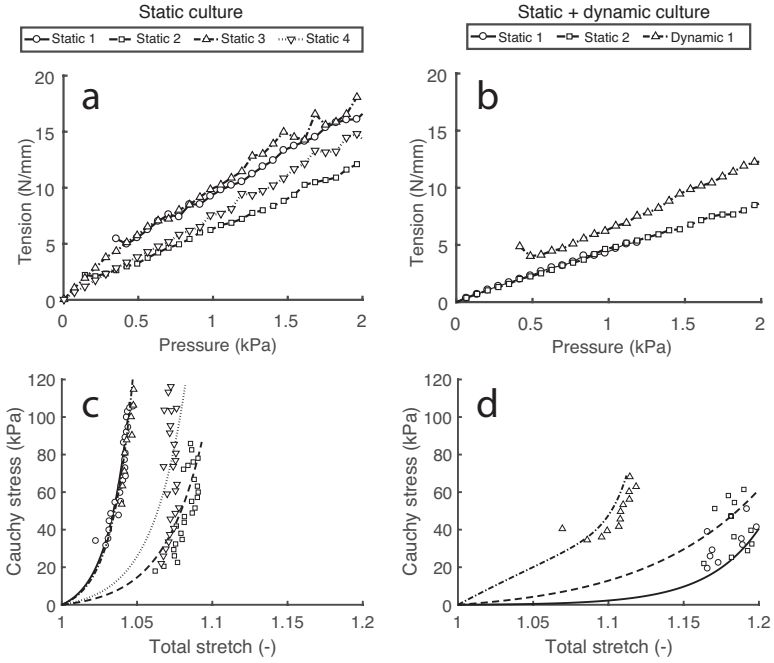

Figure 4.6: Tension-pressure relations at **(a)** the end of 3 weeks of static culture in four samples and **(b)** after 4 weeks static culture and after 3 weeks static + 1 week dynamic culture. Non-linear stress-stretch curves of 3-weeks statically cultured tissue samples **(c)** after 4 weeks of static culture and **(d)** after 3 weeks static + 1 week dynamic culture.

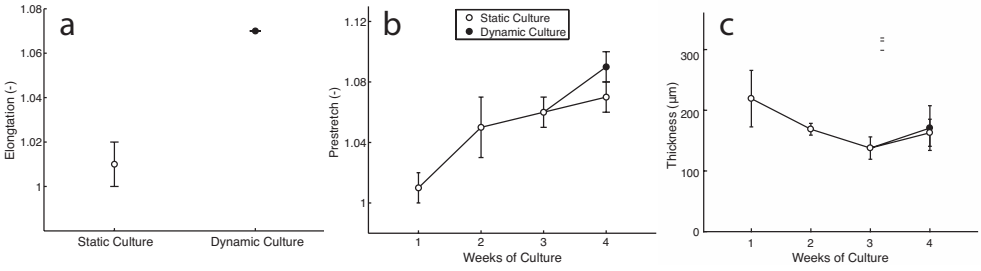

Figure 4.7: (a) Tissue elongation at 0 pressure at 4 week for statically and dynamically cultured samples; **(b)** prestretch development in the TE construct; and **(c)** Thickness (µm) development of the TE constructs during culture. All data is represented as mean value of all samples on the specific timepoint ± SEM.

4.3.5 Thickness

From the original scaffold thickness of 500 μm, tissue thickness decreased more than 50% within the first week of culture to 226±48 μm (Fig. 4.7C). Subsequently, tissue thickness further decreased to a value of ∼150 μm after which only minor changes occurred.

4.3.6 Collagen Orientation

After staining with CNA, collagen fibers could be clearly observed in the tissue samples (Fig. 4.8A). Analysis of the fiber architecture showed an in-plane fiber distribution with no clear preferred directionality, for all tissue samples, for the entire culture period (Fig. 4.8B-F).

4.3.7 Histology

The AB and hematoxylin (Fig. 4.9A-E) and PR red (Fig. 4.9F-J) staining show homogeneously distributed cells, GAGs and collagen fibers in all tissues. The collagen fibers were mainly aligned in the tissue plane and, with time, collagen fibers were observed to become thicker (Fig. 4.9K-O). Finally, the fluorescence images (Fig. 4.9P-T) show vast amounts of αSMA-positive cells (green), indicating the presence of contractile cells.

4.3.8 Biochemical Assays

The total tissue dry weight of the statically cultured samples appeared relatively constant with culture time (Fig. 4.10A). However, since the amount of PGA scaffold decreases with time, these results indicate an increase in tissue mass with time. At week 4, the dynamically cultured samples appeared to have a lower dry weight compared to the statically cultured samples.

Both the dry weight content of GAGs and hydroxyproline increased with time (Fig. 4.10B and C). The dynamically cultured samples contained a higher fraction of GAGs, and a slightly lower fraction of hydroxyproline compared to the static samples at week 4. The concentration of DNA increased up to week 3, and marginally dropped in week 4 for the static samples and more considerably for the dynamic samples (Fig. 4.10D).

4.4 Discussion

In the present study, a novel bioreactor and associated analysis techniques were developed to systematically investigate the synergy between mechanics and tissue growth and remodeling. A proof-of-principle experiment was conducted to demonstrate the proposed framework's potential.

4.4.1 Vertigro functionality

The Vertigro is a versatile bioreactor capable of dynamically culturing planar TE constructs, and simultaneously performing mechanical testing. Its unique two-chamber design allows easy and sterile

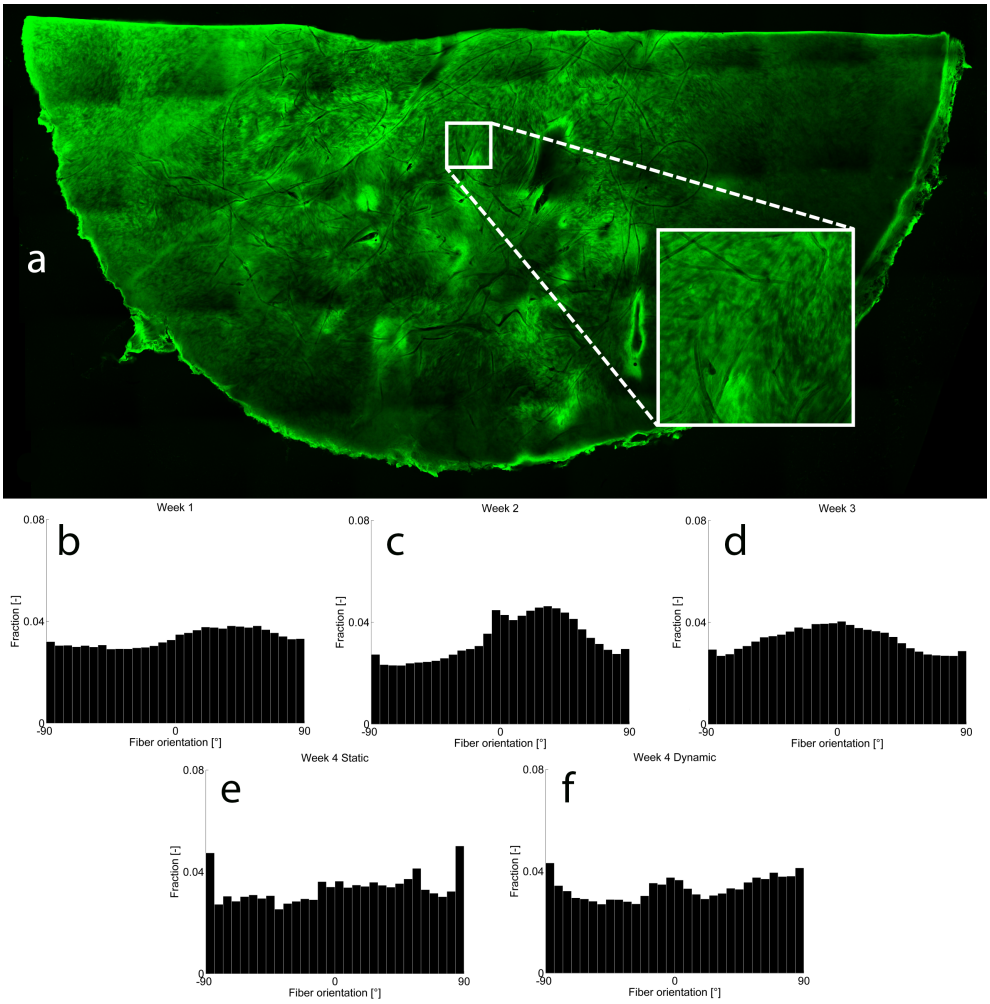

Figure 4.8: (a) Representative CNA stained sample showing the directionality of the collagen fibers. This particular sample was culture statically for 2 weeks, where the collagen was stained in green. **(b–f)** Histograms showing collagen fiber fractions for each orientation for the entire sample.

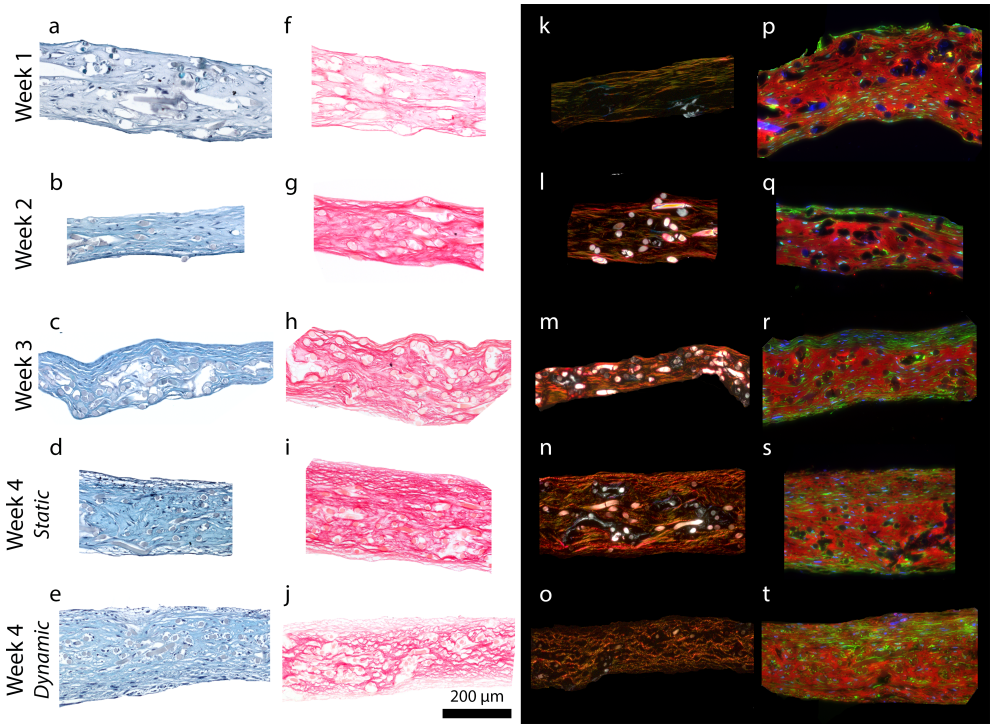

Figure 4.9: Representative histology images from all weeks (week 1-4 on the first 4 rows, the final row represents the dynamically cultured samples at week 4). **(a–e)** AB, **(f–j)** brightfield PR, **(k–j)** polarized light PR, and **(p–t)** fluorescence immuno-staining for collagen (red), cell nuclei (blue) and SMA (green). Scaffold remnants appear in bright white due to white light reflections (k–o).

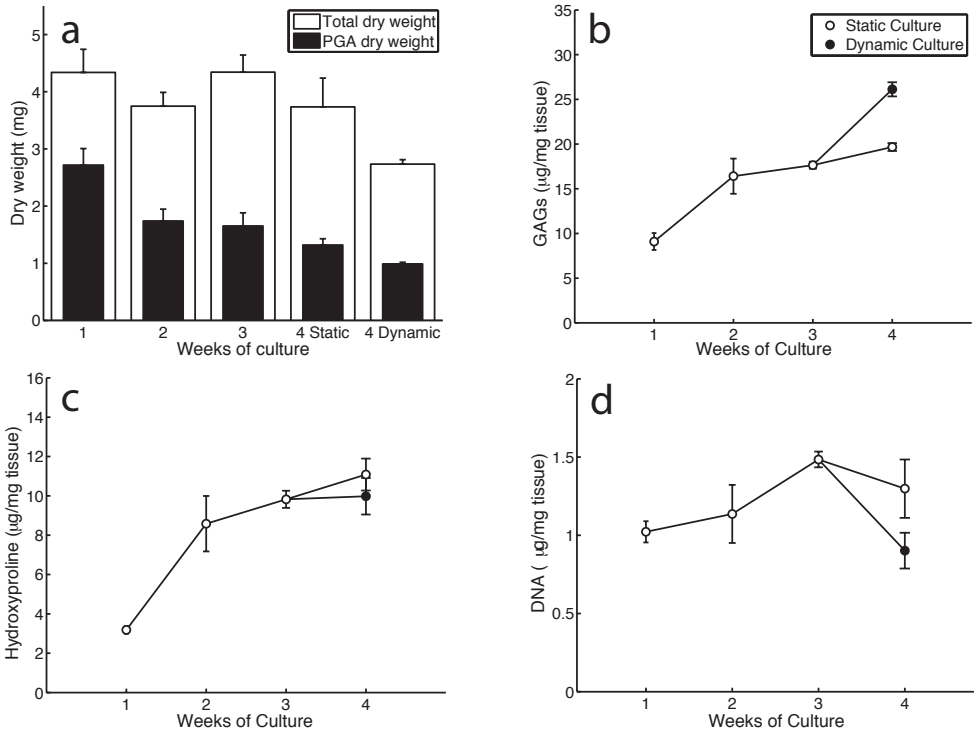

Figure 4.10: Biochemical assays. **(a)** Mean total tissue dry weight (white bars), where the black bars indicate the remaining part of the total weight composed of PGA scaffold. Dry weight concentration of GAGs **(b)**, Hydroxyproline **(c)** and DNA **(d)** for the statically and dynamically cultured samples.

handling of the tissue construct, while the dedicated bottom pressure chamber attains the pressure application. In addition, although not treated in the present study, the construct geometry can be easily changed by using removable inserts with different designs to mount tissue constructs with different geometries inside the bioreactor. The design in which currently rapidly degrading circular PGA scaffold was combined with slow degrading PCL scaffold, proved to be successful for culturing TE constructs that did not detach due to developing cell tension during static culture. Finally, the custom-made feedback system maintained the preset pressures during dynamic culturing, demonstrated here for a one-week period.

4.4.2 Tissue composition and architecture

Histological analysis (Fig. 4.9) showed the presence of GAGs, collagen fibers and αSMA positive cells in the tissue constructs. These findings were quantitatively confirmed by biochemical assays (Fig. 4.10), demonstrating that tissue dry weight remained fairly constant, where the fraction PGA scaffold was gradually substituted by cell-produced matrix components such as collagen and GAGs. Finally, CNA-stained samples confirmed the presence of vast amounts of isotropically oriented collagen fibers (Fig. 4.8), in line with the homogeneous pressure application and isotropic boundary conditions and scaffold properties.

4.4.3 Tissue geometry

Besides changes in tissue composition, the geometry of the constructs underwent notable changes (Fig. 4.3). First, tissue thickness in week 1 was halved compared to the original scaffold thickness, gradually decreasing to a constant thickness of ∼150μm. The large initial decrease in thickness is probably due to the high PGA porosity, which decreases immediately upon seeding. The consecutive decrease in thickness can be attributed to developing cell contractility that leads to tissue compaction in the unconstrained directions. These results are in line with the prestretch measurements that show an increase in prestretch with culture time, corresponding with previous observations [229] and the αSMA-positive cells observed via histology. Besides changes in thickness, the dynamically cultured samples were longer when constrained compared to their statically cultured counterparts. However, in contrast to the observed increase in unloaded length, the biochemical assays showed that the weight of the dynamic samples was lower compared to the static samples. This phenomenon may be explained by the fact that the amount of GAGs in the dynamic samples was higher compared to the static samples. The highly polar GAGs retain vast amounts of water and therefore increase tissue volume, which is not taken into account in the dry weight measurements.

4.4.4 Tissue mechanics

The bioreactor was designed to not only culture tissue samples for a prolonged time period, but also to simultaneously perform mechanical testing, by means of a classical mechanical bulge test [91,9].

This test can be performed non-destructively as the mechanical test is performed inside the bioreactor itself, while measuring the tissue deformation non-destructively using ultrasound. The stress-stretch relationships of all samples (Fig. 4.6C,D) showed the typical exponential nonlinear behavior featured in collagenous soft tissues. Furthermore, the prestretch measurements are essential when analyzing the tissue mechanics: not taking the tissue prestretch into account can lead to a significant overestimation of the tissue stiffness, dependent on the degree of prestretch[180].

4.4.5 Limitations

The use of ultrasound to measure tissue deformation during mechanical testing provides a great advantage of nondestructive testing. In fact, the suitability of ultrasound imaging to measure in vitro material functionality was recently demonstrated[108]. Nevertheless, the limited spatial resolution of the current US system and method used resulted in inaccuracies in estimating tissue thickness, which was therefore measured using microscopy in the present study. The spatial resolution can be improved by using a higher frequency ultrasound transducer and utilize the tracking of raw radio-frequency signals, allowing for non-destructive determination of tissue thickness, and high-precision tracking of the tissue[138]. Moreover, in the present study the stresses were estimated using Laplace's law, which is only valid for true membranes. In order to accurately estimate the mechanical properties in case of thick tissues, the use of an inverse finite element analysis method is recommended.

All of the 16 statically cultures samples were successfully cultured and analyzed. However, 2 of the 4 dynamically cultured samples failed in week 4. To prevent future loss of samples during dynamic culture, a smoother pressure gradient could be implemented. Currently, a square waveform function was used, but a sinoid function would lead to a smoother pressure transition. Additionally, a slow-degrading scaffold, rather than the rapidly-degrading PGA, can be used to support the tissue, which could shorten the current static culture time of three weeks that is required before the tissue construct is strong enough to withstand dynamic pressure.

4.4.6 Conclusions and outlook

In conclusion, a novel versatile bioreactor was developed that offers a potent platform to unravel underlying mechanisms of tissue growth and remodeling through a systematic analysis of the influence of, amongst others, scaffold material, cell type and pressure regimens, on tissue (mechanical) adaptation. An improved knowledge of this process is key to deliver insights in pathologies where adverse growth and remodeling occur, and essential in the fields of regenerative medicine and tissue engineering.

This versatile framework allows for tissue culture and pressure-driven mechanical stimulation under hemodynamic loading while simultaneously performing mechanical testing without sacrificing samples. This allows for the monitoring of tissue samples with time and as such has great potential for investigating mechanically-induced growth and remodeling. Due to the versatile setup

of the two-chamber bioreactor, - permissive of sterile handling while maintaining dynamic pressure profiles - many different physiological situations can be studied in a well-controlled in vitro environment. This allows for a systematic investigation of how mechanical stimuli affect tissue adaptation, for example by changing the pressure regime, degree of tissue anisotropy, scaffold material, and construct geometry. To demonstrate the successful development of the bioreactor system, a wide range of standard analysis techniques was employed to analyze the developing tissue constructs. In future studies, the current set of techniques can be extended with e.g. an inverse finite element method to accurately estimate the evolution of the mechanical properties.

CHAPTER 5

Actually, everything that can be known has a Number; for it is impossible to grasp anything with the mind or to recognize it without this.

Philolaus, ca. 470 – 385 BC

Nondestructive mechanical characterization of developing biological tissues using inflation testing

The contents of this chapter are based on:

Oomen, P. J. A., van Kelle, M. A. J., Oomens, C. W. J., Bouten, C. V. C. & Loerakker, S. (2017) Nondestructive mechanical characterization of developing biological tissues using inflation testing. *Journal of the Mechanical Behavior of Biomedical Materials* 74, 438–447.

5.1 Introduction

Biological tissues have an intriguing capacity to adapt in response to changes in their mechanical environment through growth and remodeling. While the underlying mechanisms that govern tissue growth and remodeling are not fully understood, it is well accepted that they occur at least partly to maintain a certain mechanical homeostasis[94,102,103]. An improved knowledge of this process is of key importance to understanding human tissue function during both health and disease. To date, it remains unknown what mechanical quantity determines tissue homeostasis; in fact, different measures have been associated to play important roles in this process, such as stress[104,214], strain[32,167,182] (Chapter 2), strain rate[167,232] and strain energy[232]. Moreover, mechanical homeostasis is not necessarily determined by the same mechanical parameters across different tissue types.

Identification of the main determinant(s) of mechanical homeostasis is far from straight-forward, as the mechanical constituents relate through constitutive behavior, making it challenging to study their independent effects. To this end, the mechanical properties of a tissue need to be followed during its development, which requires a nondestructive mechanical test. As the commonly used mechanical testing methods, such as tensile and indentation tests, typically require sacrificing the test specimen, we developed a bioreactor that allows for culturing planar soft tissues for a prolonged time, while being subject to dynamical loading to induce growth and remodeling (Chapter 4). This bioreactor is designed to perform mechanical testing during culture by means of a classical inflation test. Ultrasound (US) imaging to track the tissue displacement allowed for nondestructive mechanical testing, and therefore assessment of the temporal changes in the tissues's mechanical state and mechanical properties due to growth and remodeling.

Previously, inflation, or bulge, tests have been developed to measure the properties of isotropic thin films that undergo small deformations. Due to these conditions, bending effects can be neglected and an in-plane stress situation can be assumed. The stresses and strains in these tests can be calculated from a set of well-prescribed equations, using the pressure and out-of-plane sample deflection[125,101]. Furthermore, analytical solutions have been developed that relate the pressure to the apex displacement by assuming small displacements, in order to estimate linear mechanical properties in terms of the Young's modulus and Poisson's ratio[233].

However, when characterizing biological soft materials using bulge testing, these analytical solutions no longer yield an accurate representation of the mechanical state, because of the intrinsic properties and loading conditions of these tissues. First, they undergo large displacements and typically feature nonlinear material behavior, causing the analytical solution using linear material theory to no longer apply. Second, many planar biological tissues, such as skin and arteries, feature an anisotropic fiber structure, resulting in an anisotropic displacement field. Third, passive residual stretches and active cell tractions are typically present in soft tissues[35,73,105,230]. For this reason, the unloaded, pressure-free state cannot be assumed to be stress-free. Neglecting these residual stresses can lead to an underestimation of material strains and consequently to an overestimation of the

tissue stiffness[180]. Finally, biological planar tissues are not always thin enough to be considered as membranes, leading to bending moments and out-of-plane stresses. Several studies have successfully incorporated tissue nonlinearity and anisotropy in parameter estimation schemes of bulge tests[9,47,48,218,219,188]. Yet, to the best of the authors' knowledge, no study has addressed the effects of tissue thickness nor has accounted for tissue prestretch. Moreover, the properties of biological tissues have never been estimated during growth and remodeling.

The goal of the current study was to develop and validate a nondestructive mechanical test and a two-step inverse analysis method to estimate the mechanical properties of biological tissue during in vitro tissue culture. Nondestructive mechanical testing of developing tissues was realized by performing bulge tests inside a novel bioreactor (Chapter 4) while tracking tissue displacement with US imaging. The mechanical properties were estimated using a full inverse finite element (FE) method, which accounts for tissue geometry and architecture, and implementation of prestretch. To increase robustness and minimize the high computational costs that this method entails, its initial estimate was provided by an analytical estimate. The inverse method was verified by performing virtual experiments using different material models, tissue thicknesses, and prestretch magnitudes. Next, the proposed experimental and numerical methods were validated by performing both bulge and tensile tests on polymer samples and comparing their results. Finally, the method was applied to nondestructively estimate the mechanical properties of living, tissue-engineered constructs.

5.2 Methods

5.2.1 Sample preperation

To validate the proposed nondestructive mechanical characterization method, both bulge and tensile tests were performed on polydimethylsiloxane (PDMS; Sylgard 184, Dow-Corning, Midland, MI, USA, using a weight ratio of 10:1 prepolymer to curing agent) samples (n=10) with a thickness of 0.38 ± 0.03 mm. The samples for bulge tests (n=5) were cut in a circular shape with a diameter of 18 mm to fit inside the bioreactor. Tensile test samples (n=5) were cut in rectangles (15.0×8.0 mm) and sprayed with graphite to enhance image contrast for digital image correlation.

To demonstrate the method's feasibility to nondestructively characterize developing tissues, bulge tests were performed on tissue-engineered constructs, previously used in a different study. In brief, human vascular derived cells from the vena saphena magna, previously characterized as contractile, matrix-producing myofibroblasts, were seeded on rapidly degrading nonwoven polyglycolic acid (PGA) scaffolds (Biomedical Structures, Warwick, USA, 0.5 mm thickness)[158,156]. The outer edge was reinforced with a ring of polycaprolactone scaffold (PCL, thickness 0.25 mm, inner diameter 13 mm) to prevent sample rupture at the clamped edge. These constructs were cultured inside the bioreactor system in supplemented standard culture medium at 37° and 5% CO_2 for a duration of either 3 (n=4) or 4 (n=3) weeks. Additionally, samples (n=6) were statically cultured for three weeks to validate the thickness measurements.

5.2.2 Mechanical testing

Bulge tests

Mechanical bulge tests were performed inside the novel bioreactor system that allows tissue culture during growth and remodeling (Chapter 4). The bioreactor was made of polysulphone and consists of two chambers for the sake of sterility during culturing (Fig. 4.1): a tissue chamber and a pressure chamber. In the former, samples can be clamped and cultured, surrounded by culture medium, while the latter was connected to a previously developed dynamic pumping system[124]. During the bulge tests, this pump was replaced by a Harvard pump (PHD2000, Harvard Apparatus, Holliston, MA, USA) to gradually apply a pressure by increasing the fluid volume in the pressure chamber. The two chambers were connected by two silicone membranes to ensure pressure transmission between the pressure and the culture chamber, where the pressure in the culture chamber was measured by a pressure sensor (P10EZ-1, BD|SENSORS, Thierstein, Germany). To mechanically test the samples, the volume in the pressure chamber was increased until a pressure of approximately 2 kPa was applied for five cycles, of which the first four were used for pre-conditioning.

To nondestructively measure tissue displacement as a function of pressure, the sample was imaged using a MyLab 70 US system (Esaote, Maastricht, Netherlands), equipped with a 8 or 12 MHz linear transducer. The US transducer was mounted on top of the bioreactor, perpendicular to the sample surface and aligned to coincide with the sample center (Fig. 4.1). In the current study only isotropic samples were tested, although for anisotropic samples two measurements would be required: one with the US transducer aligned along the main fiber direction $\mathbf{v}_1$, and a second with the US transducer aligned perpendicularly to the main fiber direction, defined as $\mathbf{v}_2$ (Fig. 5.1c).

From the B-mode frames of the US video (frame rate 20 Hz, resolution 21.5 px/mm), the sample profile was tracked using a custom MATLAB (Mathworks, Natick, MA, USA) script (Fig. 5.1a,b). For each frame, the tissue edges were detected using Matlab's built-in edge detection function, followed by a morphological closing operation. To obtain an analytical representation of the central area of the tissue profile, a circle with radius R was fitted through the central 50% of this edge region (Fig. 5.1b). From this circle, the radius of curvature κ ($= 1/R$) and current sample length L were calculated, followed by the in-plane sample stretch due to bulging $\lambda = L/L_0$, where L_0 is the initial tissue length at the pressure-free state. The initial constrained thickness t_0 of six additional samples was measured from the raw radio-frequent signals of an ultrasound measurement, as described previously[138], and compared to microscopy measurements of the sample cross-section. The thickness was measured at approximately 15 locations along the tissue cross-section using both measurement techniques.

Tensile tests

To validate the bulge test methodology and analysis, uniaxial tensile tests were performed on a BioTester (CellScale, Waterloo, Canada). The isotropic PDMS samples were stretched to 120% of

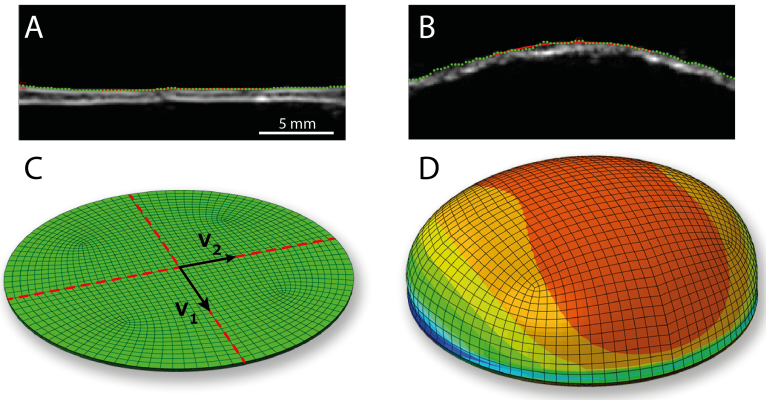

Figure 5.1: US images of a tissue-engineered construct before **(a)** after applying pressure **(b)**. The green dots indicate the top tissue profile, while the continuous red lines show the circle that was fitted to the central 50% of the sample profile. The bulge tests were simulated by a FE model, before **(c)** and after **(d)** applying pressure, where the red dashed lines in **(a)** indicate the position of the ultrasound transducer to measure the tissue deformation in the main ($\mathbf{v}_1$) and cross-fiber ($\mathbf{v}_2$) directions.

their original length with a strain rate of 100%/min for five cycles, of which the first four were used for pre-conditioning. Force data were collected with a sampling frequency of 5 Hz and images were taken with the same frequency by a CDD camera mounted perpendicular to the sample surface. From these images, sample displacements were tracked using a global digital image correlation (GDIC) algorithm, as described previously[17,162]. From these displacements, the deformation gradient tensor $\mathbf{F}$ was computed, from which the right Cauchy-Green deformation tensor $\mathbf{C} = \mathbf{F}^{\mathrm{T}}\mathbf{F}$ was obtained. From this tensor, the two in-plane principal stretches $\lambda_i = \sqrt{\mathbf{C} : (\mathbf{e}_i \otimes \mathbf{e}_i)}$ $(i = 1, 2)$ were obtained with the unit direction vector $\mathbf{e}_1$ coinciding with the tensile direction, and $\mathbf{e}_2$ with the perpendicular in-plane direction. Assuming incompressibility, the thickness t and width w of the sample during stretching could be estimated as a function of the initial thickness t_0 and width w_0 and the in-plane stretches:

$$t = \frac{t_0}{\lambda_1 \lambda_2} \tag{5.1}$$

$$w = w_0 \lambda_2 \tag{5.2}$$

Finally, the current thickness and width were used to compute the Cauchy stress σ from the measured force F:

$$\sigma = \frac{F}{tw} \tag{5.3}$$

5.2.3 Tissue prestretch

When performing a bulge test on living soft tissues, the total elastic stretch of the tissue generally does not equal the stretch from the deformation due to mechanical loading. Instead, it is the product of this stretch and both passive residual stretches and active cell tractions that were already present in the unloaded configuration, causing tissue prestretch[35,73,105,230]. Therefore, a multiplicative decomposition was employed, splitting the total elastic deformation $\mathbf{F}_e$ into a deformation part due to loading $\mathbf{F}$ and a deformation induced by tissue prestretch $\mathbf{F}_p$[180]:

$$\mathbf{F}_e = \mathbf{F}\mathbf{F}_p \tag{5.4}$$

In the tensile tests, no prestretch was measured ($\mathbf{F}_p = \mathbf{I}$) since the samples were released before mounted in the tester. However, the samples in the bioreactor used for bulge testing could have prestretch. This was measured after the bulge test: a 3x3 rectangular grid of ink markers were placed on the tissue while constrained and imaged using a high-resolution digital microscope (VHX-500, Keyence, Itasca, IL, USA, resolution 100px/mm, magnification 20x). After imaging, the tissues were dissected from the sample holder using a cork borer and immediately imaged again to quantify tissue compaction. The markers were considered as nodes spanning a quadratic quadrilateral element. Using the 'nodal' displacements, the deformation gradient tensor $\mathbf{F}_p$ accounting for prestretch was obtained, describing the deformation from the unconstrained to the constrained state.

5.2.4 Constitutive models

Two constitutive models were used to estimate material behavior. For the PDMS samples, a Neo-Hookean model was used, which has been shown to be well capable of describing the mechanical behavior of PDMS materials for stretches up to at least 1.5[120]. For the biological materials, an exponential fiber-reinforced model was used. The constitutive behavior was modeled as a function of the total elastic deformation $\mathbf{F}_e$.

Neo-Hookean model

The Cauchy stress for the Neo-Hookean model was defined as:

$$\boldsymbol{\sigma} = \frac{\mu}{J_e}\left(\mathbf{B}_e - J_e^{2/3}\mathbf{I}\right) + \kappa\frac{\ln(J_e)}{J_e}\mathbf{I} \tag{5.5}$$

where μ is the shear modulus, $\kappa = \frac{2\mu(1+\nu)}{3(1-2\nu)}$ the bulk modulus, $J_e = \det(\mathbf{F}_e)$ the total elastic Jacobian, $\mathbf{B}_e = \mathbf{F}_e\mathbf{F}_e^T$ the left Cauchy-Green deformation tensor, and $\mathbf{I}$ the second order identity tensor.

Fiber-reinforced model

The fiber-reinforced material was assumed to consist of an isotropic matrix (m) and a (potentially anisotropic) collagen fiber network (f). Both material components additively contribute to the total Cauchy stress:

$$\boldsymbol{\sigma} = (1 - \Phi_f)\boldsymbol{\sigma}_m + \Phi_f \boldsymbol{\sigma}_f \tag{5.6}$$

where Φ_f is the total fiber volume fraction, set at 0.5[56] and $\boldsymbol{\sigma}_m$ and $\boldsymbol{\sigma}_f$ are the Cauchy stress tensors of the matrix and fibrous parts, respectively. The matrix was modeled by the Neo-Hookean constitutive model (Equation 5.5), while the fiber part was modeled by an exponential Holzapfel-like model[56,97]. For the fibrous component, an equidistal angular fiber distribution was assumed of a discrete number of N fibers situated in the plane of the material. Each fiber i oriented in the direction $\mathbf{n}_0$ (in the reference configuration) contributes to the total fiber stress:

$$\boldsymbol{\sigma}_f = \sum_{i=1}^{N} \phi_f^i \boldsymbol{\sigma}_f^i \tag{5.7}$$

Each fiber has a certain volume fraction ϕ_f^i, described by a periodic version of the normal probability distribution function[56,76]:

$$\phi_f^i = A \exp\left(\frac{\cos(2(\gamma^i - \alpha)) + 1}{\beta}\right) \tag{5.8}$$

where γ^i is the fiber angle with respect to the main fiber direction $\mathbf{v}_1$, α the main orientation, β the dispersity and A a normalisation factor which is defined such that the sum of individual fiber fractions equals 1:

$$A = \left(\sum_{i=1}^{N} \exp\left(\frac{\cos(2(\gamma^i - \alpha)) + 1}{\beta}\right)\right)^{-1} \tag{5.9}$$

Due to symmetry, a semi-circular distribution was used with $N = 60$ fibers and hence an angular resolution of $\mathrm{d}\gamma = 3°$. Note that β determines the degree of anisotropy: if $\beta \to \infty$, the material is fully isotropic, whereas $\beta \to 0$ indicates a fully anisotropic architecture. The fibers were distributed equidistally in the plane spanned by the main fiber direction $\mathbf{v}_1$ and the cross-fiber direction $\mathbf{v}_2$, where the direction of each fiber in the reference configuration is given by a unit vector $\mathbf{n}_0^i$, defined with respect to $\mathbf{v}_1$ and $\mathbf{v}_2$:

$$\mathbf{n}_0^i = \cos(\gamma^i)\mathbf{v}_1 + \sin(\gamma^i)\mathbf{v}_2 \tag{5.10}$$

For each individual fiber i, its contribution to the total fiber stress (Equation 5.7) was defined by an adapted version of the Holzapfel-Gasser-Ogden model[97,54], where it was assumed that the fibers only resist tension:

$$\boldsymbol{\sigma}_f^i = k_1(\lambda_{\mathrm{e}}^i)^2 \left(\exp\left[k_2\langle(\lambda_{\mathrm{e}}^i)^2 - 1\rangle\right] - 1\right) \mathbf{n}^i \otimes \mathbf{n}^i \tag{5.11}$$

with $\langle\circ\rangle$ the Macaulay brackets, k_1 and k_2 material parameters, $\lambda_e^i = \sqrt{\mathbf{C}_e : (\mathbf{n}_0^i \otimes \mathbf{n}_0^i)}$ the total elastic stretch of fiber i, and $\mathbf{n}^i$ the unit fiber direction vector in the deformed configuration, related to the stress-free configuration by $\lambda_e^i \mathbf{n}^i = \mathbf{F}_e \mathbf{n}_0^i$.

5.2.5 Mechanical characterization

To estimate the material parameters, inverse methods are required for both bulge and tensile tests. For the bulge tests, a combination of analytical and FE methods was used to reduce computational costs and increase robustness and accuracy, whereas for the tensile tests already an analytical method sufficed. The set of material parameters to be estimated are indicated by ξ, which for the Neo-Hookean model only comprised one parameter ($\xi = \mu$), whereas the fiber-reinforced model required at least three parameters to be estimated ($\xi = [\mu, k_1, k_2]$); if the degree of anisotropy β is unknown a priori, it also needed to be estimated.

Bulge tests: initial estimate

The initial material parameter estimates were provided by the classical bulge equations. From the bulge tests (Section 5.2.2), the pressure p and the radii of curvature κ_i in the direction of $\mathbf{v}_i$ ($i = 1, 2$) were available. From these data, the stress resultants T_i were computed according to membrane theory[125,101]:

$$T_1 = \frac{p}{2\kappa_2} \tag{5.12a}$$

$$T_2 = \frac{p}{\kappa_2}\left(1 - \frac{\kappa_1}{2\kappa_2}\right) \tag{5.12b}$$

These equations were initially derived for thin axisymmetric geometries[125,101], however it has been demonstrated that they can closely approximate the stress resultants in geometries that do not necessarily deform axisymmetrically due to material anisotropy[141,140] including anisotropic tissues subjected to inflation testing[218,219,143].

To estimate the material properties, the in-plane orthogonal stress resultants were also expressed in terms of the in-plane Cauchy stresses (Equation 5.5 or 5.6) in the direction of $\mathbf{v}_i$ ($\sigma_i = \boldsymbol{\sigma} : (\mathbf{v}_i \otimes \mathbf{v}_i)$ with $i = 1, 2$)[125,101,219]:

$$T_1^{\text{est}} = \int_0^t \sigma_1\left(\lambda_e, \xi\right) \mathrm{d}z \tag{5.13a}$$

$$T_2^{\text{est}} = \int_0^t \sigma_2\left(\lambda_e, \xi\right) \mathrm{d}z \tag{5.13b}$$

with t the thickness of the deformed tissue (Eq. 5.1) and z in the direction normal to the tissue

surface, with $z = 0$ at the bottom and $z = t$ at the top of the tissue. The parameter set ξ was to be estimated, whereas the in-plane elastic stretches at the sample top surface ($\lambda^s_{e,1}$ and $\lambda^s_{e,2}$) were available from the post-processed US data (Fig. 5.1). Assuming that the curvature change through the thickness is negligible, a linear variation of the in-plane stretch through the tissue thickness was present, according to linear beam theory[219]:

$$\begin{aligned} \lambda_{e,1}(z) &= \lambda^s_{e,1} + \kappa_1 \left(z - t\right) \\ \lambda_{e,2}(z) &= \lambda^s_{e,2} + \kappa_2 \left(z - t\right) \end{aligned} \tag{5.14}$$

To estimate ξ, MATLAB's least-square optimization algorithm (*lsqnonlin*, trust-region algorithm) was employed, aiming to find the minimum difference between the analytical and estimated stress tensions (Equations 5.12 and 5.13, respectively) by varying the parameter set ξ. To this end, the following cost function was used:

$$E(\xi) = \frac{1}{N_p} \sum_{k=1}^{N_p} \sqrt{\left(T_1(p^k) - T_1^{\text{est}}(p^k, \xi)\right)^2 + \left(T_2(p^k) - T_2^{\text{est}}(p^k, \xi)\right)^2} \tag{5.15}$$

where N_p is the number of pressure steps.

Bulge tests: inverse finite element analysis

The second step in the inverse analysis employed an inverse FE analysis in order to obtain a more accurate estimate of the material parameter(s) ξ. The experiment was simulated by an FE model in Abaqus FEA (Dassault Systèmes Simulia, Providence, RI, USA). Due to symmetry, the circular sample was modeled as a quarter disk, using quadratic full integration brick elements (Fig. 5.1). Mesh convergence tests showed that at least 10 elements were required through the thickness and 20 along each radius, resulting in a total of 4800 elements. In line with the experiments, a uniform pressure was gradually applied at the bottom plane of the sample and near-incompressibility was implemented by setting the Poisson ratio to $\nu = 0.498$.

The bulge experiment provided the two principal surface profiles z_1 and z_2 (coinciding with $\mathbf{v}_1$ and $\mathbf{v}_2$, respectively) of the sample as a function of the pressure p. In this inverse method, the material parameter set ξ was adjusted until the difference between the profile displacements perpendicular to the tissue surface in the initial configuration of the experiment (Δz_1 and Δz_2) and simulation (Δz_1^{est} and Δz_2^{est}) was minimized using MATLAB's *lsqnonlin* function. This resulted in the following cost function:

$$E(\xi) = \frac{1}{N_p N_x} \sum_{k=1}^{N_p} \sum_{l=1}^{N_x} \sqrt{\left(\Delta z_1(p^k, x^l) - \Delta z_1^{\text{est}}(p^k, x^l, \xi)\right)^2 + \left(\Delta z_2(p^k, x^l) - \Delta z_2^{\text{est}}(p^k, x^l, \xi)\right)^2} \tag{5.16}$$

where N_p is the number of pressure steps and N_x the number of points along each principal surface profile with in-plane position x along $\mathbf{v}_1$ or $\mathbf{v}_2$. The initial estimate of ξ was provided by the membrane method of the first step of the inverse method (Section 5.2.5).

Tensile tests: inverse analysis

The in-plane principal stretches and Cauchy stresses were available from the tensile tests (Section 5.2.2). In order to estimate the material properties from these tests, an estimate for the Cauchy stress along the stretching direction (σ_1^{est}) was obtained by varying ξ, until the difference with the measured stress σ_1 was minimized. Once again, this was achieved through MATLAB's *lsqnonlin* function, using the following cost function:

$$E(\xi) = \frac{1}{N_s} \sum_{k=1}^{N_s} \sqrt{\left(\sigma_1(\lambda_e^k) - \sigma_1^{\text{est}}(\lambda_e^k, \xi)\right)^2} \tag{5.17}$$

where N_s is the number of stretch steps.

Inverse method validation

To verify the numerical framework, several virtual experiments were performed. FE models were generated as described in Section 5.2.5 with a diameter of 10 mm and different thicknesses (0.10–0.50 mm, no prestretch) and degrees of prestretch (1.0–1.3, thickness of 0.10 mm). Three different material types were tested: Neo-Hookean (NH), isotropic fiber-reinforced (IFR) and anisotropic fiber-reinforced (AFR).

The shear modulus for the Neo-Hookean material was (arbitrarily) chosen to be $\mu = 300$ kPa. The material parameters for the fiber-reinforced material were chosen to resemble native aortic heart valve leaflet tissue[54,19]: $\mu = 50$ kPa, $k_1 = 0.7$ kPa, $k_2 = 9.9$; with material isotropy and anisotropy enforced by setting the fiber dispersity to $\beta = 100$ and $\beta = 0.5$, respectively.

To assess the reduction of computational costs gained by the first estimation step, 5 inverse FE analyses with random initial parameter estimates were performed for each material type, for thin samples ($t_0 = 0.10$ mm) and no pre-stretch.

5.3 Results

5.3.1 Numerical verification: virtual experiments

To assess the accuracy and performance of the proposed numerical framework, several virtual experiments were performed, in which bulge tests were simulated for three different kinds of known material behavior at different sample thicknesses and prestretch magnitudes. The NH behavior was estimated closely by the initial estimate for all thicknesses and prestretch magnitudes (Fig. 5.2a,b). The stiffness of the IFR material was slightly overestimated, particularly in the lower stretch regions,

and became less accurate with increasing degrees of prestretch (Fig. 5.2c,d). Similarly, the stiffness of the AFR behavior was overestimated, particularly in the direction perpendicular to the main fiber direction, becoming more severe with higher degrees of prestretch (Fig. 5.2e,f). For both isotropic and anisotropic fiber-reinforced models, the nonlinearity was not captured for simulations with low diameter-thickness ratios and prestretches due to the low stretch intervals present in these cases.

The initial estimates were subsequently used for the inverse FE analyses. For all cases the final estimated material properties correctly described the preset material behavior of the virtual simulations. 5 Iterations were needed to estimate the shear modulus of the NH material, while as few as 2 iterations were enough to estimate the isotropic and anisotropic fiber-reinforced material parameters (Fig. 5.3). In contrast, when using random initial material parameters (n=5), 8.2 ± 3.0 iterations were required to successfully estimate the NH material's shear modulus, and 17.8 ± 13.1 and 10.6 ± 3.4 for the isotropic and anisotropic fiber-reinforced materials, respectively. Some of the estimations with random parameters needed to be restarted because of diverging parameter estimates, or failing FE simulations due to low stiffness estimates.

5.3.2 Experimental validation: comparison with biaxial tensile tests

The accuracy of the proposed methodology was assessed by performing both bulge and tensile tests on the same PDMS material (considered to behave as a Neo-Hookean material). After the bulge tests, the sample profile was successfully tracked as a function of pressure from the ultrasound images (Fig. 5.1), in order to estimate the tissue's in-plane tensions and profile displacement, which were respectively used in the initial and full FE parameter estimation steps. The shear modulus found in the initial estimate underestimated material stiffness (Fig. 5.4a,b); this estimate was improved in the inverse FE analysis (Fig. 5.4c,d), estimating a shear modulus of $\mu = 657.5 \pm 67.9$ kPa (Fig. 5.5). The tensile tests resulted in an estimated shear modulus of $\mu = 622.7 \pm 20.4$ kPa, which was similar to the one estimated from the bulge test but with a smaller standard deviation (Fig. 5.5).

5.3.3 Application to tissue-engineered constructs

Seven tissue-engineered constructs were mechanically characterized while being cultured inside the bioreactor system. The average initial thickness (and standard deviation) of the tissue-engineered constructs was determined using both nondestructive ultrasound measurements, and digital microscopy on cross-sections of dissected samples (Fig. 5.6). For each sample, the thickness was determined on approximately 15 locations throughout the tissue. Both methods showed comparable average thicknesses. The prestretch in the tissue-engineered constructs was found to be between 1.03 and 1.05.

Similarly to the PDMS samples, the initial estimate underestimated material stiffness (Fig. 5.7a,b), which was improved in the inverse FE analysis (Fig. 5.7c,d). All samples featured a nonlinear stress-stretch response, as typically seen in soft tissues (Fig. 5.8).

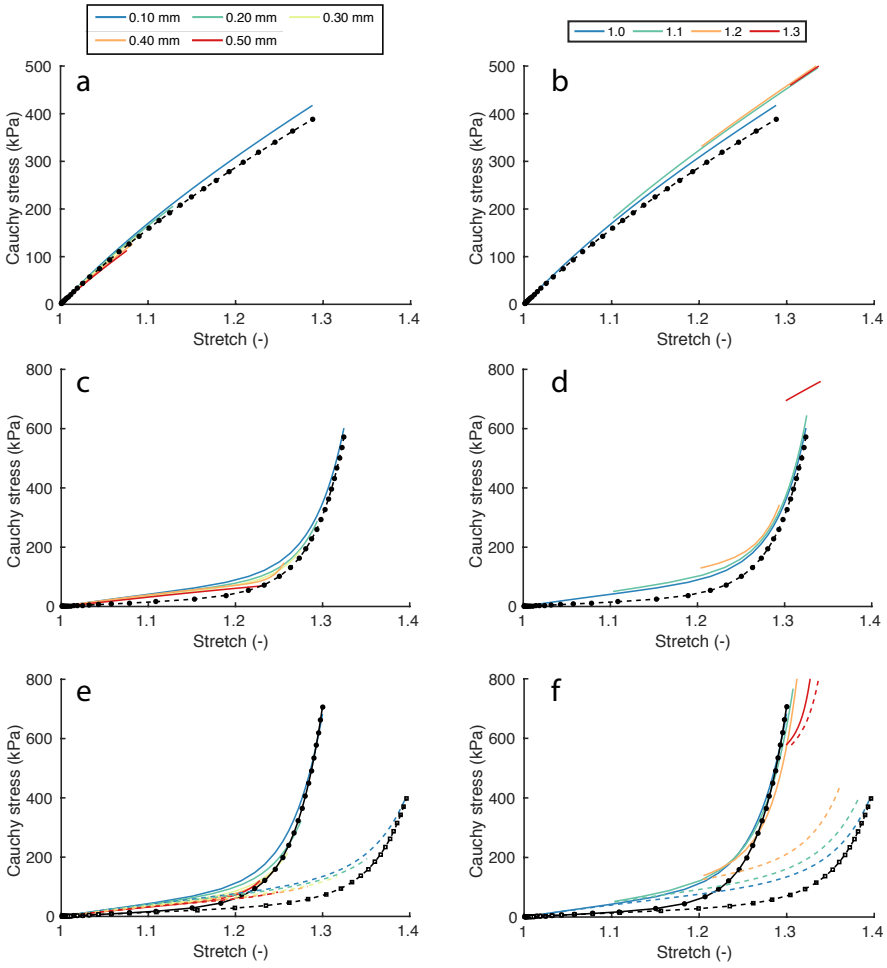

Figure 5.2: The influence of thickness and prestretch on the estimation of the stress-stretch behavior of the virtual experiments using NH **(a,b)**, IFR **(c,d)** and AFR **(e,f)** constitutive models. The black markers indicate the true stress-stretch behavior. The colored lines indicate the initial estimate of the stress-stress behavior for different tissue thicknesses **(a,c,e)** or prestretch magnitudes **(b,d,f)**. The black dashed lines indicate the material behavior estimated by the full inverse FE method, where the correct result was found for all choices of thickness and prestretch. In the AFR model, the black markers and continuous line indicate the stress in the fiber direction, while the stress in the cross-fiber direction is given by the white markers and dashed line.

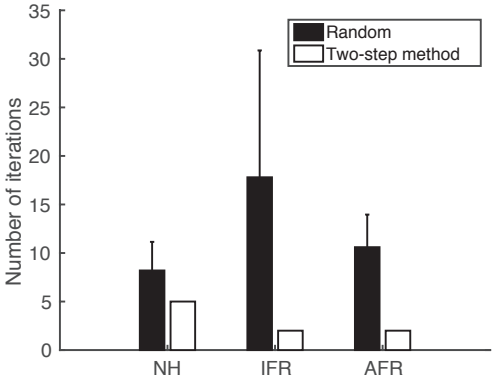

Figure 5.3: The number of iterations required to estimate the material parameters of all three materials was lower when using the two-step method, compared to starting the inverse FE with a random initial estimate (n=5 per material). The number of iterations until convergence varied per random initial estimate.

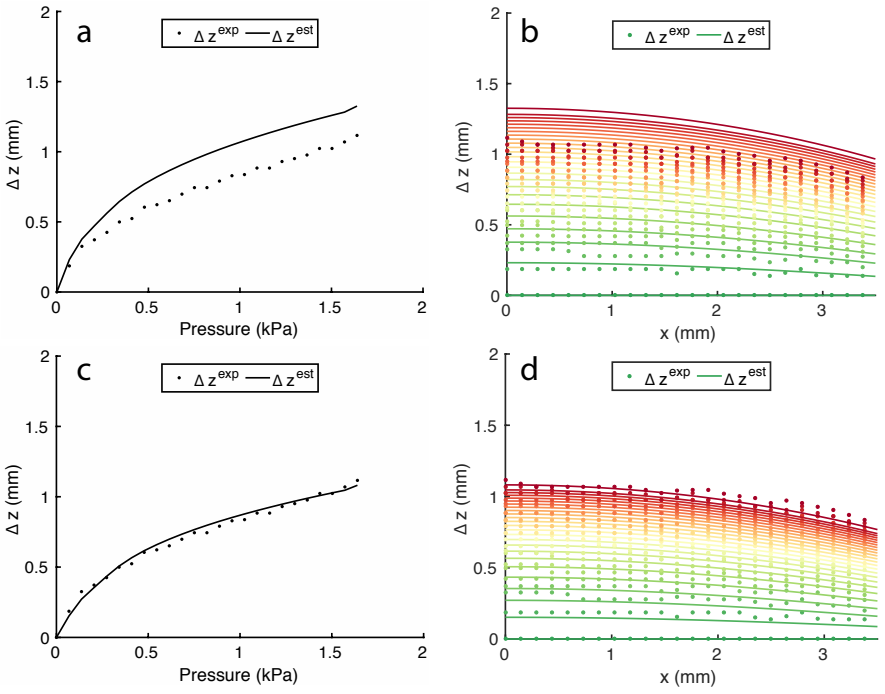

Figure 5.4: The material behavior of PDMS samples was estimated in the full inverse FE method by fitting the estimated profile displacement (continuous lines) as a function of pressure to the one measured by ultrasound (dotted markers). This figure shows the results from one representative sample, with the apex displacement as a function of pressure **(a,c)**, and the displacement of the central 50% of the sample as a function of pressure **(b,d)**, where the transition from pressure-free to maximum pressure state is indicated by the color transition from green to red. The initial material estimate **(a,b)** shows an underestimate of the material stiffness while the final estimate **(c,d)** closely describes the experimental displacement behavior.

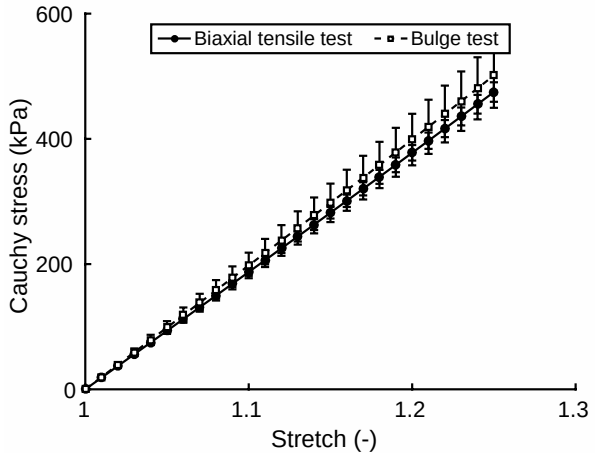

Figure 5.5: The material behavior of PDMS samples was estimated by biaxial tensile tests (continous line, circular markers) and bulge tests (dashed lines, square markers). Both methods estimated similar shear moduli, with $\mu = 622.7 \pm 20.4$ kPa for the biaxial tests and $\mu = 657.5 \pm 67.9$ kPa for the bulge tests.

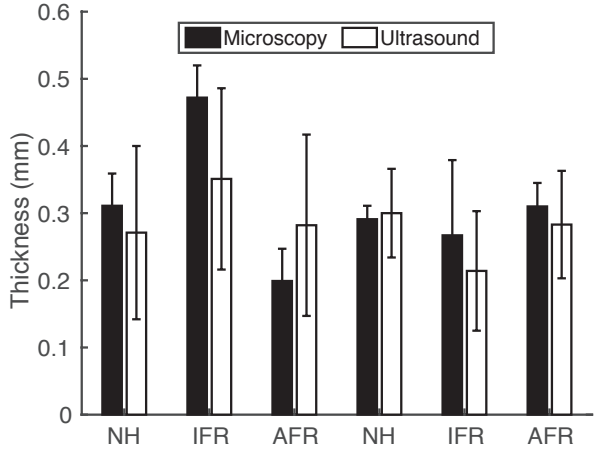

Figure 5.6: The thickness of 6 tissue-engineered samples was determined on approximately 15 locations using nondestructive ultrasound measurements, and microscopy measurements on dissected tissue cross-sections. The two methods yielded comparable results, yet the data spread was higher in the ultrasound measurements.

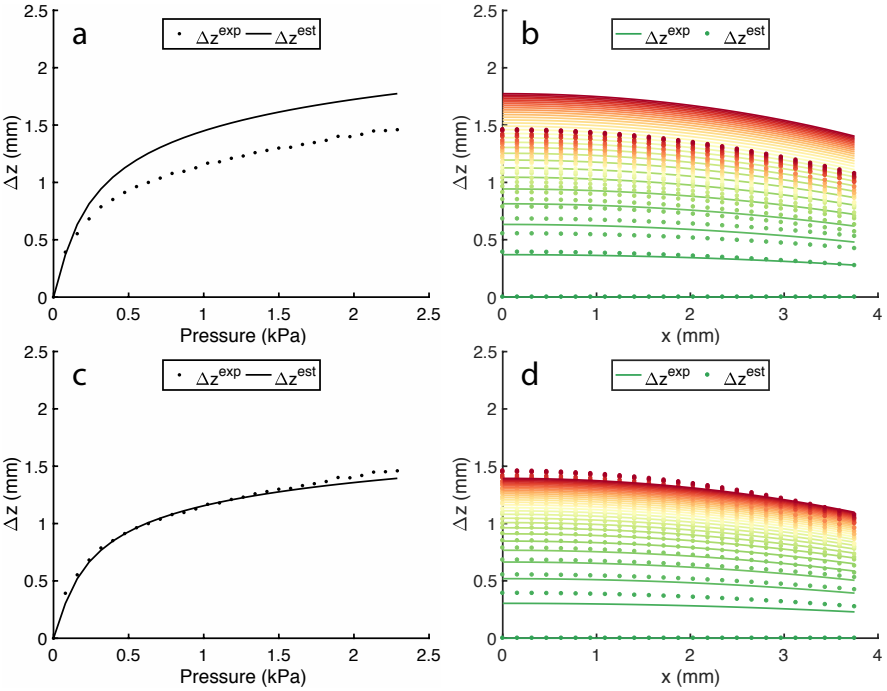

Figure 5.7: The material behavior of developing engineered tissues was estimated in the full inverse FE method by fitting the estimated profile displacement (continuous lines) as a function of pressure to the one measured by ultrasound (dotted markers). This figure shows the results from one representative sample, with the apex displacement as a function of pressure **(a,c)**, and the displacement of the central 50% of the sample as a function of pressure **(b,d)**, where the transition from pressure-free to maximum pressure state is indicated by the color transition from green to red. The initial material estimate **(a,b)** shows an underestimate of the material stiffness while the final estimate **(c,d)** closely resembles the experimental displacement behavior.

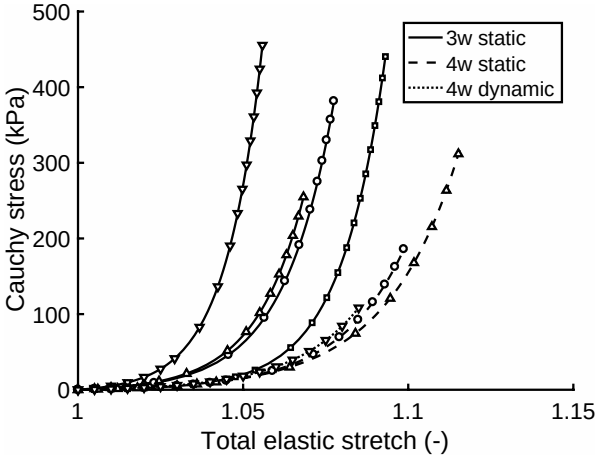

Figure 5.8: Estimated stress-stretch behavior of the tissue-engineered constructs. All samples showed a nonlinear stress-stretch response, as typically seen in soft tissues. The three-week statically cultured samples (n=4, continuous lines) showed a stiffer response than the four-week statically (n=2, dashed lines) and dynamically (n=1, dotted line) cultured samples.

5.4 Discussion

The goal of the current study was to develop and validate a mechanical characterization method to nondestructively estimate the mechanical properties of soft tissues that can be applied during tissue culture. Mechanical testing was achieved by performing a bulge test on samples inside a novel bioreactor using US (Chapter 4) and was followed by an inverse analysis to estimate the mechanical properties. The efficiency and accuracy of the proposed method was demonstrated on virtual experiments of several material types with known parameters. Furthermore, PDMS samples were used to demonstrate the method's feasibility by comparing it with tensile testing. Finally, the method was applied to estimate the material properties of tissue-engineered constructs during culture.

5.4.1 Numerical feasibility

The inverse analysis of the bulge experiments was performed in two steps. The goal of the first step was to provide a rapid, but not necessarily fully accurate, estimate of the mechanical properties. This estimate subsequently functioned as an initial estimate in the second step, where a full inverse FE scheme was used to obtain a more accurate estimate of the mechanical behavior.

In the initial estimation step, Laplace's law was used to obtain an analytical estimate of the material parameters. When characterizing true membranes, without any residual stretches, this method has been shown to be capable of providing a rapid and accurate estimate of the material parameters of soft tissues, even for nonlinear and anisotropic materials [219,143]. However, this method's accuracy decreases when the tissue thickness and prestretch increases, as shown by the virtual simulations performed in this study (Fig. 5.2). The estimate's accuracy was further decreased by a decreasing stretch range due to the structural material changes: an increasing thickness led to lower maximum stretch and stress, such that only the toe region of stress-strain curve was obtained for nonlinear materials (Fig. 5.2c,e). Increasing prestretch led to a higher minimum stretch during bulging, such that only the linear region of the stress-strain curve was obtained for nonlinear materials (Fig. 5.2d,f).

Despite these limitations, the analytical estimate still provided a reasonable and therefore important estimate of the materials' mechanical behavior, for it considerably reduced the computational costs (Fig. 5.3) and increased robustness of the second step. This reduction was most evident in the fiber-reinforced materials, where more parameters were to be estimated. Without such an initial estimate, an inverse FE analysis with 3D elements is computationally costly, therefore previous studies typically resorted to faster methods such as shell meshes [9,188,47,48,119,140] or analytical solutions as used in the initial estimate [219,143]. These methods can provide excellent estimates for thin membranes, but possibly lead to inaccurate material parameter estimates when the tissues become too thick or feature residual stretches. During the characterization of the PDMS and tissue-engineered samples, the inverse FE method was indeed able to improve on the initial estimate and closely fit the experimental pressure-displacement behavior (Figs. 5.4 and 5.7).

5.4.2 Experimental feasibility

The main advantage of the proposed method is its capability to characterize soft tissues while they are being cultured inside a bioreactor without the need to sacrifice the tissues. US imaging is key to this setup, as it allows for measurements of the tissue deformation during bulge testing inside the bioreactor. Previous studies have typically measured the tissue deformation during bulging using stereo camera setups [218,188,47,48,143,119] or advanced optical rigs [9,77], which are incompatible with the limited view of samples inside a bioreactor. In contrast, US is able to measure throughout the tissue cross-section and can therefore be easily mounted on top of a bioreactor. The custom MATLAB script that was developed successfully tracked the tissue profile displacement as a function of the applied pressure. Apart from displacement measurements, the tissue thickness could also be measured inside the bioreactor when using a high-frequent US transducer. The radio frequency data of the 12 MHz transducer that was used in the current study yielded comparable results to those obtained by microscopy of fresh tissue cross-sections, albeit with a higher spread on the measurements (Fig. 5.6).

The experimental validity of this method was demonstrated by mechanically characterizing PDMS samples by both tensile tests and bulge tests with the proposed two-step inverse analysis method. The shear modulus estimated by both tests only differed by 5%, although the spread on the bulge tests was slightly higher in the tensile tests (Fig. 5.5). Following the validation experiments, tissue-engineered constructs were successfully characterized (Figs. 5.7 and 5.8). The displacement-pressure behavior that was measured could be well-fit by the fiber-reinforced material model, resulting in the nonlinear stress-stretch response that is typically found in most biological soft tissues. Changes to a more compliant material behavior could be observed from week 3 to week 4, although the sample number used in this study was too low to draw any significant conclusions.

The tissue-engineered constructs were found to be relatively stiff, with stress stiffening already occurring from a stretch of 1.05 in the three-week cultured samples. This can be explained by the low pressures, and thefore also low stretches, that were imposed on the tissue during bulging. Biological soft tissues are known to demonstrate significant softening behavior due to the Mullins effect [159,172]. The mechanical properties can therefore be highly sensitive to the applied stretch magnitude, so when applying higher pressures one might find more compliant mechanical behavior. This is also the reason why only the PDMS samples were used to compare the proposed method to tensile testing, as this material does not exhibit softening within the tested stretch range and therefore their material behavior is not dependent on the applied load.

5.4.3 Limitations

Although US is key to the nondestructive mechanical testing method, it has a limited spatial resolution, which affects the accuracy of the tissue displacement and thickness measurements. In the current study, the radio frequency data [138] of a 12 MHz transducer was used, which is almost the maximum frequency for clinical US systems. Currently, probes with frequencies as high as 50 MHz are

available that can greatly enhance the spatial resolution, which is linearly proportional to the transducer's frequency. A limited spatial resolution is also the reason why 3D US, which would result in a full-field deformation measurement, is inadequate for accurately measuring tissue deformation and thickness.

All measurements were carried out without damaging the samples, with the exception of the prestretch that can be developed due to deposition stretch of newly deposited matrix[105] and cell traction forces[230]. Quantification of the prestretch could only be performed at the end of the experiment by taking the tissue out of the bioreactor, thereby bringing it back to a stress-free state, and measuring the dimensional changes. In order to nondestructively test tissues during culturing, it should be assumed that the prestretch remains constant after the initial tissue development, and thus the prestretch that is measured at the end of the experiment is representative for all time points. Alternatively, some samples could be sacrificed during the experiment to measure the prestretch, where it should be assumed that the prestretch is similar in the samples that were not sacrificed.

Finally, the biaxial stress and stretch states that can be explored within this testing setup are limited. With biaxial tensile testing, any arbitrary biaxial stress and stretch state can be explored, whereas with inflation testing the tissue can only be loaded by a uniform pressure, thus limiting characterization of anisotropic tissues. This leads to characterization of only a limited part of the mechanical behavior of anisotropic tissues, yet this part is most relevant for thin cardiovascular tissues at physiological loading conditions, which are mimicked by the bioreactor.

5.4.4 Future directions

In the current study, we employed a combination of experimental and inverse methods to nondestructively characterize the mechanical properties of isotropic and anisotropic soft tissues, without being limited by the presence of prestretch or excessive tissue thickness. The proposed method was applied to a novel bioreactor system but can without much effort be applied to other bioreactor systems that are capable of applying pressures to culture tissues. The inverse analysis can be combined with any experimental bulge test setup, as long as pressure and tissue displacement are measured.

The main advantage of this method is that tissues can now be cultured in a bioreactor system and mechanically characterized during their development. Using the mechanical properties, different mechanical constituents can be investigated to assess whether any determine the mechanical homeostasis, which is key to better understand how soft tissues function during both health and disease.

CHAPTER 6

Perhaps imagination is only intelligence having fun.

George Scialabba – Harvard Magazine, 1983

Initial scaffold thickness affects the emergence of a geometrical and mechanical equilibrium in engineered cardiovascular tissues

The contents of this chapter are based on:

Van Kelle, M.A.J.*, Oomen, P.J.A.*, Janssen–van den Broek, M.W.J.T., Lopata, R.G.P., Loerakker, S. & Bouten, C.V.C. Initial scaffold thickness affects the emergence of a geometrical and mechanical equilibrium in engineered cardiovascular tissues. *Submitted*

*These authors contributed equally

6.1 Introduction

Cardiovascular diseases remain the leading cause of death worldwide. If the many therapies that are available to alleviate, or slow down these diseases, fail, prostheses are available to replace end-stage diseased cardiovascular tissues. Autologous, bioprosthetic, and synthetic prostheses are widely used for replacing diseased arteries and heart valves, yet repetitive surgery is often required due to post-operative complications such as calcification, infection and aneurysm formation [168,65,211,114,173]. Moreover, the lack of growth and remodeling capacity of artificial prostheses may necessitate multiple re-operations for paediatric patients [1,131], resulting in a lower life expectancy and quality of life [175].

Tissue engineering can potentially address the shortcomings of the current cardiovascular tissue replacements, in particular their inability to grow and remodel. Tissue engineering aims to create autologous tissue replacements from biodegradable materials [187,53]. Previous studies have already shown that tissue-engineered (TE) vessels and heart valves prostheses have the potential of growth and remodeling. For instance, Hoerstrup et al. [92] implanted TE vascular grafts in the pulmonary artery of a growing lamb. While the animal's weight increased twofold during a two-year follow-up period, the graft diameter (30%) and length (45%) increased significantly. More recently, a similar animal model was used to demonstrate that decellularized vascular grafts showed a similar trend, with the diameter increasing with 56% upon a 366% increase in animal body weight. Neo-tissue formation was found in all of the explanted grafts [212], thus eliminating dilation as the only cause of increased diameter. Finally, Kluin et al. [121]. obtained a fully functional TE heart valve with mature and stable tissue formation after 12 months, using an *in situ* implanted, slow-degrading scaffold.

To date, our understanding of growth and remodeling in engineered tissues remains incomplete. In native tissues, physiological growth and remodeling is widely believed to occur in order to maintain a certain homeostatic mechanical state [72,94,102,103]. Through this principle, tissues can maintain their function regardless of changes in their mechanical environment. Several mechanical quantities have been proposed to determine mechanical homeostasis across different cardiovascular native tissues, including stretch [32,167,182] (Chapter 2), stress [214,104,224], strain energy density [40,232], and stiffness [14,66].

Interestingly, it is unclear whether or not mechanical homeostasis was reached in previous studies of TE prostheses. On the contrary, despite promising early results, adverse growth and remodeling of TE prostheses have led to geometrical instabilities, i.e. aneurysm formation in TE vascular grafts [134,147,118], and leaflet shortening in TE heart valves that causes valvular insufficiency [200,57,183]. We believe that the scaffold design of (*in situ*) TE prostheses is crucial to obtain and maintain mechanical and geometrical homeostasis. Many design parameters can be tuned when producing scaffolds for tissue engineering, for instance: scaffold thickness, porosity, fiber alignment, fiber diameter, compliance, degradation rate, and polymer composition. All of these parameters influence the mechanical properties of scaffolds, and can therefore influence growth and remodeling and subsequently the establishment of homeostasis. Previously, both in vivo [238] and in silico [154] models have been used to assess the influence of scaffold properties on growth and remodeling in TE prosthe-

ses. Most recently, Best et al. [18] clearly demonstrated in an in vivo study that decreasing the scaffold thickness to diameter ratio positively affects long-term growth and remodeling of TE vascular grafts.

In the current study, we aim to determine and understand the effects of initial scaffold thickness on establishing a geometrical and mechanical equilibrium in engineered cardiovascular tissues. To this end, a recently developed in vivo bioreactor (Chapter 4) was used to culture two groups of TE cardiovascular constructs with different initial thicknesses (relevant for cardiovascular tissue engineering), under the same dynamic loading conditions. In order to investigate whether geometrical and/or mechanical equilibrium was established in the TE constructs, temporal changes in tissue geometry and mechanical state were quantified at several time points during development, by means of nondestructive ultrasound imaging and inverse analysis (Chapter 5). At the end of culture, the TE constructs' composition and structure were determined by biochemical assays, histology and in-plane collagen organization.

It was found that a mechanically steady state was reached for both sample thicknesses, although at different magnitudes of the investigated mechanical quantities (strain, stress, strain energy density, and tangent). A stable geometrical state was only reached in the thicker samples, while the thinner constructs continued to dilate. This indicates that obtaining a geometrically and mechanically stable state in tissue-engineered constructs is highly dependent on functional scaffold design, in this particular case the initial scaffold thickness.

6.2 Methods

6.2.1 Scaffold production

Two supramolecular scaffold sheets with respective thicknesses of 0.31 ± 0.01 and 0.47 ± 0.01 mm were produced in-house via electrospinning. Polycarpolactone-bisurea (PCL-bu) polymer [237] (SyMO-Chem, Eindhoven, The Netherlands) was dissolved in chloroform to a 15 wt% concentration and electrospun in a climate-controlled electrospinning cabinet (IME Technology, Geldrop, Netherlands). The cabinet was equipped with a 14G nozzle (flow rate of 55 µL/min) and a distance of 16 cm was maintained between nozzle and the grounded target drum (0.31×12.0 cm), rotating at 100 rpm. The climate chamber was set to 23°C, 30% relative humidity, and a voltage of 15 kV was applied to the nozzle. After spinning, the two sheets were dried overnight under vacuum at room temperature. Each sheet was inspected with scanning electron microscopy. Additionally, the thicknesses of the sheets was assessed using a VHX-500 Keyence digital microscope.

6.2.2 Scaffold mechanical (fatigue) testing

Fatigue tests were performed on the bare scaffold materials, using an ElectroForce LM1 TestBench by BOSE equipped with 5 N load cells. Two rectangular samples (15×6.5 mm) were cut from each sheet, which were uniaxially stretched for 1.8 million cycles (equal to 21 days of dynamic culturing, see Section 6.2.3) with increasing maximum actuator displacements of 5, 10, 15, and 20% of the initial

sample length. Every displacement stage consisted of two periods of 225,000 sinusoid displacement cycles at 10 Hz, each followed by a rest period of equal duration to cyclic displacement (22,500 seconds). During testing, the samples were submerged in a physiological salt solution at 37°C. From this test, the peak first Piola-Kirchhoff stresses were calculated from the force acting on the load cells as a function of time.

Uniaxial tensile tests of the scaffolds were perfomed before and after fatigue testing on a BioTester (CellScale, Waterloo, Canada). The samples were stretched to 115% of the initial length with a strain rate of 100%/min for 10 cycles, of which the first 9 were considered pre-conditioning. During testing, the samples were again submerged in a physiological salt solution at 37° C. The force was measured by a 1.5 N load cell, and images were taken by a CCD camera mounted perpendicular to the sample surface. All data were collected with a sampling frequency of 5 Hz. Again the first Piola-Kirchhof stresses were calculated from the force data. The in-plane sample stretches were obtained from the images using a global digital image correlation algorithm[162].

6.2.3 Tissue culture in bioreactor

To culture TE constructs, the 'versatile tissue growth and remodeling' (Vertigro) bioreactor[227] was utilized (Fig. 4.1). Inside this bioreactor, a circular insert with a diameter of 15mm containing a cell-seeded construct can be placed which is then consecutively cultured under pressure-driven dynamic loading conditions. Regardless of geometrical and mechanical changes in the construct, the applied pressures were maintained by a custom LabVIEW (National Instruments, Austin, USA) program.

The electrospun PCL-bu scaffolds (Section 6.2.1) (both n=8) were clamped in the inserts and sterilized using UV-light. Next 0.25 mg/mL L-ascorbic 2-phosphate acid (Sigma-Aldrich, St. Louis, MO, USA) supplemented standard culture medium (TE medium) was added to the inserts after which they were placed in an incubator overnight. Primary myofibroblast-like cells were isolated from human vena saphena samples, according to the Dutch guidelines for use of secondary materials. These cells exhibit a contractile phenotype, and are known to produce abundant amounts of extracellular matrix[156], making them ideal for cardiovascular tissue-engineering. The cells were cultured in advanced Dulbecco's Modified Eagle Medium (Invitrogen, Carlsbac, CA, USA), supplemented with 10% Fetal Bovine Serum (Greiner Bio One, Frinckenhausen, Germany), 1% Glutamax (Invitrogen) and 1% penicillin/streptomycin (Lonza, Basel, Switserland) which was changed twice per week. At passage 7, the cells were harvested and seeded on the PCL-bu scaffolds using a seeding density of 15 million cells/cm^3 using fibrin as a cell carrier[158]. After seeding, TE medium was added to the constructs which were then statically cultured at 37, 100% humidity and 5% CO_2 to allow for initial tissue development. After this period, the inserts containing the constructs were placed in the bioreactor and cultured for 21 days at a dynamic loading regime with a maximum pressure of 4 kPa at 1 Hz.

6.2.4 Nondestructive geometrical and mechanical characterisation during culture

Changes in tissue geometry and mechanical state were nondestructively characterised at day 0, 3, 7, 14, and 21 of dynamic culturing. At each time point, a 12 MHz linear ultrasound transducer (LA435) connected to a MyLab 70 Ultrasound system (Esaote Europe, Maastricht, Netherlands) was positioned on top of the bioreactor, perpendicular to the construct surface and aligned with the centre of the construct. The transducer was positioned at the same location as during previous measurements. To prevent infections during culture, the measurements were performed inside a laminar air flow cabinet, with the ultrasound probe contained in a sterile probe cover (Civco, Coralville, IA, US). To assess the construct thickness, raw radio-frequency (RF) data were acquired without applying any pressure. From this data the thickness was determined in approximately 20 locations using MATLAB´s (Mathworks, Natick, MA, USA) *findpeaks* algorithm, of which the median thickness was used as initial construct thickness t_0.

Next, a mechanical test was performed during which a pressure (p) of 4 kPa (the same maximal pressure used during dynamic culturing) was gradually applied to the constructs, while imaging the constructs deformation with the ultrasound scanner. Three pressure cycles were applied in each test, of which the first two were considered as preconditioning. The pressure was measured by a pressure sensor (P10EZ-1, BD|SENSORS, Thierstein, Germany). The constructs' geometries were assumed to be axisymmetric and their mechanical properties isotropic, hence one measurement in any given direction was assumed to be representative for all other directions.

The sample profile as a function of pressure was tracked in the B-mode images (frame rate 25 Hz, resolution 21 px/mm) using a custom MATLAB script (Section 4.2.4). First, the two attachment points of the constructs were selected, then the tissue apex was manually selected in each frame. A circle was subsequently fitted through the attachment points and the apex to describe the tissue profile. This profile was used to calculate the construct curvature k and current length L. The unloaded construct length L_0 was defined at $p = 0$, and the construct stretch during pressure application as $\lambda = L/L_0$.

6.2.5 Mechanical properties and mechanical state during culture

Constitutive model

The material behavior of the TE constructs was modeled by a hyperelastic fiber-reinforced constitutive model, where the Cauchy stress $\boldsymbol{\sigma}$ was obtained from a strain energy density function Ψ as a function of a set of material parameters ξ:

$$\boldsymbol{\sigma} = \frac{2}{J}\mathbf{F} \cdot \frac{\partial \Psi(\xi)}{\partial \mathbf{C}} \cdot \mathbf{F}^{\mathrm{T}} \tag{6.1}$$

with $\mathbf{F}$ the deformation gradient tensor, $\mathbf{C} = \mathbf{F}^{\mathrm{T}} \cdot \mathbf{F}$ the right Cauchy-Green deformation tensor and $J = \det(\mathbf{F})$ the Jacobian,. The strain energy density function consisted of an isotropic matrix

part m and anisotropic fibrous part f with fiber volume fraction Φ_f, arbitrarily set at 0.5[56]:

$$\Psi = (1 - \Phi_f)\Psi_m + \Phi_f \Psi_f \tag{6.2}$$

The constitutive behavior of the isotropic matrix part was described by a Neo-Hookean constitutive model,

$$\Psi_m = \frac{\kappa}{2} \ln^2(J) + \frac{\mu}{2} (I_1 - 3 - 2\ln(J)) \tag{6.3}$$

where $\kappa = \frac{2\mu(1+\nu)}{3(1-2\nu)}$ is the bulk modulus, μ the shear modulus, and $I_1 = \mathbf{C} : \mathbf{I}$ the first invariant of the right Cauchy-Green deformation tensor. Quasi-incompressibility was enforced by setting the Poisson ratio at $\nu = 0.498$. The fiber part was modeled as a discrete fiber distribution oriented in the plane of the sample. Each fiber i with unit direction vector $\mathbf{e}_f^i$ (in the reference configuration) additively contributed[56] to the total fiber strain energy density function Ψ_f. The strain energy density function Ψ_f^i for each individual fiber i was given by an exponential model (similar to[56,135], as described in Section 3.2.4):

$$\Psi_f^i = \frac{k_1}{2k_2} \left(\exp \left[k_2 \left\langle (\lambda^i)^2 - 1 \right\rangle \right] - k_2 \langle (\lambda^i)^2 - 1 \rangle - 1 \right) \tag{6.4}$$

with k_1 and k_2 material parameters, $(\lambda^i)^2 = \mathbf{C} : (\mathbf{e}_f^i \otimes \mathbf{e}_f^i)$ the squared elastic fiber stretch, and $\langle \circ \rangle$ the Macaulay brackets to enforce that the fibers only resist tension.

Estimation of material properties

From each nondestructive mechanical test, the construct's profile as a function of pressure was recorded at each time point. Using this information, the material properties ξ (here $\xi = [\mu, k_1, k_2]$) of the constructs at each time point were determined using a two-step inverse method that was developed in Chapter 5. In the first step, shell theory was used to obtain a rapid analytical estimate of the material properties. This estimate was used as an initial estimate of the second step, where an inverse finite element analysis was used to obtain a more accurate estimate of the material properties. In this step, the experiments were simulated by a finite element model in Abaqus FEA (Dassault Systèmes Simulia Corp., Providence, RI, USA). Only one quarter of the tissue geometry (at $p = 0$) was modeled due to symmetry. A uniform pressure was applied to the bottom plane of the construct, while the nodes on the sample edge were fully constrained. MATLAB's $lsqnonlin$ function was utilised to adjust the material parameter set ξ until the difference between the surface profile as a function of pressure $z(p)$ between the experiment (exp) and the estimate (est) was minimised. This resulted in the following cost function:

$$E(\xi) = \frac{1}{N_p N_x} \sum_{j=1}^{N_p} \sum_{k=1}^{N_x} \sqrt{z(p_j, x_k, \xi)^{\text{exp}} - z(p_j, x_k, \xi)^{\text{est}}} \tag{6.5}$$

with N_p the number or pressure steps, N_x the number of in-plane positions x along the tissue profile.

Analysis of the mechanical state

After the material parameter estimation, the strain energy density, the Cauchy stress tensor and deformation gradient tensor at every node in the central 50% of the construct were obtained from the final simulation of the inverse finite element analysis. Subsequently, the maximum principal stress σ_{max} and its direction $\mathbf{n}_{\text{max}}$ were determined. The stretch λ_{max} in the same direction $\mathbf{n}_{\text{max}}$ was then obtained from $\lambda_{\text{max}} = 1/\sqrt{\mathbf{B}^{-1} : (\mathbf{n}_{\text{max}} \otimes \mathbf{n}_{\text{max}})}$, with $\mathbf{B}$ the left Cauchy-Green deformation tensor. The local tangent of the principal stress-stretch curve was determined at $p = 4$ kPa.

6.2.6 Tissue analysis after culture

After culture (day 21 of dynamic culture), the constructs were cut into three pieces. Two quarters were fixed in 3.7% formaldehyde and used for histology and collagen orientation analysis, respectively. The other half of the samples were lyophilized overnight and used to quantify the amounts of DNA, glycosaminoglycans (GAGs) and hydroxyproline (HYP, as measure for the amount of collagen).

From each sample, the first quarter was embedded in paraffin and sectioned into slices of 7 µm. The embedded samples were stained for general tissue structure (Hematoxylin & Eosin (HE)), collagen (Picrosirius red (PR)) and GAGs (Safranin O (SO)). These sections were imaged under a bright-field microscope (Axio Observer Z1, Carl Zeiss AG, Oberkochen, Germany), and the PR stain was also imaged using polarized light. In addition, fluorescent stainings were performed for collagen type III, (Tropo)elastin and a costaining for collagen type I, α-smooth muscle actin (αSMA), and cell nuclei, which all were imaged using an Axiovert 200M microscope (Zeiss).

The other quarter of the samples was incubated with a collagen-specific CNA35[22] probe for 1 hour, after which the gross collagen organisation was imaged via a tilescan on each side (excitation 488 nm, emission 520 nm, magnification 10x) using a confocal laser scanning microscope (TCS SP5X; Leica Microsystems, Wetzlar, Germany). To quantify the in-plane collagen fiber organisation, a custom-made MATLAB script was used[70], which quantifies the fraction of fibers oriented in each in-plane direction.

Finally, the lyophilized halves of the constructs were snap-frozen and disintegrated using a Mikro-Dismembrator (Model S, Sartorius, Goettingen, Germany), followed by digestion using a papain digestion buffer (60 , 16 hours). The constructs' total GAG content were determined using an adapted protocol by[63], with a standard curve of chondroitin sulfate (Shark Cartilage, Sigma-Aldrich). A HYP assay was performed[109] using a trans-4-hydroxyproline (Sigma-Aldrich) standard curve. To obtain a measure for cellular activity, construct GAG and hydroxyproline content were normalised to the tissue's total DNA content, which was determined with the Hoechst dye method[29].

6.2.7 Statistics & Sample Numbers

During the experiment, unfortunately a few samples were excluded due to an infection. For the thin samples, one sample was excluded during the second week, and two samples in the final week of dynamic culture. For the thick samples, in both the second and final week one sample was excluded. This resulted in analyses at the end of the experiment for n=5 and n=6 samples for the thin and thick group respectively. The geometrical and mechanical measurements of samples before drop-out were still taken into account. All data are presented as mean value $\pm$ the standard error of mean. For the biochemical assay data, comparisons between groups were made using the Wilcoxon signed-rank statistical test in MATLAB. The geometrical and mechanical data were analyzed in IBM SPSS Statistics for Macintosh (IBM Corp., Armonk, NY, USA), using linear mixed model analysis, according to Duricki et al. [59]. This is a statistical approach that accounts for multiple measurements in the same (in this case) constructs, while accommodating for possible dropout of samples during the experiment. Post hoc analyses using Fisher's least significant difference tests were used to test for statistical different between adjacent time points within each initial construct thickness group, and between the two groups at the same time point. Differences were considered statistically different when $p<0.05$.

6.3 Results

6.3.1 Geometrical changes during culture

The geometrical changes of the tissue constructs are depicted in Fig. 6.1. Initially, both groups started with a tissue length L_0 of 15 mm (in accordance with the diameter of the bioreactor insert) (Fig. 6.1a). However, after only 3 days of dynamic culturing the samples both elongated significantly, where the length of the thinner samples was larger than that of the thicker samples. This trend continued over time for the initially thinner tissues, while the thicker construct length did not significantly change with time. At the end of culture, the length of the tissues of both groups had significantly increased (Fig. 6.1e,f) compared to the start of culture (Fig. 6.1c,d). The construct thickness t_0 at the start of the dynamic culturing face was similar to the initial scaffold thickness (Fig. 6.1b). Next, both groups followed a similar trend, where first a significant decrease in thickness was observed up to day 7, after which the thickness slightly increased again up to day 21.

6.3.2 Construct mechanics during culture

Several mechanical constituents were quantified during dynamic culture in the central 50% of the constructs. The elastic stretch, maximum principal Cauchy stress, strain energy density, and local tangent of the principal stress-stretch curve at $p = 4$ kPa in the thin constructs were higher than in the thick constructs (Fig. 6.2). During tissue development, the elastic stretch of the constructs in the two groups diverged towards significantly different equilibrium states, with the stretch in the

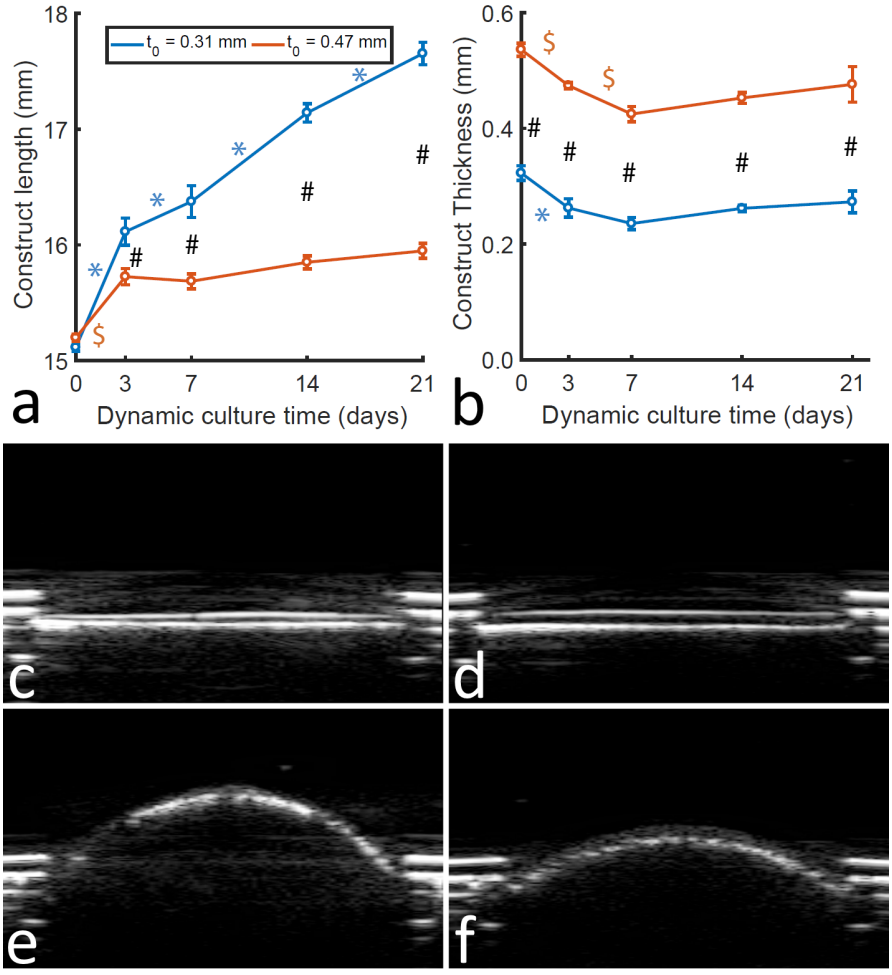

Figure 6.1: Geometrical changes of the constructs during dynamic culture: Changes in tissue length L_0 (**a**) and construct thickness t_0 (**b**) for starting scaffold thicknesses of 0.31mm (blue) and 0.47mm (red). Significant changes ($p<0.05$) between adjacent time points within the initially thinner and thicker constructs are indicated by * and $, respectively, while significant differences between the two groups at the same time point are indicated by #. Representative ultrasound images (with $p = 0$) of the thin (**c,e**) and thick (**d,f**) constructs at the start (**c,d**) and end (**e,f**) of the dynamic culturing.

thin constructs slightly increasing and the stretch in the thick constructs decreasing with time. The strain energy density stabilised during development, with no significant changes between adjacent time points observed during dynamic culture. The maximum principal Cauchy stress of the thin samples appeared to decrease with culture time, while the stress in the thicker samples increased up to day 7, followed by a decrease. Finally, the tangent in both groups appeared to decrease during development, albeit in the thick samples after an initial increase and with no significant changes between adjacent time points. No significant differences were found between the local tangents of the two groups after the start of dynamic culture.

6.3.3 Bare scaffold features progressive viscoelastic and plastic deformation

Fatigue tests were performed on both scaffold thicknesses, during which increasing actuator displacements were applied to stretch the scaffolds (Fig. 6.3a). During each actuator displacement stage, the peak First Piola-Kirchhoff stress decreased, which can be attributed to progressive plastic (permanent) length change of the scaffolds (Fig. 6.3c,d). After the rest period that was applied during each displacement stage, the stress only partially recovered to the same magnitude as found before the rest period. This indicates that stress relaxation occurred during each stage, thus identifying the scaffolds as viscoelastic materials.

Despite the plastic deformation that occurred during fatigue testing, additional uniaxial tests performed before and after fatigue testing showed no clear differences in the mechanical behavior between both scaffold groups (Fig. 6.3b). Both the fatigue and additional tensile tests indicated that the thin scaffolds were more compliant than the thick scaffolds.

6.3.4 Collagen formation occurs isotropically in-plane

An in-plane isotropically distributed collagen organisation was observed on both sides of a quarter of the engineered constructs (Fig. 6.4). Using fiber tracking software, this was also confirmed quantitatively, as indicated in the histograms of Fig. 6.4. When comparing both sides of the samples, the top part has a more dense collagen fiber network compared to the bottom part, which contains more thick bundles of fibers.

6.3.5 Layered tissue formation throughout the samples thickness

Fig. 6.5 shows representative histological images for the thin (left column) and thick (right column) samples (note that the scaffold was dissolved during the embedding process). The HE stain showed a more dense structural organisation in the thick samples, compared to the thin samples (a,b). In addition, a distinct layer formation was present on the top side of both sample groups, which was also visible in the PR stain (c,d). When looking at this latter stain under polarized light to asses the maturity of the fibers, the bright-red mature fibers were found opposite of this top layer at the pressurized sides of the samples. α-SMA positive cells were mostly located in the top layer of

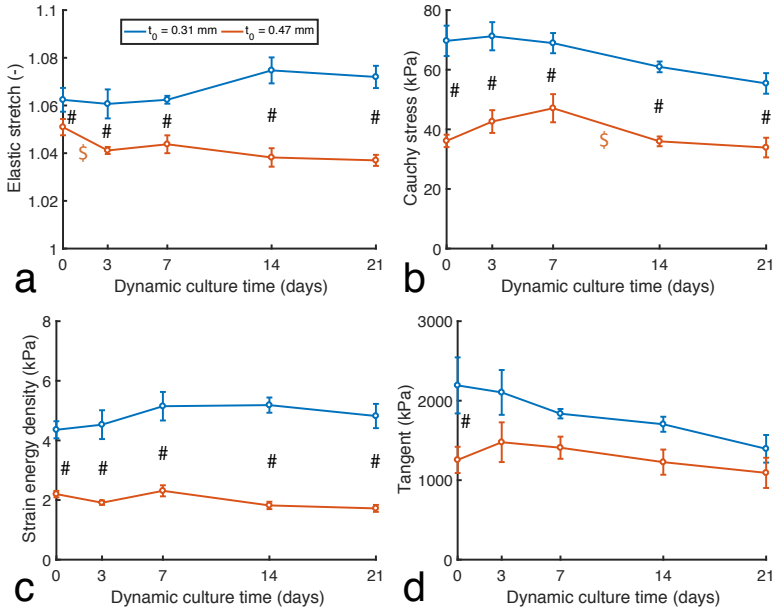

Figure 6.2: Assessment of the constructs' mechanical state during dynamic culture. In all constructs, the stretch **(a)**, maximum principal Cauchy stress **(b)**, strain energy density **(c)**, and tangent of the principal stress-stretch curve at $p = 4$ kPa **(d)** were nondestructively quantified. Significant changes ($p<0.05$) between adjacent time points within the initially thinner and thicker samples are indicated by * and $, respectively, while significant differences between the two groups at the same time point are indicated by #.

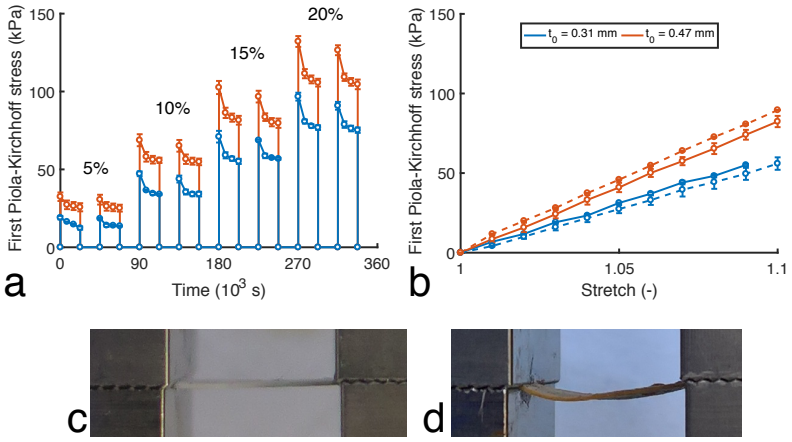

Figure 6.3: Mechanical testing of the bare scaffold. First Piola-Kirchhoff stress during fatigue testing with increasing actuator displacements **(a)**. Images were captured before **(c)** and several hours after **(d)** fatigue testing, here shown for a sample of $t_0 = 0.31$ mm. The stress-stretch behavior of each sample was characterised before (continuous lines) and after (dashed lines) fatigue testing **(b)**.

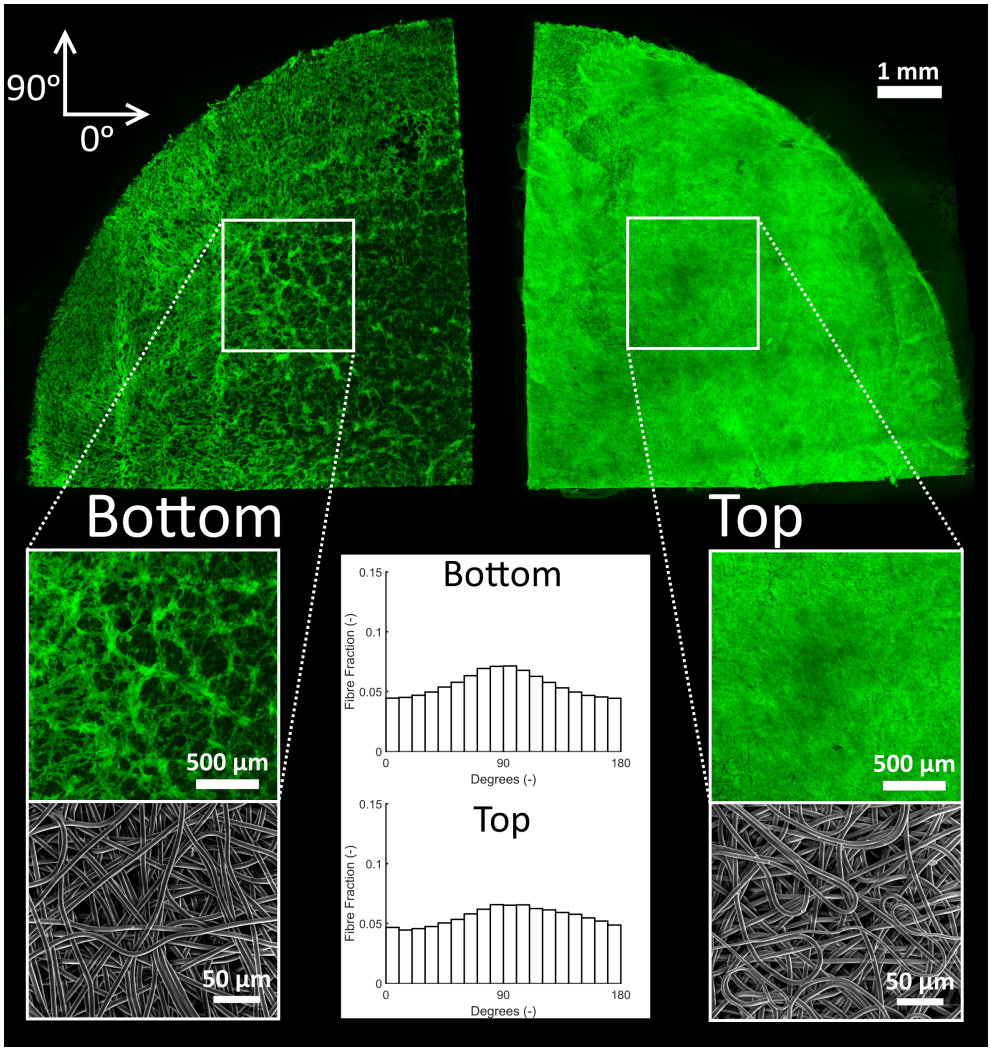

Figure 6.4: The top (right) and bottom (left) side of a representative collagen-stained quarter of one of the constructs. Zoomed-in images are indicated between the white squares, with below them scanning electron images of the scaffold prior to seeding. The histograms indicates the fraction of collagen fibers oriented in each direction for the entire sample.

the tissue, together with relatively immature collagen type III (g,h,i,j). On the other hand, some elastin fibers were present on the pressured sides of the samples (Fig. k,l). Finally, GAGs were most abundant in the thicker samples, also evenly distributed throughout the thickness.

6.3.6 Increased GAG formation in thick constructs

Fig. 6.6 shows the results for the biochemical assays performed on the lyophilized samples at the end of the experiment. The mean DNA content (μgram) for each group is slightly higher in the thicker samples (Fig. 6.6a), these values were used to normalize the total GAG and HYP content. The constructs' GAGs per DNA (Fig. 6.6b) content was significantly ($p=0.03$) higher for the thick samples, while the opposite is true for the amount of HYP per DNA (Fig. 6.6c).

6.4 Discussion

The current study sought to determine in vivo whether a geometrical and/or mechanical equilibrium state could be reached in engineered cardiovascular constructs depending on initial scaffold thickness. Towards this end, temporal changes in geometry and mechanical properties in dynamically cultured constructs were assessed over time using non-destructive ultrasound imaging.

6.4.1 Geometrical equilibrium is dependent on initial scaffold thickness

In the fatigue tests performed on the bare scaffold material (Fig. 6.3) both the thin and thick samples plastically deformed at all of the applied levels of actuator displacement. Moreover, the electrospun materials showed viscoelastic behavior, as indicated by the increase in peak First Piola-Kirchoff stress after a period of rest. It should be noted that both permanent deformation and viscoelastic behavior will likely have the same lengthening effects in vivo, as the material will never experience an unloaded state.

The cell-seeded scaffolds experienced a similar type of dynamic loading compared to the bare scaffolds, during which lengthening of the sample was compensated by the feedback system of the bioreactor, in order to maintain a constant peak pressure. As with the bare scaffolds, construct length increased during dynamic culture, and was dependent on the initial scaffold thickness (Fig. 6.1). Strikingly, the initially thin construct length continued to increase, whereas the thicker constructs length stabilized after three days of dynamic culture. In the thin samples, this apparently caused the tissue length to continue to dilate, whereas the thicker samples are able to counteract this lengthening. A possible explanation could be attributed to the fact that there is more ECM production in the thick samples, in the form of cell-produced GAGs (Fig. 6.6). Moreover, a more dense collagen structure was observed in the thicker samples (Fig. 6.5g,h), which could also explain the stabilizing lengthening behavior. Although, this could also simply be caused by the fact that the scaffold is thicker, therefore leading to lower internal stretches and stresses.

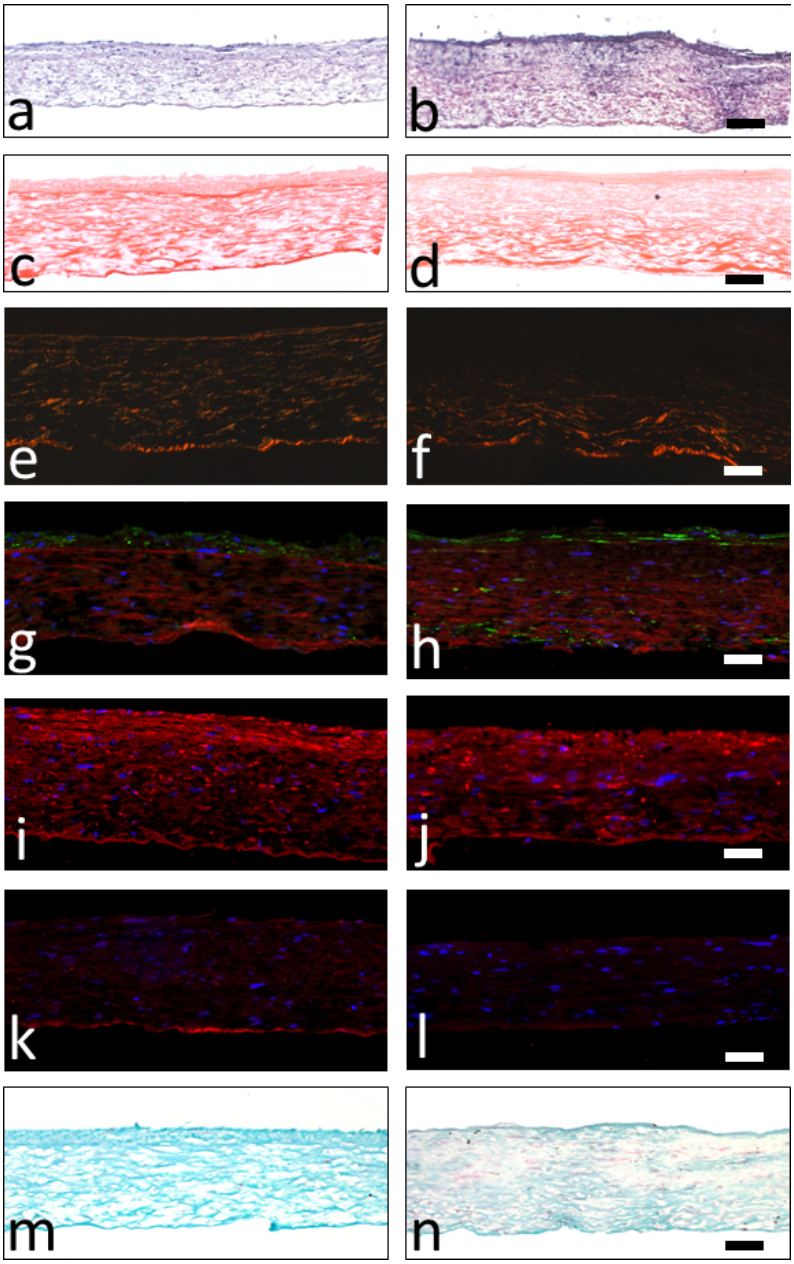

Figure 6.5: Representative histological images of the middle section for the thin (left column) and thick (right column) samples at t=21 days of dynamic culture, where the bottom side of all samples coincides with the pressurized side in the bioreactor. **a,b**) HE stain showing the general tissue composition, with a distinct layer formation on the top side of the samples. **c,d**) PR stain showed general collagen organisation (red). **e,f**) PR stain visualized with polarized light, depicting relatively mature collagen fibers (red). **g,h**) Fluorescent images with α-SMA positive cells in green, cell nuclei in blue and collagen in red. **i,j**) Fluorescent stain for collagen type III. **k,l**) Co-fluorescent stain for elastin (ref) and cell nuclei (blue). **m,n**) SO stain depicting GAGs in red. The scale of the images is indicated by the black and white bars (100µm) (abbreviations: HE: Hematoxylin & Eosin, PR: Picosirius Red, SO: Safarin-O

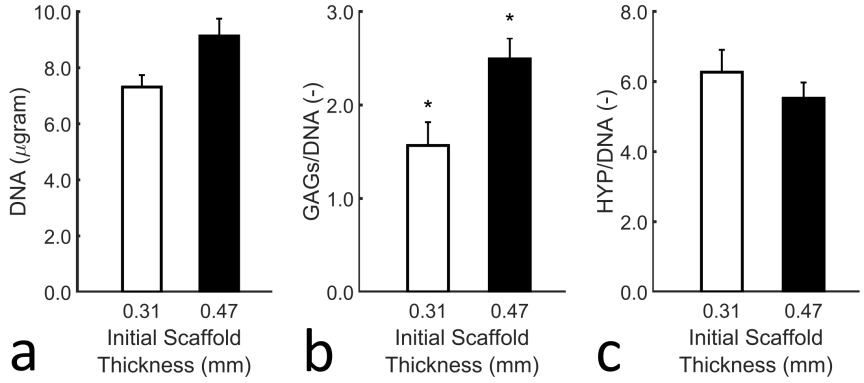

Figure 6.6: Biochemical Assays: Total DNA content (μgram) (**a**) GAGs per DNA (**b**) and HYP per DNA (**c**) for initial scaffold thicknesses 0.31mm (white bars) and 0.47mm (black bars).

For both the thin and thick constructs the thickness followed similar trends, first decreasing with culture time up to day 7, after which there was a slight increase in thickness. The initial thinning can be ascribed to the Poisson effect, as the samples are plastically deformed in the in-plane directions. The slight thickening of the samples could a direct consequence of subsequent tissue formation on top of the scaffold (Fig. 6.5), which was also observed by van Vlimmeren et al. [231] in statically cultured samples containing the same cells, after four weeks of culture.

Overall, these results indicate that these electrospun polymer materials, often used for tissue engineering purposes, experience viscoelastic and plastic behavior, and that different scaffold design parameters can have large implications for reaching a geometrically stable state. This was for instance also reported by Best et al. [18] who, by merely increasing the initial lumen diameter in *in situ* TE vascular grafts, could promote enhanced neointimal tissue formation and matched the final size of the lumen to that of the native situation. Similarly, this study demonstrates that the initial thickness of cardiovascular TE grafts can greatly influence the eventual dimensions of these constructs. In this particular case, a geometrical equilibrium state was only found for the thicker samples.

6.4.2 Mechanical equilibrium at distinctly different magnitudes

For all mechanical constituents, a clear distinction can be observed between the two samples groups (Fig. 6.2), which can simply be explained by the differences in initial scaffold thicknesses. For instance, the stretches in both sample groups start at different magnitudes, and slightly increase and decrease for the thin and thick samples respectively, after which they seem to reach a steady state. This seems particularly odd, since the unloaded construct length continued to dilate in the thinner samples, while it stabilizes for the thicker samples. Apparently, the tissue stretch in the thinner sample is maintained at a constant level, although the unloaded state increases over time.

For the thick samples the Cauchy stresses initially increased, followed by a gradual decrease. A

simple explanation can be found in the trend of the sample thickness over time, which appeared to follow an inverse trend. Contrary, the thinner samples follow a similar trend after day 7, but do not show the initial increase in stress. The temporal changes in tangent stiffness converge to a similar value for the two groups at the end of the experiment, which gives rise to speculation what would happen beyond this time point.

Contrary to earlier findings using this bioreactor system [227], no prestretch was present in any of the tested samples, although histology showed that presence of αSMA positive contractile cells (Fig. 6.5g,h). A possible explanation is that in these experiments, a non-degrading scaffold was used, which impairs cell-mediated contraction of the tissue construct, or lies in the fact that these cells predominantly reside in the top layer of the tissue, thus being unable to compact the entire construct.

In these particular experiments, the scaffold seems very important for the mechanical behavior of the constructs (as is the phase in the initial case for many *in situ* TE applications). In future experiments, it would be interesting to see what would happen to the tissue mechanical properties if a more compliant or partially degraded scaffold is used [165,166]. Finally, knowing the typical loading pattern in these types of constructs can be very insightful, as this to a great extend determines ECM production and degradation [21,103,193,244]

6.4.3 Tissue composition is similar to the native situation

Although clear differences in mechanical behavior between the two groups were observed, little differences in tissue composition were found. Apart from a significant increase in the GAG per number of cells, no significant difference in cell-produced collagen were found. Also no clear differences could be observed qualitatively between the groups (Fig. 6.5). Perhaps culture times in these experiments were too short to give rise to such significant differences, or the scaffold mechanical properties dominated the overall mechanical response of the constructs.

Interesting observations can be made within the tissue samples themselves i. First, a clear top layer is present (Fig. 6.5a,b) containing mainly αSMA positive cells, collagen type III and GAGs (Fig. 6.5c,d,g,h). The presence of the latter three components indicates that this layer is relatively immature, and has probably formed in the later stage of the experiment [231]. Second, thick bundles of collagen type I (Fig. 6.5e,f) and even traces of elastin (Fig. 6.5k,l) are present on the bottom of the samples, implying that this layer is relatively mature. The existence of these thick bundles of collagen fibers can also be seen in the CNA-stained images (Fig. 6.4, left). Noteworthy is the presence of elastin (which appears more abundant in the thinner samples compared to the thick samples), which is rarely observed in similar in vivo experiments [157]. Finally, when looking at the gross organization of all the tissue components, they resemble the build-up shown in some in vivo TE studies. For instance, we found thick bundles of collagen on the pressurized (bottom) side of our constructs, which coincides with densely organized collagen fibers found in the fibrosa (pressurized) side of native and TE heart valves. In addition, elastin was also found on this side of our samples, which is consistent with a recent study by Kluin et al. [121], who also found elastin bundles mainly on the

pressurized pulmonary side of TE valve constructs.

6.4.4 Comparison to in vivo studies

Lengthening of implanted vascular grafts, and subsequent aneurysm formation, has been observed in previous studies[118,170], which could be explained by relatively small initial wall thicknesses. On the contrary, a recent study by Talacua et al. [215] opted for an electrospun PCL scaffold as a vascular graft with a thickness of 0.275 mm, enforced by an additional Gore-tex patch. Over the course of 3 months they reported a constant lumen diameter, possible caused by the relatively thick combined PCL and Gore-tex graft. In another study Kluin et al. [121], used a polycarbonate-bisurea valvular graft with a thickness of 0.4 mm, implanted at the pulmonary position in sheep. In agreement with our study, at similar loading pressures (3.3 vs 4 kPa) and comparable initial scaffold thicknesses (0.4 vs 0.47 mm, compared to the thicker group in this study) they also observed a constant tissue length over time. Moreover, the tissue formation in both studies samples is very similar, with elastin and thick collagen bundle formation on the pressurized side of the samples.

6.4.5 Limitations & Future directions

In this particular case, a relatively simple design parameter, scaffold thickness, significantly influenced TE construct mechanics and geometrical stability. Naturally, other scaffold properties are of paramount importance to obtain a mechanical and geometrical stable state, for instance the effect of scaffold degradation during in vitro or in vivo experiments. Moreover, this study only focused on isotropically organized constructs, while cardiovascular tissues tend to exhibit an anisotropic tissue organization. A future study should focus on inducing anisotropic loads in the TE constructs, for instance by using an anisotropic scaffold or by altering the bioreactor insert shape. Finally, different scaffold mechanical properties and external loading magnitudes could potentially influence experimental outcomes.

6.4.6 Conclusion

In this study we sought to elucidate if a simple scaffold design parameters such as initial thickness could influence the emergence of a mechanical and geometrical equilibrium state in in vivo TE constructs. A mechanically steady state was reached in both groups, albeit at different magnitudes of the investigated mechanical quantities (elastic stretch, Cauchy stress, strain energy density, and tangent stiffness). A stable geometrical situation was only established in the thicker samples, while the thinner constructs continuously elongated. This demonstrates that reaching geometrical and mechanical stability in tissue-engineered constructs is highly dependent on functional scaffold design.

CHAPTER 7

Mischief managed.

Fred and/or George Weasley

General discussion

7.1 Background and objectives

7.1.1 Growth and remodeling in native heart valves

From a biomechanical perspective, it is now well accepted that growth and remodeling occur in response to changes in the tissue's mechanical environment, and in order to maintain a certain mechanical homeostasis[72,94,102,103]. To date, no consensus has been reached on which mechanical constituent(s) determine(s) mechanical homeostasis across different native tissue types, including cardiovascular tissues. The first goal of this thesis was therefore to determine which mechanical quantity determines mechanical homeostasis in native cardiovascular tissues, in this case heart valves (Chapter 2), and what the relative roles of growth and remodeling are in maintaining it (Chapter 3).

7.1.2 Growth and remodeling in engineered cardiovascular tissues

Growth and remodeling are not only pivotal for the functioning of native tissues, but are also of high importance for tissue engineering. The growth and remodeling potential of tissue-engineered prostheses make them an exciting alternative for current valvular and vascular tissue replacements. Yet, in contrast to the native tissues they ought to replace, mechanical and geometrical instabilities have led to failure of tissue-engineered heart valves[57,85,183,200] and vascular grafts[118,134,147]. So, if engineered cardiovascular tissues are to be successful in the long term, further research on growth and remodeling in engineered cardiovascular tissues is required. Therefore, the second overall aim of this thesis was to investigate if mechanical homeostasis can also be established in engineered tissues. We hypothesized that scaffold design is crucial to guide growth and remodeling towards mechanical and geometrical homeostasis, as it is the scaffold (alongside hemodynamic loading) that primarily determines the engineered tissue's mechanical environment immediately after implantation (Chapter 6). A novel in vitro platform was presented in this thesis to test this hypothesis (Chapters 4 and 5).

7.1.3 General discussion outline

The goal of this chapter is to discuss the presented results, their limitations, and potential clinical and scientific impact. First, the stretch-driven tissue homeostasis that we found in human native valves during aging is discussed. Second, we discuss the emerging importance of functional scaffold on reaching geometrical and mechanical stability in tissue-engineered cardiovascular constructs. Moreover, the sometimes contradicting results that we obtained in native and engineered tissues are discussed. Finally, we explore possible future applications and developments of the in vitro platform to study growth and remodeling in engineered cardiovascular tissues.

7.2 Growth and remodeling in native heart valves

7.2.1 Age-dependent changes indicate that a stretch-driven homeostasis is maintained in native heart valves

In Chapter 2, age-related changes in native heart valves were studied to unravel which mechanical quantity determines mechanical homeostasis in native tissues during postnatal development. To this end, an extensive data set was generated of paired human aortic and pulmonary native valves of fetal to adult origin. Each valve was structurally, geometrically, and mechanically characterized. The outcomes were used to predict age-dependent changes in stress and stretch in the leaflet tissue via finite element modeling. The results indicated that the circumferential leaflet stress was different between the aortic and pulmonary valve, and that the aortic valve stress increases considerably over time (Fig ??). Strikingly, relatively small differences were found in stretch with time and between the aortic and pulmonary valve. These results indicate that growth and remodeling in native heart valves occur in order to maintain a stretch-driven homeostasis. Using these results, we demonstrated in Chapter 3 that growth and remodeling play opposing roles in preserving tissue stretch homeostasis during physiological development. In particular, our numerical models indicated that during early development (infant to adolescent) tissue stretch was maintained by growth and increased by remodeling, and vice versa during late development (adolescent to adult).

7.2.2 Comparison with the literature

Age-related changes in the semilunar heart valves

Age-related changes in the structural and mechanical properties of the native semilunar heart valves have been widely investigated. The leaflets' collagen architecture has been found to mature with age, represented by thicker fiber bundles[3,116] and increased cross-linking[11]. Consequently, as also seen in Figs. 2.3 and 3.5, the stiffness of the leaflets generally increases with age[11,116,207,209,226].

To the best of our knowledge, we are the first to directly correlate mechanical, geometrical, and structural changes to mechanically-driven growth and remodeling in the semilunar heart valves. However, interesting comparisons can be drawn with previous studies in native mitral valves. These valves have a vastly different geometry than aortic valves, yet feature the same cell types and tissue structure. We thereby assume that the mitral valve properties change in a similar age-dependent fashion as the semilunar heart valves.

Growth and remodeling in the mitral valve

Recently, Ayoub et al.[10] used an experimental-numerical approach to study the cellular deformation and protein activity of mitral valve interstitial cells in response to varying cyclic strain magnitudes applied by a bioreactor system[151] (Table 1.1). They found that cellular deformation correlated with overall mitral valve leaflet deformation, and found a range of cellular deformation values in

which cell activity appeared to be homeostatic. From these results they concluded that mitral valve deformation is the key player in leaflet tissue homeostatic regulation. Their findings in the mitral valve agree with our finding that mechanical homeostasis is stretch-driven in the semilunar heart valves.

Still in the mitral valve, Dal-Bianco et al. [45] and Rausch et al. [182] used an ovine model in which the papillary muscles of the left ventricle were tethered to induce elevated mitral valve stretches and stresses. Both studies reported mitral leaflet growth in response to these changes, yet speculated differently on their cause, without claiming to have identified a growth and remodeling mechanism. Dal-Bianco et al. suggested that mitral leaflet growth occurred in response to stress, whereas Rausch et al. speculated that stretch was driving leaflet growth.

Stretch vs. stress

Though the two in vivo studies had contrasting thoughts on the underlying cause, it is interesting to note that they found similar growth and remodeling outcomes in mitral valves. Naturally, stress and stretch relate through constitutive laws, so changing one leads to changes in the other. This might be the reason that stress and stretch are often used interchangeably in the aforementioned two studies, and in many others in the literature. This would pose no problem in a linear isotropic material, as stress and stretch would relate proportionally in all directions. However, the mechanical behavior of native heart valves is highly nonlinear and anisotropic (Figs. 2.1 and 2.3), with the leaflets being much stiffer in the circumferential direction. Therefore, a small change in leaflet circumferential stretch can lead to a large change in circumferential stress. Conversely, a large change in radial leaflet stretch could only result in a small increase in radial stress.

To the best of our knowledge, previous studies never directly compared the time course of changes in different mechanical quantities such as stretch and stress. We therefore believe that our study, for the first time, provides clear evidence of a stretch mechanical homeostasis in native heart valves – at least on the tissue scale.

7.2.3 Beyond the tissue scale

Cells are believed to drive tissue growth and remodeling

The evidence we provided of a stretch-driven mechanical homeostasis on the tissue scale raises the question through which mechanism it is maintained. As discussed briefly in Section 1.2.2, the cells residing in the ECM of cardiovascular tissues, in this case valvular interstitial cells, are believed to be responsible for maintaining mechanical homeostasis. These cells can secrete important ECM components such as collagen, elastin, and GAGs, as well as metalloproteinases (MMPs) that degrade these components [160]. Moreover, the secretion of these proteins is affected by changes in the cell's mechanical environment [33,34,94,103,133,189].

The molecular signaling pathways that govern the secretion of ECM proteins and MMPs are highly complex and outside the scope of this thesis; the interested reader is referred to the comprehensive reviews by Chiquet et al. [34] and Hoffman et al. [94]. Most important in the context of tissue growth and remodeling is to know what mechanical cue(s) activate(s) these pathways.

A cellular mechanism to sense changes in mechanical environment

The concept of mechanical homeostasis implies that there is a cellular mechanism that senses changes in the cell's mechanical environment and subsequently initiates the signaling cascades responsible for ECM production or degradation. Such a sensing mechanism is thought to be mediated by mechanically-induced conformation changes of cellular proteins. A change in protein conformation can expose certain binding sites that initiate cellular signaling pathways which mediate secretion of ECM proteins.

Thus, could one conclude that the stretch homeostasis that we found in native heart valves indicates that the 'mechanical sensor' of vascular interstitial cells senses stretch? Not necessarily, as cells have different structural and mechanical properties than the ECM, so the stresses and strains that they experience may differ from those on the tissue scale. However, recent findings in mitral valves indicated that valvular interstitial cellular deformation directly correlates with overall tissue deformation[10].

The literature is divided on the existence of a possible 'cellular stretch sensor, with sound arguments having been made both for and against. On the one hand, Omens [169] postulated that "it is likely that any cellular transducer is actually a strain or deformation transducer. This is certainly the case for man-made force gauges, which detect stress or force indirectly through the deformation of a compliant structure." On the other hand, Humphrey [100] argued that the same can be said for stretch, as a stretch can only be measured when knowing a reference configuration, something that is hard to experimentally define in native cardiovascular tissues as they are never in an unloaded state. Tissue growth only complicates this problem, as noted by Cowin [36]: "The question is one of gage length. If the gage length is changing, how can one measure strain?".

Hence, neither stress, stretch, or other mechanical quantities, are straight-forward to measure by even the most advanced men-made equipment, so the question remains how cells would be able to sense any of these (or strain energy density, strain rate, etc.). Finding conclusive evidence for a (sub)cellular mechanism that modulates growth and remodeling would involve measuring these mechanical constituents on the subcellular scale, which remains a daunting task. Provided that evidence actually exists, with Humphrey [100] arguing: "Stress and strain are merely convenient mathematical concepts; they are not unique observables or physical quantities. (...) Why should we expect cells to sense directly and respond to these mathematical constructs?." Nevertheless, based on the growing body of evidence, including this thesis, that show a correlation between mechanical factors on the tissue scale and tissue growth and remodeling, it seems likely that mechanical forces are sensed at some subcellular level. Research on this length scale is required to identify the underlying

processes of mechanically-driven growth and remodeling.

7.2.4 Future perspective of stretch-driven growth and remodeling in native heart valves

Until the (sub)cellular mechanism that drives cardiovascular growth and remodeling is fully unraveled, we have to be satisfied with an empirical correlations between mechanics and growth and remodeling. Such correlation have nonetheless be proven to be relevant for clinical applications; we do not necessarily have to understand how growth and remodeling occur, as long as we can predict their outcome. During the past years, numerical models (see Section 1.4.3) have been developed that can predict growth and remodeling in native tissues. Widely ranging in complexity and methodology, all these models generally aim to drive a certain mechanical constituent towards a homeostatic value via tissue growth and remodeling. Note that the constrained mixture models even take evolving reference states into account for multiple tissue components when attempting to predict tissue growth and remodeling[105].

In native heart valves, we now found that stretch appears to be this driving factor, across different age groups. This finding could drive the development of numerical models for clinical applications.

Clinical example: mitral valve repair

A clinical application for numerical models of growth and remodeling could be mitral valve repair, in which impaired mitral valve leaflet coaptation and flow is restored by ring annuloplasty[28]. This surgical procedure aims to correcting mitral valve insufficiency by implanting an annuloplasty device at the native annulus. The recurrence rate of mitral valve insufficiency is 60%[149] three to five years after surgery. This recurrence is believed to be caused by adverse leaflet growth and remodeling in response to a strain field that is changed by the adjusted annulus shape[10]. Several annuloplasty devices are available to surgeons, yet it remains unclear which device best suits each patient's needs. Stretch-driven computational models could predict leaflet growth and remodeling in response to this surgical procedure, and thus aid surgeons in selecting an annuloplasty device which would optimize leaflet growth and remodeling. Additionally, computational models of growth and remodeling could guide the design of new annuloplasty devices.

7.3 Growth and remodeling in engineered cardiovascular tissues

After we identified that growth and remodeling in native heart valves appear to maintain a mechanical stretch homeostasis, we set out to investigate if a similar homeostatic mechanism emerged in engineered cardiovascular tissues under the influence of different scaffold thicknesses (Chapter 6). Relatively thin and thick scaffolds (0.31 and 0.47 mm, respectively) were used to culture engineered constructs under dynamic pressure conditions (Chapter 4), during which their geometrical and mechanical properties were quantified nondestructively (Chapter 5). A stable mechanical state was reached in both relatively thin and thick scaffolds, with significantly different end-stage values for

elastic stretch, stress, and strain energy density between the two groups. Interestingly, a geometrically stable state was only reached for the thicker constructs, while the thinner constructs continuously dilated. These findings are promising for the field of tissue engineering, as they provide reasonable grounds to believe that well-designed scaffolds could produce engineered tissue replacements that remain mechanically and geometrically stable in vivo.

7.3.1 The importance of scaffold design

The continuous dilation of the thinner scaffolds that we observed in vitro (Fig. 6.1) would lead to aneurysm formation in engineered vascular grafts. Aneurysm formation has emerged as a common issue in previous in vivo studies and eventually leads to graft failure[118,134,147]. It is therefore of paramount importance to prevent this from occurring in vivo.

To the best of our knowledge, no in vivo studies have been performed in which different scaffold thicknesses were compared while keeping the other geometrical parameters constant. However, Kluin et al.[121] recently implanted a valvular graft made from the same scaffold material as in our study in the pulmonary position in a sheep model. In agreement with our study, they observed a constant tissue length over time at similar loading pressures (3.3 vs. 4 kPa) and initial scaffold thicknesses (0.4 vs. 0.47 mm, compared to the thicker group in this study). Moreover, the tissue formation in both studies was very similar, with elastin and thick collagen bundle formation on the pressurized side of the samples. So, relatively thicker scaffolds could indeed provide the foundation for a stable engineered tissue in vivo.

Scaffold plastic deformation

Mechanical fatigue tests of the scaffold material indicated that continuous construct dilation in the thinner scaffolds was mainly governed by plastic deformation of the scaffold material (Fig. 6.3). Unfortunately, most natural and synthetic electrospun scaffolds that are currently used for cardiovascular tissue engineering[23] are prone to such plastic deformation. Until this issue is resolved, increasing scaffold thickness provides a way of limiting, or possibly eliminating, plastic deformation. With relatively thicker scaffolds, scaffold stress and strain are lower for a given pressure. This consequently leads to less plastic deformation, and can potentially enable cell-induced prestretch (which was not observed in our in vitro study) to counteract permanent tissue dilation in vivo. A computational study by Loerakker et al.[137] indicated that the latter is only possible for lower tissue deformations, which would indeed be the case if opting for thicker scaffolds.

Scaffold design parameters

In this thesis, we investigated the effect of scaffold thickness on growth and remodeling of engineered tissues. Clearly, other scaffold parameters (e.g. fiber diameter and alignment, chemical composition, and stiffness) could have similar impacts. All these parameters can alter the scaffolds me-

chanical properties and thus influence not only the amount of plastic deformation that could occur, but also growth and remodeling. A wider study could be performed in which scaffold design parameters are systematically perturbed using our bioreactor. To reduce the number of perturbations, parameter values of interest could be identified a priori by a numerical model, as shown by Miller et al. [154].

7.3.2 Possible consequences of different mechanical states

In contrast to the geometry of the engineered tissues, the mechanics of the thick *and* thin engineered constructs reached a stable state within the time span of our in vitro experiment. Yet, the final states were significantly different between the two scaffold groups (Fig. 6.2). The mechanical constituents that we quantified, stretch [10,32,45,167], stress [66,104,214,224], strain energy density [40,232], and stiffness [14,66,202], have all been associated with mechanical homeostasis in several tissue types. Aside from assessing if a mechanical homeostasis was present in engineered cardiovascular tissues, we also aimed to identify what mechanical metric would determine homeostasis, similar to the native heart valve study. However, no clear evidence was found for just a single one of these factors determining tissue homeostasis in engineered cardiovascular tissues. Instead, all of the mechanical quantities were found to reach a steady state, albeit a different one for each scaffold thickness (Fig. 6.2).

We hypothesize that these (different) apparently stable mechanical states may may not necessarily lead to tissue homeostasis. For instance, when the tissue stretch is too high (e.g. due to low tissue thickness), growth and remodeling may not be able to recover the stretch to a homeostatic value that is located at a much lower stretch. Instead, excessive growth and remodeling may occur as the tissue attempts to, but is unable to, reach mechanical homeostasis. Thus, differences in any of the mechanical measures that we quantified could lead to different long-term growth and remodeling outcomes, which could prove to be essential in vivo.

7.3.3 Bringing tissue engineering forward: combining experimental data with computational predictions

The geometric and mechanical stable states that were observed are promising for cardiovascular tissue engineering. Yet, as discussed in the previous section, this does not necessarily mean that a long-term tissue homeostasis will be established in vivo. A longer in vitro experiment would be required to gain more insight in long-term remodeling, unfortunately this is beyond the capabilities of our current system. Alternatively, computational models could be used to predict long-term growth and remodeling of engineered cardiovascular tissues. The short-term growth and remodeling predictions of such a model could be calibrated using our in vitro results. There ar4 also several in vivo studies who may provide a less comprehensive data set, but crucial insights in long-term in vivo tissue state of tissue-engineered heart valves [57,68,85,121,183,200,206] and vascular grafts and arteries [15,118,134,147,222].

Most recently, a computationally inspired tissue-engineered heart valve design [135,197] was implanted as pulmonary valve replacement in a sheep model and monitored for one year [60]. Not only did these valves feature long-term in vivo performance and remodeling comparable to native heart valves, their remodeling was correctly predicted by the computational model [136]. Their model currently includes mechanically-driven cellular traction forces and collagen alignment, but growth is yet to be included in order to predict longer term adaptation. This would be particularly relevant when predicting development of engineered tissues in pediatric patients, who still undergo somatic growth. Nevertheless, these results highlight the potency of combining numerical models with experimental data in order to improve the design and functionality of engineered tissues. Our in vitro setup can be a valuable tool for calibrating numerical models of growth and remodeling and bring the field of tissue engineering forward by improving the design of these novel prostheses.

7.4 Growth and remodeling in native and engineered cardiovascular tissues

In the previous sections, we discussed growth and remodeling in both native and engineered tissues. In native tissues, we found evicence of a stretch homeostasis in human native semilunar heart valves. The most convincing evidence was the similarity in tissue stretch between the aortic and pulmonary valves and with age. In contrast, the Cauchy stress differed significantly between the aortic and pulmonary valve, with the stress continuously increasing with age in the aortic valve. Interestingly, the results of the engineered tissues in our vitro experiment indicated differences in tissue stretch *and* stress (and strain energy density) between engineered constructs with different thicknesses, with only small changes in all mechanical constituents during development. So, although the mechanical state of the engineered tissues appeared to be stable regardless of thickness, in contrast to native heart valves, we found no clear evidence of a single mechanical stretch homeostasis in the engineered cardiovascular tissues. Moreover, we believe that the engineered tissues may not yet have reached homeostasis, as histology revealed immature tissue areas at the end of the experiment (Fig. 6.5). In the next three sections, we discuss three major differences that may have caused these contradictions: cell type, the presence of a synthetic scaffold, and time scale.

7.4.1 Cell type

The most obvious difference between the engineered tissues and native heart valves might be the cells, which ultimately govern growth and remodeling. The cells that were used in Chapters 4-6 to engineer cardiovascular constructs are healthy cells originating from the human vena saphena. These cells have been previously characterized as myofibroblasts, and were found to be contractile and able to produce abundant amounts of ECM [156]. They have been widely used for in vitro studies in our lab [49,69,191,192,230,231]. In the native heart valves, the cells that are mainly responsible for ECM production and maintenance are valvular interstitial cells. These cells can either have a myofibrob-

last or fibroblast phenotype [3,177], the latter of which is the predominant phenotype during postnatal development. It is possible that these different cell types feature differences in the mechanosensitive pathways that govern tissue growth and remodeling (Section 7.2.3). Moreover, differences in cellular structures can lead to different mechanical properties and consequently cause differences in the mechanical loads that they perceive. A stiffer cell will be more sensitive to small changes in tissue stress than a more compliant one, as, for instance, only a small change in cell strain can lead to a relatively big change in stress. This will subsequently affect tissue growth and remodeling that is observed on the tissue scale.

7.4.2 Presence of scaffold material

The scaffold that was used to engineer cardiovascular tissues in Chapter 6 consisted of slow-degrading PCL-BU. This scaffold material did not degrade significantly within the timespan of the experiment and was relatively stiffer than the neo-tissue that was formed during dynamic culture [7,26]. The scaffold material could therefore have dominated the mechanical behavior of the engineered tissues. Consequently, this may have prevented tissue growth and remodeling from establishing a mechanical homeostasis similar to the one found in the native heart valves.

In Chapter 4, we attempted to circumvent this issue by culturing tissues using a rapidly degrading PGA scaffold. Unfortunately, the rapid degradation of this scaffold lead to failure in the majority of the engineered constructs before a stable tissue was formed by the cells. An alternative approach would be to oxidatively degrade the PCL-BU scaffold after a stable tissue has been formed, thus eliminating the scaffold's mechanical integrity [26] and simulating long-term in vivo growth and remodeling, where the scaffold will eventually be degraded.

7.4.3 A matter of time

The engineered cardiovascular tissues were cultured for a total of five weeks, of which three were dynamic culture. This time span is almost negligible compared to the many years that set apart the native valves that were analyzed. In vitro, the pressure was increased from 0 to 4 kPa within two days, while the native transvalvular pressure changes only ever so slowly during physiological postnatal development (Fig. 2.2). One could therefore hypothesize that the native valves are always in homeostasis, as the slow temporal changes of the valves' mechanical environment give growth and remodeling ample time to restore any possible deviations from homeostatic stretch. In contrast, the rapid changes that were imposed on the engineered tissues may lead to different growth and remodeling responses, or even imply that these tissues did not (yet) reach homeostasis.

Recent computational studies suggest growth and remodeling are influenced by the rate of change of external loading. In their constrained mixture model (Section 1.4.3), Ramachandra et al. predicted that gradual (3-8 days), rather than step changes, of pressure and flow ameliorates maladaptation [178,179]. In accordance with experimental studies [44,224], they concluded that maladaptation was likely caused by an insufficient rate of matrix production. Increasing the pressure in the bioreactor

from 0 to 4 kPa within 2 days therefore may have influenced the development of our engineered tissues. A more gradual pressure increase should therefore be considered in future experiments. This might not be an issue for in situ tissue engineering, as tissue will be developing while constantly being subjected to a reasonable constant physiological pressure.

7.5 Future outlook for the bioreactor

In Chapters 4 and 5, we presented an in vitro platform to study tissue growth and remodeling in engineered cardiovascular tissues. The main novelty of this system is its potential to nondestructively quantify the mechanical properties of the engineered tissues during development. This novel platform was used in Chapter 6 to investigate how scaffold design effects geometrical and mechanical changes in engineered cardiovascular tissues, and how it is dependent on the scaffold design, as discussed in the previous section. In this case we studied variations in scaffold thickness. By changing only this simple scaffold design parameter, we demonstrated differences in various mechanical measures (elastic stretch, stress, strain energy density, and stiffness) of engineered cardiovascular tissues. Clearly, the influence of various scaffold parameters, other than scaffold thickness, on growth and remodeling of engineered tissues could be easily studied using our system. Moreover, in Section 7.3.3 the bioreactors potential value for the development of numerical growth and remodeling models was discussed. Yet, the bioreactor's versatile design itself also allows for other modifications, which has promising perspectives for future research.

7.5.1 Bioreactor modifications

Thus far, we only cultured isotropic tissues under uniform mechanical loading in our bioreactor system. Yet, native arteries and heart valves are highly anisotropic and feature heterogeneous stress and strain fields. To improve our system, we could therefore opt to change the design of the sample holders (Fig. 4.3) from a circular to a, for instance, elliptical shape. This would impose larger strains and stresses in the short axis compared to the long axis of the ellipse, and could therefore lead to different growth and remodeling outcomes on these two directions. Alternatively, an anisotropic rather than isotropic scaffold fiber alignment could be used, which could guide cell and collagen via contact guidance[88]. It would also be interesting to use the system to evaluate those options simultaneously and study the resulting cellular and collagen orientation, as mechanical cues have been found to conflict with contact guidance in strain-based in vitro experiments[49,69].

Another direction could see the bioreactor being used for studying growth and remodeling of (engineered) cardiac tissues, to study the adverse growth and remodeling that occurs during dilated cardiomyopathy (by increasing medium volume), and hypertrophic cardiomyopathy (by increasing pressure). Cardiac growth and remodeling can occur well within a time span of three weeks[112,161,198], so the effects could potentially be observed within the maximum dynamic culture time of the current system.

7.5.2 Pathologies and pharmocology

The focus of this thesis was to study the effect of physiological changes in the mechanical environment on growth and remodeling. Interestingly, one could also use the bioreactor to study growth and remodeling under pathological situations. In our current studies, we used healthy myofibroblast-like cells from the human vena saphena to engineer cardiovascular constructs, since they are representative of cells that are found in healthy human arteries[156]. Using different cell types, our system can also be used as to study the effect of pathologies on cardiovascular growth and remodeling. One example would be the use of Lmna knockout fibroblast cells. A mutation in the Lmna gene is typically found in patients suffering from diseases such as muscle dystrophy and cardiomyopathy[25,110,228]. Fibroblasts with this genetic defect lack the structural components connecting them with the ECM, and therefore cannot 'sense' their mechanical environment, leading to an impaired capacity for tissue growth and remodeling. By culturing cardiovascular constructs with these cells in our bioreactor, we could investigate tissue growth and remodeling in patients suffering from muscle dystrophy and cardiomyopathy.

From a clinical perspective, it is also important to investigate the influence that pharmocological treatments have on cardiovascular growth and remodeling. After all, the majority of the patients suffering from cardiovascular diseases are prescribed such drug treatments. For instance, hypertensive patients often receive vasodilators to decrease blood pressure[74]. These drugs target specific cellular pathways that are important for cardiovascular growth and remodeling, such as the RHO-associated protein kinase pathway[103,236]. By introducing both current and potential future drug components in the medium of our bioreactor system, we could quantify their effect on overall tissue growth and remodeling. This may be particularly relevant for patients that in the future may receive tissue-engineered prostheses, as they often suffer from concomitant cardiovascular diseases that require drug treatment.

7.6 Main conclusions

This thesis focused on the biomechanics of growth and remodeling in native and engineered cardiovascular tissues. Its overall aims were (1) to identify what mechanical quantity determines mechanical homeostasis in native cardiovascular tissues, in this case heart valves, and (2) to investigate if mechanical homeostasis could also be established in engineered cardiovascular tissues.

A stretch-driven homeostasis was identified in native semilunar heart valves, and it was found that growth and remodeling play contradicting roles in preserving this homeostasis during physiological development. Whilst not providing definite insights in the underlying mechanisms of growth and remodeling, these empirical findings can drive the development of computational models that could lead to the development of new medical devices and therapies to treat valvular disease.

Shifting gears to engineered cardiovascular tissues, we developed and validated a bioreactor system with an integrated nondestructive mechanical characterization method. This novel in vitro plat-

form was used to demonstrate that a geometrical and mechanical stable state could be established in engineered cardiovascular tissues, albeit dependent on the scaffold design, in this case thickness. Evidence of such a stable state in engineered cardiovascular tissues, similar to the native tissues that they ought to replace, is promising for the field of tissue engineering.

References

[1] Ackermann, K., Balling, G., Eicken, A., Günther, T., Schreiber, C., & Hess, J. (2007). Replacement of the systemic atrioventricular valve with a mechanical prosthesis in children aged less than 6 years: late clinical results of survival and subsequent replacement. *The Journal of Thoracic and Cardiovascular Surgery*, 134(3), 750–756.

[2] Aggarwal, A., Pouch, A. M., Lai, E., Lesicko, J., Yushkevich, P. A., Gorman Iii, J. H., Gorman, R. C., & Sacks, M. S. (2016). In-vivo heterogeneous functional and residual strains in human aortic valve leaflets. *Journal of Biomechanics*, 49(12), 2481–2490.

[3] Aikawa, E., Whittaker, P., Farber, M., Mendelson, K., Padera, R. F., Aikawa, M., & Schoen, F. J. (2006). Human semilunar cardiac valve remodeling by activated cells from fetus to adult: implications for postnatal adaptation, pathology, and tissue engineering. *Circulation*, 113(10), 1344–1352.

[4] Aldous, I. G., Lee, J. M., & Wells, S. M. (2010). Differential Changes in the Molecular Stability of Collagen from the Pulmonary and Aortic Valves During the Fetal-to-Neonatal Transition. *Annals of Biomedical Engineering*, 38(9), 3000–3009.

[5] Ali, M. L., Kumar, S. P., Bjornstad, K., & Duran, C. M. (1996). The sheep as an animal model for heart valve research. *Cardiovascular Surgery*, 4(4), 543–549.

[6] Ambrosi, D., Ateshian, G. A., Arruda, E. M., Cowin, S. C., Dumais, J., Goriely, A., Holzapfel, G. A., Humphrey, J. D., Kemkemer, R., Kuhl, E., Olberding, J. E., Taber, L. A., & Garikipati, K. (2011). Perspectives on biological growth and remodeling. *Journal of the Mechanics and Physics of Solids*, 59(4), 863–883.

[7] Argento, G., Simonet, M., Oomens, C. W. J., & Baaijens, F. P. T. (2012). Multi-scale mechanical characterization of scaffolds for heart valve tissue engineering. *Journal of Biomechanics*, 45(16), 2893–2898.

[8] Ascenzi, A. (1993). Biomechanics and Galileo Galilei. *Journal of Biomechanics*, 26(2), 95–100.

[9] Avril, S., Badel, P., & Duprey, A. (2010). Anisotropic and hyperelastic identification of in vitro human arteries from full-field optical measurements. *Journal of Biomechanics*, 43(15), 2978–2985.

[10] Ayoub, S., Lee, C.-H., Driesbaugh, K. H., Anselmo, W., Hughes, C. T., Ferrari, G., Gorman, R. C., Gorman, J. H., & Sacks, M. S. (2017). Regulation of valve interstitial cell homeostasis by mechanical deformation: implications for heart valve disease and surgical repair. *Journal of The Royal Society Interface*, 14(135).

[11] Balguid, A., Rubbens, M. P., Mol, A., Bank, R. A., Bogers, A. J. J. C., Van Kats, J. P., De Mol, B. A. J. M., Baaijens, F. P. T., & Bouten, C. V. C. (2007). The role of collagen cross-links in biomechanical behavior of human aortic heart valve leaflets - Relevance for tissue engineering. *Tissue Engineering*, 13(7), 1501–1511.

[12] Bashey, R. I., Torii, S., & Angrist, A. (1967). Age-Related Collagen and Elastin Content of Human Heart Valves. *Journal of gerontology*, 22(2), 203–208.

[13] Bayer, I. M., Adamson, S. L., & Langille, B. L. (1999). Atrophic remodeling of the artery-cuffed artery. *Arteriosclerosis, Thrombosis, and Vascular Biology*, 19(6), 1499–1505.

[14] Bellini, C., Bersi, M. R., Caulk, A. W., Ferruzzi, J., Milewicz, D. M., Ramirez, F., Rifkin, D. B., Tellides, G., Yanagisawa, H., & Humphrey, J. D. (2017). Comparison of 10 murine models reveals a distinct biomechanical phenotype in thoracic aortic aneurysms. *Journal of The Royal Society Interface*, 14(130).

[15] Bersi, M. R., Bellini, C., Wu, J., Montaniel, K. R. C., Harrison, D. G., & Humphrey, J. D. (2016). Excessive Adventitial Remodeling Leads to Early Aortic Maladaptation in Angiotensin-Induced Hypertension. *Hypertension (Dallas, Tex. : 1979)*, 67(5), 890–896.

[16] Bersi, M. R., Ferruzzi, J., Eberth, J. F., Gleason, R. L. J., & Humphrey, J. D. (2014). Consistent Biomechanical Phenotyping of Common Carotid Arteries from Seven Genetic, Pharmacological, and Surgical Mouse Models. *Annals of Biomedical Engineering*, 42(6), 1207–1223.

[17] Besnard, G., Hild, F., & Roux, S. (2006). "Finite-element" displacement fields analysis from digital images: application to Portevin–Le Châtelier bands. *Experimental Mechanics*, 46, 789–803.

[18] Best, C. A., Fukunishi, T., Drews, J., Khosravi, R., Hor, K., Mahler, N., Yi, T., Humphrey, J. D., Johnson, J., Breuer, C. K., & Hibino, N. (2018). Oversized biodegradable arterial grafts promote enhanced neointimal tissue formation. *Tissue Engineering Part A*, (pp. ten.TEA.2017.0483).

[19] Billiar, K. L. & Sacks, M. S. (2000a). Biaxial mechanical properties of the native and glutaraldehyde-treated aortic valve cusp: Part II – A structural constitutive model. *Journal of Biomechanical Engineering*, 122(4), 327–335.

[20] Billiar, K. L. & Sacks, M. S. (2000b). Biaxial mechanical properties of the natural and glutaraldehyde treated aortic valve cusp: Part I – Experimental results. *Journal of Biomechanical Engineering*, 122(1), 23–30.

[21] Boerboom, R. A., Driessen, N., & Bouten, C. (2003). Finite element model of mechanically induced collagen fiber synthesis and degradation in the aortic valve. *Annals of biomedical ....*

[22] Boerboom, R. A., Krahn, K. N., Megens, R. T. A., van Zandvoort, M. A. M. J., Merkx, M., & Bouten, C. V. C. (2007). High resolution imaging of collagen organisation and synthesis using a versatile collagen specific probe. *Journal of Structural Biology*, 159(3), 392–399.

[23] Bouten, C. V. C., Dankers, P. Y. W., Driessen-Mol, A., Pedron, S., Brizard, A. M. A., & Baaijens, F. P. T. (2011). Substrates for cardiovascular tissue engineering. *Advanced Drug Delivery Reviews*, 63(4), 221–241.

[24] Brennan, M. P., Dardik, A., Hibino, N., Roh, J. D., Nelson, G. N., Papademitris, X., Shinoka, T., & Breuer, C. K. (2008). Tissue-engineered vascular grafts demonstrate evidence of growth and development when implanted in a juvenile animal model. *Annals of Surgery*, 248(3), 370–376.

[25] Broers, J. L. V., Ramaekers, F. C. S., Bonne, G., Ben Yaou, R., & Hutchison, C. J. (2006). Nuclear lamins: Laminopathies and their role in premature ageing. *Physiological Reviews*, 86(3), 967–1008.

[26] Brugmans, M. C. P., Soñtjens, S. H. M., Cox, M. A. J., Nandakumar, A., Bosman, A. W., Mes, T., Janssen, H. M., Bouten, C. V. C., Baaijens, F. P. T., & Driessen-Mol, A. (2015). Hydrolytic and oxidative degradation of electrospun supramolecular biomaterials: In vitro degradation pathways. *Acta Biomaterialia*, 27, 21–31.

[27] Buganza Tepole, A., Ploch, C. J., Wong, J., Gosain, A. K., & Kuhl, E. (2011). Growing skin: A computational model for skin expansion in reconstructive surgery. *Journal of the Mechanics and Physics of Solids*, 59(10), 2177–2190.

[28] Carpentier, A., Chauvaud, S., Fabiani, J. N., Deloche, A., Relland, J., Lessana, A., Dallaines, C., Blondeau, P., Piwnica, A., & Dubost, C. (1980). Reconstructive Surgery of Mitral-Valve Incompetence - 10-Year Appraisal. *Journal of Thoracic and Cardiovascular Surgery*, 79(3), 338–&.

[29] Cesarone, C. F., Bolognesi, C., & Santi, L. (1979). Improved microfluorometric DNA determination in biological material using 33258 Hoechst. *Analytical Biochemistry*, 100(1), 188–197.

[30] Chai, C.-K., Speelman, L., Oomens, C. W. J., & Baaijens, F. P. T. (2014). Compressive mechanical properties of atherosclerotic plaques–indentation test to characterise the local anisotropic behaviour. *Journal of Biomechanics*, 47(4), 784–792.

[31] Chaput, M., Handschumacher, M. D., Guerrero, J. L., Holmvang, G., Dal-Bianco, J. P., Sullivan, S., Vlahakes, G. J., Hung, J., Levine, R. A., & Leducq Foundation MITRAL Transatlantic Network (2009). Mitral leaflet adaptation to ventricular remodeling: prospective changes in a model of ischemic mitral regurgitation. *Circulation*, 120(suppl 1), S99–103.

[32] Chaput, M., Handschumacher, M. D., Tournoux, F., Hua, L., Guerrero, J. L., Vlahakes, G. J., & Levine, R. A. (2008). Mitral leaflet adaptation to ventricular remodeling: occurrence and adequacy in patients with functional mitral regurgitation. *Circulation*, 118(8), 845–852.

[33] Chiquet, M. (1999). Regulation of extracellular matrix gene expression by mechanical stress. 18(5), 417–426.

[34] Chiquet, M., Gelman, L., Lutz, R., & Maier, S. (2009). From mechanotransduction to extracellular matrix gene expression in fibroblasts. *Biochimica et Biophysica Acta (BBA) - Molecular Cell Research*, 1793(5), 911–920.

[35] Chuong, C. J. & Fung, Y. C. (1986). On Residual Stresses in Arteries. *Journal of Biomechanical Engineering*, 108(2), 189–192.

[36] Cowin, S. C. (1996). Strain or deformation rate dependent finite growth in soft tissues. *Journal of Biomechanics*, 29(5), 647–649.

[37] Cox, M. A. J., Driessen, N. J. B., Boerboom, R. A., Bouten, C. V. C., & Baaijens, F. P. T. (2008). Mechanical characterization of anisotropic planar biological soft tissues using finite indentation: experimental feasibility. *Journal of Biomechanics*, 41(2), 422–429.

[38] Cox, M. A. J., Driessen, N. J. B., Bouten, C. V. C., & Baaijens, F. P. T. (2006). Mechanical characterization of anisotropic planar biological soft tissues using large indentation: a computational feasibility study. *Journal of Biomechanical Engineering*, 128(3), 428–436.

[39] Cyron, C. J., Aydin, R. C., & Humphrey, J. D. (2016). A homogenized constrained mixture (and mechanical analog) model for growth and remodeling of soft tissue. *Biomechanics and Modeling in Mechanobiology*, 15(6), 1389–1403.

[40] Cyron, C. J. & Humphrey, J. D. (2014). Vascular homeostasis and the concept of mechanobiological stability. *International Journal of Engineering Science*, 85(C), 203–223.

[41] Cyron, C. J. & Humphrey, J. D. (2017). Growth and Remodeling of Load-Bearing Biological Soft Tissues. *Meccanica*, 52(3), 645–664.

[42] Cyron, C. J., Wilson, J. S., & Humphrey, J. D. (2014). Mechanobiological stability: a new paradigm to understand the enlargement of aneurysms? *Journal of the Royal Society Interface*, 11(100), 20140680–20140680.

[43] Dahl, S. L. M., Vaughn, M. E., Hu, J.-J., Driessen, N. J. B., Baaijens, F. P. T., Humphrey, J. D., & Niklason, L. E. (2008). A Microstructurally Motivated Model of the Mechanical Behavior of Tissue Engineered Blood Vessels. *Annals of Biomedical Engineering*, 36(11), 1782–1792.

[44] Dajnowiec, D. & Langille, B. L. (2007). Arterial adaptations to chronic changes in haemodynamic function: coupling vasomotor tone to structural remodelling. *Clinical Science*, 113(1), 15–23.

[45] Dal-Bianco, J. P., Aikawa, E., Bischoff, J., Guerrero, J. L., Handschumacher, M. D., Sullivan, S., Johnson, B., Titus, J. S., Iwamoto, Y., Wylie-Sears, J., Levine, R. A., & Carpentier, A. (2009). Active adaptation of the tethered mitral valve: insights into a compensatory mechanism for functional mitral regurgitation. *Circulation*, 120(4), 334–342.

[46] Dasi, L. P., Simon, H. A., Sucosky, P., & Yoganathan, A. P. (2009). Fluid mechanics of artificial heart valves. *Clinical and Experimental Pharmacology & Physiology*, 36(2), 225–237.

[47] Davis, F. M., Luo, Y., Avril, S., Duprey, A., & Lu, J. (2015). Pointwise characterization of the elastic properties of planar soft tissues: application to ascending thoracic aneurysms. *Biomechanics and Modeling in Mechanobiology*, 14(5), 967–978.

[48] Davis, F. M., Luo, Y., Avril, S., Duprey, A., & Lu, J. (2016). Local mechanical properties of human ascending thoracic aneurysms. *Journal of the Mechanical Behavior of Biomedical Materials*, 61, 235–249.

[49] de Jonge, N., Kanters, F. M. W., Baaijens, F. P. T., & Bouten, C. V. C. (2013). Strain-induced collagen organization at the micro-level in fibrin-based engineered tissue constructs. *Annals of Biomedical Engineering*, 41(4), 763–774.

[50] Delfino, A., Stergiopulos, N., Moore, J. E., & Meister, J. J. (1997). Residual strain effects on the stress field in a thick wall finite element model of the human carotid bifurcation. *Journal of Biomechanics*, 30(8), 777–786.

[51] Delgadillo, J. V. & Delorme, S. (2010). Effect of freezing on the biaxial mechanical properties of arterial samples. *Journal of Biomechanical Engineering*.

[52] Deshpande, V. S., McMeeking, R. M., & Evans, A. G. (2007). A model for the contractility of the cytoskeleton including the effects of stress-fibre formation and dissociation. *Proceedings of the Royal Society A: Mathematical, Physical and Engineering Sciences*, 463(2079), 787–815.

[53] Dijkman, P. E., Driessen-Mol, A., Frese, L., Hoerstrup, S. P., & Baaijens, F. P. T. (2012). Decellularized homologous tissue-engineered heart valves as off-the-shelf alternatives to xeno- and homografts. *Biomaterials*, 33(18), 4545–4554.

[54] Driessen, N. J., Bouten, C. V., & Baaijens, F. P. T. (2005). A structural constitutive model for collagenous cardiovascular tissues incorporating the angular fiber distribution. *Journal of Biomechanical Engineering*, 127, 494–503.

[55] Driessen, N. J. B., Cox, M. A. J., Bouten, C. V. C., & Baaijens, F. P. T. (2008). Remodelling of the angular collagen fiber distribution in cardiovascular tissues. *Biomechanics and Modeling in Mechanobiology*, 7(2), 93–103.

[56] Driessen, N. J. B., Mol, A., Bouten, C. V. C., & Baaijens, F. P. T. (2007). Modeling the mechanics of tissue-engineered human heart valve leaflets. *Journal of Biomechanics*, 40(2), 325–334.

[57] Driessen-Mol, A., Emmert, M. Y., Dijkman, P. E., Frese, L., Sanders, B., Weber, B., Cesarovic, N., Sidler, M., Leenders, J., Jenni, R., Grünenfelder, J., Falk, V., Baaijens, F. P. T., & Hoerstrup, S. P. (2014). Transcatheter implantation of homologous "off-the-shelf" tissue-engineered heart valves with self-repair capacity: long-term functionality and rapid in vivo remodeling in sheep. *Journal of the American College of Cardiology*, 63(13), 1320–1329.

[58] Dumont, K., Yperman, J., Verbeken, E., Segers, P., Meuris, B., Vandenberghe, S., Flameng, W., & Verdonck, P. R. (2002). Design of a new pulsatile bioreactor for tissue engineered aortic heart valve formation. *Artificial Organs*, 26(8), 710–714.

[59] Duricki, D. A., Soleman, S., & Moon, L. D. F. (2016). Analysis of longitudinal data from animals with missing values using SPSS. *Nature Protocols*, 11(6), 1112–1129.

[60] Emmert, M. Y., Schmitt, B. A., Loerakker, S., Sanders, B., Spriestersbach, H., Fioretta, E. S., Bruder, L., Brakmann, K., Motta, S. E., Lintas, V., Dijkman, P. E., Frese, L., Berger, F., Baaijens, F. P. T., & Hoerstrup, S. P. (2018). Computational modeling guides tissue-engineered heart valve design for long-term in vivo performance in a translational sheep model. *Science Translational Medicine*, 10(440).

[61] Engelmayr, G. C., Hildebrand, D. K., Sutherland, F., Mayer, J. E., & Sacks, M. S. (2003). A novel bioreactor for the dynamic flexural stimulation of tissue engineered heart valve biomaterials. *Biomaterials*, 24(14), 2523–2532.

[62] Fan, R., Bayoumi, A. S., Chen, P., Hobson, C. M., Wagner, W. R., Mayer, J. E. J., & Sacks, M. S. (2013). Optimal elastomeric scaffold leaflet shape for pulmonary heart valve leaflet replacement. *Journal of Biomechanics*, 46(4), 662–669.

[63] Farndale, R., Buttle, D., & Barrett, A. (1986). Improved quantitation and discrimination of sulphated glycosaminoglycans by use of dimethylmethylene blue. *Biochimica et Biophysica Acta (BBA) - General Subjects*, 883(2), 173–177.

[64] Farrar, E. J., Pramil, V., Richards, J. M., Mosher, C. Z., & Butcher, J. T. (2016). Valve interstitial cell tensional homeostasis directs calcification and extracellular matrix remodeling processes via RhoA signaling. *Biomaterials*, 105, 25–37.

[65] Fernandez, G., Costa, F., Fontan, F., Naftel, D. C., Blackstone, E. H., & Kirklin, J. W. (1989). Prevalence of Reoperation for Pathway Obstruction After Fontan Operation. *The Annals of Thoracic Surgery*, 48(5), 654–659.

[66] Ferruzzi, J., Bersi, M. R., Mecham, R. P., Ramirez, F., Yanagisawa, H., Tellides, G., & Humphrey, J. D. (2016). Loss of Elastic Fiber Integrity Compromises Common Carotid Artery Function: Implications for Vascular Aging. *Artery Research*, 14, 41–52.

[67] Fisher, C. I., Chen, J., & Merryman, W. D. (2013). Calcific nodule morphogenesis by heart valve interstitial cells is strain dependent. *Biomechanics and Modeling in Mechanobiology*, 12(1), 5–17.

[68] Flanagan, T. C., Sachweh, J. S., Frese, J., Schnoering, H., Gronloh, N., Koch, S., Tolba, R. H., Schmitz-Rode, T., & Jockenhoevel, S. (2009). In Vivo Remodeling and Structural Characterization of Fibrin-Based Tissue-Engineered Heart Valves in the Adult Sheep Model. *Tissue Engineering Part A*, 15(10), 2965–2976.

[69] Foolen, J., Deshpande, V. S., Kanters, F. M. W., & Baaijens, F. P. T. (2012). The influence of matrix integrity on stress-fiber remodeling in 3D. *Biomaterials*, 33(30), 7508–7518.

[70] Frangi, A. F., Niessen, W. J., Vincken, K. L., & Viergever, M. A. (1998). Multiscale vessel enhancement filtering. *Medical Image Computing and Computer-Assisted Intervention - Miccai'98*, 1496, 130–137.

[71] Frey, N. & Olson, E. N. (2003). Cardiac hypertrophy: the good, the bad, and the ugly. *Annual Review of Physiology*, 65(1), 45–79.

[72] Fung, Y. C. (1990). Biomechanical Aspects of Growth and Tissue Engineering. In *Biomechanics* (pp. 499–546). New York, NY: Springer, New York, NY.

[73] Fung, Y. C. (1991). What are the residual stresses doing in our blood vessels? *Annals of Biomedical Engineering*, 19(3), 237–249.

[74] Galiè, N., Humbert, M., Vachiery, J.-L., Gibbs, S., Lang, I., Torbicki, A., Simonneau, G., Peacock, A., Noordegraaf, A. V., Beghetti, M., Ghofrani, A., Sanchez, M. A. G., Hansmann, G., Klepetko, W., Lancellotti, P., Matucci, M., McDonagh, T., Pierard, L. A., Trindade, P. T., Zompatori, M., & Hoeper, M. (2015). 2015 ESC/ERS Guidelines for the diagnosis and treatment of pulmonary hypertension. *European Heart Journal*, 37(1), 67–119.

[75] Galilei, G. (1638). *Discorsi e Dimostrazioni Matematiche Intorno a Due Nuove Scienze*. Elzevir, Leiden.

[76] Gasser, T. C., Ogden, R. W., & Holzapfel, G. A. (2006). Hyperelastic modelling of arterial layers with distributed collagen fibre orientations. *Journal of the Royal Society Interface*, 3(6), 15–35.

[77] Genovese, K. (2009). A video-optical system for time-resolved whole-body measurement on vascular segments. *Optics and Lasers in Engineering*, 47(9), 995–1008.

[78] Gerson, C. J., Goldstein, S., & Heacox, A. E. (2009). Retained structural integrity of collagen and elastin within cryopreserved human heart valve tissue as detected by two-photon laser scanning confocal microscopy. *Cryobiology*, 59(2), 171–179.

[79] Gibbons, G. H. & Dzau, V. J. (1994). The Emerging Concept of Vascular Remodeling. *New England Journal of Medicine*, 330(20), 1431–1438.

[80] Glagov, S., Weisenberg, E., Zarins, C. K., Stankunavicius, R., & Kolettis, G. J. (1987). Compensatory Enlargement of Human Atherosclerotic Coronary Arteries. *New England Journal of Medicine*, 316(22), 1371–1375.

[81] Gleason, R. L., Dye, W. W., Wilson, E., & Humphrey, J. D. (2008). Quantification of the mechanical behavior of carotid arteries from wild-type, dystrophin-deficient, and sarcoglycan-δ knockout mice. *Journal of Biomechanics*, 41(15), 3213–3218.

[82] Göktepe, S., Abilez, O. J., & Kuhl, E. (2010a). A generic approach towards finite growth with examples of athlete's heart, cardiac dilation, and cardiac wall thickening. *Journal of the Mechanics and Physics of Solids*, 58(10), 1661–1680.

[83] Göktepe, S., Abilez, O. J., Parker, K. K., & Kuhl, E. (2010b). A multiscale model for eccentric and concentric cardiac growth through sarcomerogenesis. *Journal of Theoretical Biology*, 265(3), 433–442.

[84] Gott, V. L., Alejo, D. E., & Cameron, D. E. (2003). Mechanical heart valves: 50 years of evolution. *The Annals of Thoracic Surgery*.

[85] Gottlieb, D., Kunal, T., Emani, S., Aikawa, E., Brown, D. W., Powell, A. J., Nedder, A., Engelmayr, G. C., Melero-Martin, J. M., Sacks, M. S., & Mayer, J. E. (2010). In vivo monitoring of function of autologous engineered pulmonary valve. *The Journal of Thoracic and Cardiovascular Surgery*, 139(3), 723–731.

[86] Gould, R. A., Chin, K., Santisakultarm, T. P., Dropkin, A., Richards, J. M., Schaffer, C. B., & Butcher, J. T. (2012). Cyclic strain anisotropy regulates valvular interstitial cell phenotype and tissue remodeling in three-dimensional culture. *Acta Biomaterialia*, 8(5), 1710–1719.

[87] Grande-Allen, K. J., Borowski, A. G., Troughton, R. W., Houghtaling, P. L., DiPaola, N. R., Moravec, C. S., Vesely, I., & Griffin, B. P. (2005). Apparently normal mitral valves in patients with heart failure demonstrate biochemical and structural derangements - An extracellular matrix and echocardiographic study. *Journal of the American College of Cardiology*, 45(1), 54–61.

[88] Guido, S. & Tranquillo, R. T. (1993). A methodology for the systematic and quantitative study of cell contact guidance in oriented collagen gels. Correlation of fibroblast orientation and gel birefringence. *Journal of Cell Science*, 105 (Pt 2), 317–331.

[89] Hammer, P. E., Pacak, C. A., Howe, R. D., & del Nido, P. J. (2014). Straightening of curved pattern of collagen fibers under load controls aortic valve shape. *Journal of Biomechanics*, 47(2), 341–346.

[90] Hasan, A., Ragaert, K., Swieszkowski, W., Selimović, Š., Paul, A., Camci-Unal, G., Mofrad, M. R. K., & Khademhosseini, A. (2014). Biomechanical properties of native and tissue engineered heart valve constructs. *Journal of Biomechanics*, 47(9), 1949–1963.

[91] Hayashi, K. (1993). Experimental Approaches on Measuring the Mechanical Properties and Constitutive Laws of Arterial Walls. *Journal of Biomechanical Engineering*, 115(4B), 481–488.

[92] Hoerstrup, S. P., Cummings Mrcs, I., Lachat, M., Schoen, F. J., Jenni, R., Leschka, S., Neuenschwander, S., Schmidt, D., Mol, A., Günter, C., Gössi, M., Genoni, M., & Zund, G. (2006). Functional growth in tissue-engineered living, vascular grafts: follow-up at 100 weeks in a large animal model. *Circulation*, 114(suppl 1), 159–166.

[93] Hoerstrup, S. P., Sodian, R., Daebritz, S., & Wang, J. (2000). Functional living trileaflet heart valves grown in vitro. *Circulation*, 102(suppl 3), III–44–49.

[94] Hoffman, B. D., Grashoff, C., & Schwartz, M. A. (2011). Dynamic molecular processes mediate cellular mechanotransduction. *Nature*, 475(7356), 316–323.

[95] Hoffman, J. & Kaplan, S. (2002). The incidence of congenital heart disease. *Journal of the American College of Cardiology*, 39(12), 1890–1900.

[96] Hollweck, T., Akra, B., Häussler, S., Überfuhr, P., Schmitz, C., Pfeifer, S., Eblenkamp, M., Wintermantel, E., & Eissner, G. (2011). A Novel Pulsatile Bioreactor for Mechanical Stimulation of Tissue Engineered Cardiac Constructs. *Journal of Functional Biomaterials*, 2(4), 107–118.

[97] Holzapfel, G. A., Gasser, T. C., & Ogden, R. W. (2000). A new constitutive framework for arterial wall mechanics and a comparative study of material models. *Journal of Elasticity*, 61, 1–48.

[98] Hu, J.-J., Humphrey, J. D., & Yeh, A. T. (2009). Characterization of Engineered Tissue Development Under Biaxial Stretch Using Nonlinear Optical Microscopy. *Tissue Engineering Part A*, 15(7), 1553–1564.

[99] Huang, C. & Yannas, I. V. (1977). Mechanochemical Studies of Enzymatic Degradation of Insoluble Collagen-Fibers. *Journal of Biomedical Materials Research Part B: Applied Biomaterials*, 11(1), 137–154.

[100] Humphrey, J. D. (2001). Stress, strain, and mechanotransduction in cells. *Journal of Biomechanical Engineering*, 123(6), 638–641.

[101] Humphrey, J. D. (2002). *Cardiovascular solid mechanics: cells, tissues, and organs*. New York, NY: Springer-Verlag.

[102] Humphrey, J. D. (2008). Vascular adaptation and mechanical homeostasis at tissue, cellular, and sub-cellular levels. *Cell Biochemistry and Biophysics*, 50(2), 53–78.

[103] Humphrey, J. D., Dufresne, E. R., & Schwartz, M. A. (2014). Mechanotransduction and extracellular matrix homeostasis. *Nature Reviews Molecular Cell Biology*, 15, 802–812.

[104] Humphrey, J. D., Eberth, J. F., Dye, W. W., & Gleason, R. L. (2009). Fundamental role of axial stress in compensatory adaptations by arteries. *Journal of Biomechanics*, 42(1), 1–8.

[105] Humphrey, J. D. & Rajagopal, K. R. (2002). A constrained mixture model for growth and remodeling of soft tissues. *Mathematical Models & Methods in Applied Sciences*, 12(3), 407–430.

[106] Humphrey, J. D., Schwartz, M. A., Tellides, G., & Milewicz, D. M. (2015). Role of Mechanotransduction in Vascular Biology Focus on Thoracic Aortic Aneurysms and Dissections. *Circulation Research*, 116(8), 1448–1461.

[107] Humphrey, J. D., Wells, P. B., Baek, S., Hu, J. J., McLeroy, K., & Yeh, A. T. (2008). A theoretically-motivated biaxial tissue culture system with intravital microscopy. *Biomechanics and Modeling in Mechanobiology*, 7(4), 323–334.

[108] Hurtado-Aguilar, L. G., Mulderrig, S., Moreira, R., Hatam, N., Spillner, J., Schmitz-Rode, T., Jockenhoevel, S., & Mela, P. (2016). Ultrasound for In Vitro, Noninvasive Real-Time Monitoring and Evaluation of Tissue-Engineered Heart Valves. *Tissue Engineering Part C: Methods*, 22(10), 974–981.

[109] Huszar, G., Maiocco, J., & Naftolin, F. (1980). Monitoring of collagen and collagen fragments in chromatography of protein mixtures. *Analytical Biochemistry*, 105(1), 424–429.

[110] Isermann, P. & Lammerding, J. (2013). Nuclear Mechanics and Mechanotransduction in Health and Disease. *Current Biology*, 23(24), R1113–R1121.

[111] Jawad, H., Ali, N. N., Lyon, A. R., Chen, Q. Z., Harding, S. E., & Boccaccini, A. R. (2007). Myocardial tissue engineering: a review. *Journal of Tissue Engineering and Regenerative Medicine*, 1(5), 327–342.

[112] Jugdutt, B. I., Khan, M. I., Jugdutt, S. J., & Blinston, G. E. (1995). Effect of enalapril on ventricular remodeling and function during healing after anterior myocardial infarction in the dog. *Circulation*, 91(3), 802–812.

[113] Jun, I., Han, H.-S., Edwards, J., & Jeon, H. (2018). Electrospun Fibrous Scaffolds for Tissue Engineering: Viewpoints on Architecture and Fabrication. *International Journal of Molecular Sciences*, 19(3), 745–14.

[114] Kannan, R. Y., Salacinski, H. J., Butler, P. E., Hamilton, G., & Seifalian, A. M. (2005). Current status of prosthetic bypass grafts: A review. *Journal of Biomedical Materials Research Part B: Applied Biomaterials*, 74B(1), 570–581.

[115] Karsaj, I. & Humphrey, J. D. (2012). A multilayered wall model of arterial growth and remodeling. *Mechanics of Materials*, 44, 110–119.

[116] Kasyanov, V., Moreno-Rodriguez, R. A., Kalejs, M., Ozolanta, I., Stradins, P., Wen, X., Yao, H., & Mironov, V. (2013). Age-related analysis of structural, biochemical and mechanical properties of the porcine mitral heart valve leaflets. *Connective Tissue Research*, 54(6), 394–402.

[117] Kerckhoffs, R. C. P., Omens, J., & McCulloch, A. D. (2012). A single strain-based growth law predicts concentric and eccentric cardiac growth during pressure and volume overload. *Mechanics Research Communications*, 42, 40–50.

[118] Khosravi, R., Best, C. A., Allen, R. A., Stowell, C. E. T., Onwuka, E., Zhuang, J. J., Lee, Y.-U., Yi, T., Bersi, M. R., Shinoka, T., Humphrey, J. D., Wang, Y., & Breuer, C. K. (2016). Long-Term Functional Efficacy of a Novel Electrospun Poly(Glycerol Sebacate)-Based Arterial Graft in Mice. *Annals of Biomedical Engineering*, 44(8), 2402–2416.

[119] Kim, J.-H., Avril, S., Duprey, A., & Favre, J.-P. (2011a). Experimental characterization of rupture in human aortic aneurysms using a full-field measurement technique. *Biomechanics and Modeling in Mechanobiology*, 11(6), 841–853.

[120] Kim, T. K., Kim, J. K., & Jeong, O. C. (2011b). Measurement of nonlinear mechanical properties of PDMS elastomer. *Microelectronic Engineering*, 88(8), 1982–1985.

[121] Kluin, J., Talacua, H., Smits, A. I. P. M., Emmert, M. Y., Brugmans, M. C. P., Fioretta, E. S., Dijkman, P. E., Söntjens, S. H. M., Duijvelshoff, R., Dekker, S., Janssen-van den Broek, M. W. J. T., Lintas, V., Vink, A., Hoerstrup, S. P., Janssen, H. M., Dankers, P. Y. W., Baaijens, F. P. T., & Bouten, C. V. C. (2017). In situ heart valve tissue engineering using a bioresorbable elastomeric implant - From material design to 12 months follow-up in sheep. *Biomaterials*, 125, 101–117.

[122] Komeda, M., Glasson, J. R., Bolger, A. F., Daughters, G. T., Ingels, N. B., & Miller, D. C. (1997). Papillary muscle-left ventricular wall "complex". *Journal of Thoracic and Cardiovascular Surgery*, 113(2), 292–300.

[123] Kortsmit, J., Driessen, N. J. B., Rutten, M. C. M., & Baaijens, F. P. T. (2009a). Nondestructive and Noninvasive Assessment of Mechanical Properties in Heart Valve Tissue Engineering. *Tissue Engineering Part A*, 15(4), 797–806.

[124] Kortsmit, J., Rutten, M. C. M., Wijlaars, M. W., & Baaijens, F. P. T. (2009b). Deformation-controlled load application in heart valve tissue engineering. *Tissue Engineering Part C: Methods*, 15(4), 707–716.

[125] Kraus, H. (1967). *Thin elastic shells – An Introduction to the Theoretical Foundations and the Analysis of Their Static and Dynamic Behavior*. New York, NY: John Wiley and Sons.

[126] Kroon, W., Delhaas, T., Arts, T., & Bovendeerd, P. (2009). Computational modeling of volumetric soft tissue growth: application to the cardiac left ventricle. *Biomechanics and Modeling in Mechanobiology*, 8(4), 301–309.

[127] Kuhl, E. (2014). Growing matter: a review of growth in living systems. *Journal of the Mechanical Behavior of Biomedical Materials*, 29, 529–543.

[128] Kural, M. H. & Billiar, K. L. (2014). Mechanoregulation of valvular interstitial cell phenotype in the third dimension. *Biomaterials*, 35(4), 1128–1137.

[129] Langer, R. & Vacanti, J. P. (1993). Tissue Engineering. *Science*, 260(5110), 920–926.

[130] Larsen, W. J. (2015). *Larsen's Human Embryology*. Churchill Livingstone, Philidelphia, 5th edition.

[131] Lee, C., Park, C. S., Lee, C.-H., Kwak, J. G., Kim, S.-J., Shim, W.-S., Song, J. Y., Choi, E. Y., & Lee, S. Y. (2011). Durability of bioprosthetic valves in the pulmonary position: Long-term follow-up of 181 implants in patients with congenital heart disease. *Journal of Thoracic and Cardiovascular Surgery*, 142(2), 351–358.

[132] Legant, W. R., Pathak, A., Yang, M. T., Deshpande, V. S., McMeeking, R. M., & Chen, C. S. (2009). Microfabricated tissue gauges to measure and manipulate forces from 3D microtissues. *Proceedings of the National Academy of Sciences of the United States of America*, 106(25), 10097–10102.

[133] Leung, D. Y., Glagov, S., & Mathews, M. B. (1976). Cyclic stretching stimulates synthesis of matrix components by arterial smooth muscle cells in vitro. *Science*, 191(4226), 475–477.

[134] L'Heureux, N., Dusserre, N., Konig, G., Victor, B., Keire, P., Wight, T. N., Chronos, N., Kyles, A. E., Gregory, C. R., Hoyt, G., Robbins, R. C., & McAllister, T. N. (2006). Human tissue-engineered blood vessels for adult arterial revascularization. *Nature Medicine*, 12(3), 361–365.

[135] Loerakker, S., Argento, G., Oomens, C. W. J., & Baaijens, F. P. T. (2013). Effects of valve geometry and tissue anisotropy on the radial stretch and coaptation area of tissue-engineered heart valves. *Journal of Biomechanics*, 46(11), 1792–1800.

[136] Loerakker, S., Obbink-Huizer, C., & Baaijens, F. P. T. (2014). A physically motivated constitutive model for cell-mediated compaction and collagen remodeling in soft tissues. *Biomechanics and Modeling in Mechanobiology*, 13(5), 985–1001.

[137] Loerakker, S., Ristori, T., & Baaijens, F. P. T. (2016). A computational analysis of cell-mediated compaction and collagen remodeling in tissue-engineered heart valves. *Journal of the Mechanical Behavior of Biomedical Materials*, 58, 173–187.

[138] Lopata, R. G. P., Nillesen, M. M., Hansen, H. H. G., Gerrits, I. H., Thijssen, J. M., & de Korte, C. L. (2009). Performance evaluation of methods for two-dimensional displacement and strain estimation using ultrasound radio frequency data. *Ultrasound in Medicine & Biology*, 35(5), 796–812.

[139] Lowery, J. L., Datta, N., & Rutledge, G. C. (2010). Effect of fiber diameter, pore size and seeding method on growth of human dermal fibroblasts in electrospun poly(e-caprolactone) fibrous mats. *Biomaterials*, 31(3), 491–504.

[140] Lu, J., Hu, S., & Raghavan, M. L. (2013). A Shell-Based Inverse Approach of Stress Analysis in Intracranial Aneurysms. *Annals of Biomedical Engineering*, 41(7), 1505–1515.

[141] Lu, J., Zhou, X., & Raghavan, M. L. (2008). Inverse method of stress analysis for cerebral aneurysms. *Biomechanics and Modeling in Mechanobiology*, 7(6), 477–486.

[142] Maron, B. J. & Hutchins, G. M. (1974). The development of the semilunar valves in the human heart. *American Journal of Pathology*, 74(2), 331–344.

[143] Marra, S. P., Kennedy, F. E., Kinkaid, J. N., & Fillinger, M. F. (2006). Elastic and Rupture Properties of Porcine Aortic Tissue Measured Using Inflation Testing. *Cardiovascular Engineering*, 6(4), 123–131.

[144] Martin, C. & Sun, W. (2012). Biomechanical characterization of aortic valve tissue in humans and common animal models. *Journal of Biomedical Materials Research Part B: Applied Biomaterials*, 100A(6), 1591–1599.

[145] Martufi, G. & Gasser, T. C. (2012). Turnover of fibrillar collagen in soft biological tissue with application to the expansion of abdominal aortic aneurysms. *Journal of The Royal Society Interface*, 9(77), 3366–3377.

[146] Matsumoto, T. & Hayashi, K. (1994). Mechanical and Dimensional Adaptation of Rat Aorta to Hypertension. *Journal of Biomechanical Engineering*, 116(3), 278–283.

[147] McAllister, T. N., Maruszewski, M., Garrido, S. A., Wystrychowski, W., Dusserre, N., Marini, A., Zagalski, K., Fiorillo, A., Avila, H., Manglano, X., Antonelli, J., Kocher, A., Zembala, M., Cierpka, L., de la Fuente, L. M., & LHeureux, N. (2009). Effectiveness of haemodialysis access with an autologous tissue-engineered vascular graft: a multicentre cohort study. *The Lancet*, 373(9673), 1440–1446.

[148] McDonald, P. C., Wilson, J. E., McNeill, S., Gao, M., Spinelli, J. J., Rosenberg, F., Wiebe, H., & McManus, B. M. (2002). The challenge of defining normality for human mitral and aortic valves: geometrical and compositional analysis. *Cardiovascular Pathology*, 11(4), 193–209.

[149] McGee, E. C., Gillinov, A. M., Blackstone, E. H., Rajeswaran, J., Cohen, G., Najam, G., Najam, F., Shiota, T., Sabik, J. F., Lytle, B. W., McCarthy, P. M., & Cosgrove, D. M. (2004). Recurrent mitral regurgitation after annuloplasty for functional ischemic mitral regurgitation. *Journal of Thoracic and Cardiovascular Surgery*, 128(6), 916–924.

[150] McPherson, J. M. & Piez, K. A. (1988). Collagen in Dermal Wound Repair. In *The Molecular and Cellular Biology of Wound Repair* (pp. 471–496). Boston, MA: Springer US.

[151] Merryman, W. D., Liao, J., Parekh, A., Candiello, J. E., Lin, H., & Sacks, M. S. (2007a). Differences in tissue-remodeling potential of aortic and pulmonary heart valve interstitial cells. *Tissue Engineering*, 13(9), 2281–2289.

[152] Merryman, W. D., Lukoff, H. D., Long, R. A., Engelmayr, G. C., Hopkins, R. A., & Sacks, M. S. (2007b). Synergistic effects of cyclic tension and transforming growth factor-beta1 on the aortic valve myofibroblast. *Cardiovascular Pathology*, 16(5), 268–276.

[153] Midwood, K. S., Williams, L. V., & Schwarzbauer, J. E. (2004). Tissue repair and the dynamics of the extracellular matrix. *The International Journal of Biochemistry & Cell Biology*, 36(6), 1031–1037.

[154] Miller, K. S., Khosravi, R., Breuer, C. K., & Humphrey, J. D. (2015). A hypothesis-driven parametric study of effects of polymeric scaffold properties on tissue engineered neovessel formation. *Acta Biomaterialia*, 11, 283–294.

[155] Mol, A., Driessen, N., Rutten, M., Hoerstrup, S. P., Bouten, C., & Baaijens, F. (2005a). Tissue engineering of human heart valve leaflets: A novel bioreactor for a strain-based conditioning approach. *Annals of Biomedical Engineering*, 33(12), 1778–1788.

[156] Mol, A., Rutten, M. C. M., Driessen, N. J. B., Bouten, C. V. C., Zund, G., Baaijens, F. P. T., & Hoerstrup, S. P. (2006). Autologous human tissue-engineered heart valves: prospects for systemic application. *Circulation*, 114(1 Suppl), I152–8.

[157] Mol, A., Smits, A. I. P. M., Bouten, C. V. C., & Baaijens, F. P. T. (2009). Tissue engineering of heart valves: advances and current challenges. *Expert Review of Medical Devices*, 6(3), 259–275.

[158] Mol, A., van Lieshout, M. I., Veen, C., Neuenschwander, S., Hoerstrup, S. P., Baaijens, F., & Bouten, C. (2005b). Fibrin as a cell carrier in cardiovascular tissue engineering applications. *Biomaterials*, 26(16), 3113–3121.

[159] Mullins, L. (1947). Effect of stretching on the properties of rubber. *Rubber Research*, 16, 275–289.

[160] Nagase, H., Visse, R., & Murphy, G. (2006). Structure and function of matrix metalloproteinases and TIMPs. *Cardiovascular Research*, 69(3), 562–573.

[161] Nagatomo, Y., Carabello, B. A., Hamawaki, M., Nemoto, S., Matsuo, T., & McDermott, P. J. (1999). Translational mechanisms accelerate the rate of protein synthesis during canine pressure-overload hypertrophy. *American Journal of Physiology. Heart and Circulatory Physiology*, 277(6), H2176–H2184.

[162] Neggers, J., Hoefnagels, J. P. M., Hild, F., Roux, S., & Geers, M. G. D. (2012). A Global Digital Image Correlation Enhanced Full-Field Bulge Test Method. *Procedia IUTAM*, 4, 73–81.

[163] Neggers, J., Hoefnagels, J. P. M., Hild, F., Roux, S., & Geers, M. G. D. (2014). Direct Stress-Strain Measurements from Bulged Membranes Using Topography Image Correlation. *Experimental Mechanics*, 54(5), 717–727.

[164] NIH (2005). *The Fourth Report on Diagnosis, Evaluation, and Treatment of High Blood Pressure in Children and Adolescents*. Technical report, U.S. Department of Health and Human Services.

[165] Niklason, L. E., Gao, J., Abbott, W. M., Hirschi, K. K., Houser, S., Marini, R., & Langer, R. (1999). Functional Arteries Grown in Vitro. *Science*, 284(5413), 489–493.

[166] Niklason, L. E., Yeh, A. T., Calle, E. A., Bai, Y., Valentin, A., & Humphrey, J. D. (2010). Enabling tools for engineering collagenous tissues integrating bioreactors, intravital imaging, and biomechanical modeling. *Proceedings of the National Academy of Sciences of the United States of America*, 107(8), 3335–3339.

[167] Obbink-Huizer, C., Oomens, C. W. J., Loerakker, S., Foolen, J., Bouten, C. V. C., & Baaijens, F. P. T. (2013). Computational model predicts cell orientation in response to a range of mechanical stimuli. *Biomechanics and Modeling in Mechanobiology*, 13(1), 227–236.

[168] O'Hara, P. J., Hertzer, N. R., Beven, E. G., & Krajewski, L. P. (1986). Surgical-Management of Infected Abdominal Aortic Grafts - Review of a 25-Year Experience. *Journal of Vascular Surgery*, *3*(5), 725–731.

[169] Omens, J. H. (1998). Stress and strain as regulators of myocardial growth. *Progress in Biophysics and Molecular Biology*, *69*(2-3), 559–572.

[170] Ong, C. S., Zhou, X., Huang, C. Y., Fukunishi, T., Zhang, H., & Hibino, N. (2017). Tissue engineered vascular grafts: current state of the field. *Expert Review of Medical Devices*, *14*(5), 383–392.

[171] Otsuji, Y., Handschumacher, M. D., Schwammenthal, E., Jiang, L., Song, J. K., Guerrero, L., Vlahakes, G. J., & Levine, R. A. (1997). Insights from three-dimensional echocardiography into the mechanism of functional mitral regurgitation - Direct in vivo demonstration of altered leaflet tethering geometry. *Circulation*, *96*(6), 1999–2008.

[172] Peña, E., Peña, J. A., & Doblaré, M. (2009). On the Mullins effect and hysteresis of fibered biological materials: A comparison between continuous and discontinuous damage models. *International Journal of Solids and Structures*, *46*(7), 1727–1735.

[173] Pibarot, P. & Dumesnil, J. G. (2009). Prosthetic heart valves: selection of the optimal prosthesis and long-term management. *Circulation*, *119*(7), 1034–1048.

[174] Prajapati, R. T., Chavally-Mis, B., Herbage, D., Eastwood, M., & Brown, R. A. (2000). Mechanical loading regulates protease production by fibroblasts in three-dimensional collagen substrates. *Wound Repair and Regeneration*, *8*(3), 226–237.

[175] Puvimanasinghe, J. P., Steyerberg, E. W., Takkenberg, J. J., Eijkemans, M. J., van Herwerden, L. A., Bogers, A. J., & Habbema, J. D. (2001). Prognosis after aortic valve replacement with a bioprosthesis: predictions based on meta-analysis and microsimulation. *Circulation*, *103*(11), 1535–1541.

[176] Raaz, U., Zöllner, A. M., Schellinger, I. N., Toh, R., Nakagami, F., Brandt, M., Emrich, F. C., Kayama, Y., Eken, S., Adam, M., Maegdefessel, L., Hertel, T., Deng, A., Jagger, A., Buerke, M., Dalman, R. L., Spin, J. M., Kuhl, E., & Tsao, P. S. (2015). Segmental aortic stiffening contributes to experimental abdominal aortic aneurysm development. *Circulation*, *131*(20), 1783–1795.

[177] Rabkin-Aikawa, E., Farber, M., Aikawa, M., & Schoen, F. J. (2004). Dynamic and reversible changes of interstitial cell phenotype during remodeling of cardiac valves. *Journal of Heart Valve Disease*, *13*(5), 841–847.

[178] Ramachandra, A. B., Humphrey, J. D., & Marsden, A. L. (2017). Gradual loading ameliorates maladaptation in computational simulations of vein graft growth and remodelling. *Journal of The Royal Society Interface*, *14*(130), 20160995–12.

[179] Ramachandra, A. B., Sankaran, S., Humphrey, J. D., & Marsden, A. L. (2015). Computational simulation of the adaptive capacity of vein grafts in response to increased pressure. *Journal of Biomechanical Engineering*, *137*(3), 031009.

[180] Rausch, M. K. & Kuhl, E. (2013). On the effect of prestrain and residual stress in thin biological membranes. *Journal of the Mechanics and Physics of Solids*, *61*(9), 1955–1969.

[181] Rausch, M. K. & Kuhl, E. (2014). On the mechanics of growing thin biological membranes. *Journal of the Mechanics and Physics of Solids*, *63*, 128–140.

[182] Rausch, M. K., Tibayan, F. A., Miller, D. C., & Kuhl, E. (2012). Evidence of adaptive mitral leaflet growth. *Journal of the Mechanical Behavior of Biomedical Materials*, *15*, 208–217.

[183] Reimer, J., Syedain, Z., Haynie, B., Lahti, M., Berry, J., & Tranquillo, R. (2017). Implantation of a Tissue-Engineered Tubular Heart Valve in Growing Lambs. *Annals of Biomedical Engineering*, *45*(2), 439–451.

[184] Roccabianca, S., Bellini, C., & Humphrey, J. D. (2014). Computational modelling suggests good, bad and ugly roles of glycosaminoglycans in arterial wall mechanics and mechanobiology. *Journal of The Royal Society Interface*, *11*(97), 20140397–20140397.

[185] Rock, C. A., Han, L., & Doehring, T. C. (2014). Complex collagen fiber and membrane morphologies of the whole porcine aortic valve. *PLOS One*, *9*(1), e86087.

[186] Rodriguez, E. K., Hoger, A., & McCulloch, A. D. (1994). Stress-dependent finite growth in soft elastic tissues. *Journal of Biomechanics*, *27*(4), 455–467.

[187] Roh, J. D., Sawh-Martinez, R., Brennan, M. P., Jay, S. M., Devine, L., Rao, D. A., Yi, T., Mirensky, T. L., Nalbandian, A., Udelsman, B., Hibino, N., Shinoka, T., Saltzman, W. M., Snyder, E., Kyriakides, T. R., Pober, J. S., & Breuer, C. K. (2010). Tissue-engineered vascular grafts transform into mature blood vessels via an inflammation-mediated process of vascular remodeling. *Proceedings of the National Academy of Sciences of the United States of America*, *107*(10), 4669–4674.

[188] Romo, A., Badel, P., Duprey, A., Favre, J.-P., & Avril, S. (2014). In vitro analysis of localized aneurysm rupture. *Journal of Biomechanics*, 47(3), 607–616.

[189] Rosen, L. A., Hollis, T. M., & Sharma, M. G. (1974). Alterations in Bovine Endothelial Histidine Decarboxylase Activity Following Exposure to Shearing Stresses. *Experimental and Molecular Pathology*, 20(3), 329–343.

[190] Rubbens, M. P., Driessen-Mol, A., Boerboom, R. A., Koppert, M. M. J., van Assen, H. C., TerHaar Romeny, B. M., Baaijens, F. P. T., & Bouten, C. V. C. (2009a). Quantification of the temporal evolution of collagen orientation in mechanically conditioned engineered cardiovascular tissues. *Annals of Biomedical Engineering*, 37(7), 1263–1272.

[191] Rubbens, M. P., Mol, A., Boerboom, R. A., Bank, R. A., Baaijens, F. P. T., & Bouten, C. V. C. (2009b). Intermittent Straining Accelerates the Development of Tissue Properties in Engineered Heart Valve Tissue. *Tissue Engineering Part A*, 15(5), 999–1008.

[192] Rubbens, M. P., Mol, A., van Marion, M. H., Hanemaaijer, R., Bank, R. A., Baaijens, F. P. T., & Bouten, C. V. C. (2009c). Straining Mode-Dependent Collagen Remodeling in Engineered Cardiovascular Tissue. *Tissue Engineering Part A*, 15(4), 841–849.

[193] Ruberti, J. W. & Hallab, N. J. (2005). Strain-controlled enzymatic cleavage of collagen in loaded matrix. *Biochemical and Biophysical Research Communications*, 336(2), 483–489.

[194] Ruff, C., Holt, B., & Trinkaus, E. (2006). Who's afraid of the big bad Wolff?: "Wolff's law" and bone functional adaptation. *American Journal of Physical Anthropology*, 129(4), 484–498.

[195] Sacks, M. S., Smith, D. B., & Hiester, E. D. (1998). The aortic valve microstructure: effects of transvalvular pressure. *Journal of Biomedical Materials Research Part B: Applied Biomaterials*, 41(1), 131–141.

[196] Sáez, P., Peña, E., Martínez, M. A., & Kuhl, E. (2013). Computational modeling of hypertensive growth in the human carotid artery. *Computational Mechanics*, 53(6), 1183–1196.

[197] Sanders, B., Loerakker, S., Fioretta, E. S., Bax, D. J. P., Driessen-Mol, A., Hoerstrup, S. P., & Baaijens, F. P. T. (2016). Improved Geometry of Decellularized Tissue Engineered Heart Valves to Prevent Leaflet Retraction. *Annals of Biomedical Engineering*, 44(4), 1061–1071.

[198] Sasayama, S., Ross, J., Franklin, D., Bloor, C. M., Bishop, S., & Dilley, R. B. (1976). Adaptations of the left ventricle to chronic pressure overload. *Circulation Research*, 38(3), 172–178.

[199] Sauren, A. A., Kuijpers, W., van Steenhoven, A. A., & Veldpaus, F. E. (1980). Aortic valve histology and its relation with mechanics-preliminary report. *Journal of Biomechanics*, 13(2), 97–104.

[200] Schmidt, D., Dijkman, P. E., Driessen-Mol, A., Stenger, R., Mariani, C., Puolakka, A., Rissanen, M., Deichmann, T., Odermatt, B., Weber, B., Emmert, M. Y., Zund, G., Baaijens, F. P. T., & Hoerstrup, S. P. (2010). Minimally-Invasive Implantation of Living Tissue Engineered Heart Valves A Comprehensive Approach From Autologous Vascular Cells to Stem Cells. *Journal of the American College of Cardiology*, 56(6), 510–520.

[201] Schoen, F. J. (2012). Mechanisms of function and disease of natural and replacement heart valves. *Annual Review of Pathology*, 7(1), 161–183.

[202] Shadwick, R. E. (1999). Mechanical design in arteries. *Journal of Experimental Biology*, 202(23), 3305–3313.

[203] Shaikh, F. M., O'Brien, T. P., Callanan, A., Kavanagh, E. G., Burke, P. E., Grace, P. A., & McGloughlin, T. M. (2010). New Pulsatile Hydrostatic Pressure Bioreactor for Vascular Tissue-engineered Constructs. *Artificial Organs*, 34(2), 153–158.

[204] Silverthorn, D. & Johnson, B. (2010). *Human Physiology: An Integrated Approach. 5th edition.* Pearson/Benjamin Cummings.

[205] Smits, A. I. P. M., Bonito, V., & Stoddart, M. (2016). In Situ Tissue Engineering: Seducing the Body to Regenerate. *Tissue Engineering Part A*, 22(17-18), 1061–1062.

[206] Sodian, R., Hoerstrup, S. P., Sperling, J. S., & Daebritz, S. (2000). Early in vivo experience with tissue-engineered trileaflet heart valves. *Circulation*.

[207] Stephens, E. H., de Jonge, N., McNeill, M. P., Durst, C. A., & Grande-Allen, K. J. (2010). Age-related changes in material behavior of porcine mitral and aortic valves and correlation to matrix composition. *Tissue Engineering Part A*, 16(3), 867–878.

[208] Stoppel, W. L., Kaplan, D. L., & Black, L. D. I. (2016). Electrical and mechanical stimulation of cardiac cells and tissue constructs. *Advanced Drug Delivery Reviews*, 96, 135–155.

[209] Stradins, P., Lacis, R., Ozolanta, I., Purina, B., Ose, V., Feldmane, L., & Kasyanov, V. (2004). Comparison of biomechanical and structural properties between human aortic and pulmonary valve. *European Journal of Cardio-Thoracic Surgery*, 26(3), 634–639.

[210] Struijk, P. C., Mathews, V. J., Loupas, T., Stewart, P. A., Clark, E. B., Steegers, E. A. P., & Wladimiroff, J. W. (2008). Blood pressure estimation in the human fetal descending aorta. *Ultrasound in Obstetrics and Gynecology*, 32(5), 673–681.

[211] Suma, H. (1999). Arterial grafts in coronary bypass surgery. *Annals of Thoracic and Cardiovascular Surgery*, 5(3), 141–145.

[212] Syedain, Z., Reimer, J., Lahti, M., Berry, J., Johnson, S., & Tranquillo, R. T. (2016). Tissue engineering of acellular vascular grafts capable of somatic growth in young lambs. *Nature Communications*, 7, 12951.

[213] Syedain, Z. H., Meier, L. A., Bjork, J. W., Lee, A., & Tranquillo, R. T. (2011). Implantable arterial grafts from human fibroblasts and fibrin using a multi-graft pulsed flow-stretch bioreactor with noninvasive strength monitoring. *Biomaterials*, 32(3), 714–722.

[214] Taber, L. A. & Humphrey, J. D. (2001). Stress-modulated growth, residual stress, and vascular heterogeneity. *Journal of Biomechanical Engineering*, 123(6), 528–535.

[215] Talacua, H., Smits, A. I. P. M., Muylaert, D. E. P., van Rijswijk, J. W., Vink, A., Verhaar, M. C., Driessen-Mol, A., van Herwerden, L. A., Bouten, C. V. C., Kluin, J., & Baaijens, F. P. T. (2015). In Situ Tissue Engineering of Functional Small-Diameter Blood Vessels by Host Circulating Cells Only. *Tissue Engineering Part A*, 21(19-20), 2583–2594.

[216] Taramasso, M., Emmert, M. Y., Reser, D., Guidotti, A., Cesarovic, N., Campagnol, M., Addis, A., Nietlispach, F., Hoerstrup, S. P., & Maisano, F. (2015). Pre-clinical In Vitro and In Vivo Models for Heart Valve Therapies. *Journal of Cardiovascular Translational Research*, 8(5), 319–327.

[217] Thoma, R. (1893). *Untersuchagen uber die Histogenese and Histomechanik des Gefassystems*. Stuttgart: Enke.

[218] Tonge, T. K., Atlan, L. S., Voo, L. M., & Nguyen, T. D. (2013a). Full-field bulge test for planar anisotropic tissues: Part I - Experimental methods applied to human skin tissue. *Acta Biomaterialia*, 9(4), 5913–5925.

[219] Tonge, T. K., Voo, L. M., & Nguyen, T. D. (2013b). Full-field bulge test for planar anisotropic tissues: Part II - A thin shell method for determining material parameters and comparison of two distributed fiber modeling approaches. *Acta Biomaterialia*, 9(4), 5926–5942.

[220] Tongprasert, F., Srisupundit, K., Luewan, S., Sirichotiyakul, S., Piyamongkol, W., Wanapirak, C., & Tongsong, T. (2011). Reference ranges of fetal aortic and pulmonary valve diameter derived by STIC from 14 to 40 weeks of gestation. 31(5), 439–445.

[221] Tözeren, A. & Skalak, R. (1988). Interaction of Stress and Growth in a Fibrous Tissue. *Journal of Theoretical Biology*, 130(3), 337–350.

[222] Udelsman, B. V., Khosravi, R., Miller, K. S., Dean, E. W., Bersi, M. R., Rocco, K., Yi, T., Humphrey, J. D., & Breuer, C. K. (2014). Characterization of evolving biomechanical properties of tissue engineered vascular grafts in the arterial circulation. *Journal of Biomechanics*, 47(9), 2070–2079.

[223] Vaenkatesan, V., Li, Z., Vellinga, W.-P., & de Jeu, W. H. (2006). Adhesion and friction behaviours of polydimethylsiloxane – A fresh perspective on JKR measurements. *Polymer*, 47(25), 8317–8325.

[224] Valentin, A., Cardamone, L., Baek, S., & Humphrey, J. D. (2009). Complementary vasoactivity and matrix remodelling in arterial adaptations to altered flow and pressure. *Journal of the Royal Society Interface*, 6(32), 293–306.

[225] Valentin, A., Humphrey, J. D., & Holzapfel, G. A. (2013). A finite element-based constrained mixture implementation for arterial growth, remodeling, and adaptation: Theory and numerical verification. *International Journal for Numerical Methods in Biomedical Engineering*, 29(8), 822–849.

[226] van Geemen, D., Soares, A. L. F., Oomen, P. J. A., Driessen-Mol, A., Janssen-van den Broek, M. W. J. T., van den Bogaerdt, A. J., Bogers, A. J. J. C., Goumans, M.-J. T. H., Baaijens, F. P. T., & Bouten, C. V. C. (2016). Age-Dependent Changes in Geometry, Tissue Composition and Mechanical Properties of Fetal to Adult Cryopreserved Human Heart Valves. *PLOS One*, 11(2), e0149020.

[227] van Kelle, M. A. J., Oomen, P. J. A., Bulsink, J. A., Janssen-van den Broek, M. W. J. T., Lopata, R. G. P., Rutten, M. C. M., Loerakker, S., & Bouten, C. V. C. (2017). A Bioreactor to Identify the Driving Mechanical Stimuli of Tissue Growth and Remodeling. *Tissue Engineering Part C: Methods*, 23(6), 377–387.

[228] van Loosdregt, I. A. E. W., Kamps, M. A. F., Oomens, C. W. J., Loerakker, S., Broers, J. L. V., & Bouten, C. V. C. (2017). Lmna knockout mouse embryonic fibroblasts are less contractile than their wild-type counterparts. *Integrative Biology : Quantitative Biosciences from Nano to Macro*, 9(8), 709–721.

[229] van Vlimmeren, M. A. A., Driessen-Mol, A., Oomens, C. W. J., & Baaijens, F. P. T. (2011). An In Vitro Model System to Quantify Stress Generation, Compaction, and Retraction in Engineered Heart Valve Tissue. *Tissue Engineering Part C: Methods*, 17(10), 983–991.

[230] van Vlimmeren, M. A. A., Driessen-Mol, A., Oomens, C. W. J., & Baaijens, F. P. T. (2012). Passive and active contributions to generated force and retraction in heart valve tissue engineering. *Biomechanics and Modeling in Mechanobiology*, 11(7), 1015–1027.

[231] van Vlimmeren, M. A. A., Driessen-Mol, A., Oomens, C. W. J., & Baaijens, F. P. T. (2013). The Potential of Prolonged Tissue Culture to Reduce Stress Generation and Retraction in Engineered Heart Valve Tissues. *Tissue Engineering Part C: Methods*, 19(3), 205–215.

[232] Vigliotti, A., Ronan, W., Baaijens, F. P. T., & Deshpande, V. S. (2016). A thermodynamically motivated model for stress-fiber reorganization. *Biomechanics and Modeling in Mechanobiology*, 15(4), 761–789.

[233] Vinci, R. P. & Vlassak, J. J. (1996). Mechanical behavior of thin films. *Annual Review of Materials Science*, 26, 431–462.

[234] Wang, Z., Zheng, W., Wu, Y., Wang, J., Zhang, X., Wang, K., Zhao, Q., Kong, D., Ke, T., & Li, C. (2016). Differences in the performance of PCL-based vascular grafts as abdominal aorta substitutes in healthy and diabetic rats. *Biomaterials Science*, 4(10), 1485–1492.

[235] Wilson, J. S., Baek, S., & Humphrey, J. D. (2013). Parametric study of effects of collagen turnover on the natural history of abdominal aortic aneurysms. *Proceedings. Mathematical, Physical, and Engineering Sciences*, 469(2150), 20120556–20120556.

[236] Wirth, A. (2010). Rho kinase and hypertension. *Biochimica Et Biophysica Acta-Molecular Basis of Disease*, 1802(12), 1276–1284.

[237] Wisse, E., Govaert, L. E., Meijer, H. E. H., & Meijer, E. W. (2006). Unusual Tuning of Mechanical Properties of Thermoplastic Elastomers Using Supramolecular Fillers. *Macromolecules*, 39(21), 7425–7432.

[238] Wissing, T. B., Bonito, V., Bouten, C. V. C., & Smits, A. I. P. M. (2017). Biomaterial-driven in situ cardiovascular tissue engineering-a multi-disciplinary perspective. *NPJ Regenerative medicine*, 2(1), 18.

[239] Witzenburg, C. M. & Holmes, J. W. (2017). A Comparison of Phenomenologic Growth Laws for Myocardial Hypertrophy. *Journal of Elasticity*, 129(1-2), 257–281.

[240] Wolff, J. (1986). *The Law of Bone Remodeling*. Berlin Heidelberg New York: Springer (translation of the German 1892 edition).

[241] Wolinsky, H. (1972). Long-Term Effects of Hypertension on the Rat Aortic Wall and Their Relation to Concurrent Aging Changes: Morphological and Checmical Studies. *Circulation Research*, 30(3), 301–309.

[242] Wolinsky, H. & Glagov, S. (1967). A lamellar unit of aortic medial structure and function in mammals. *Circulation Research*, 20(1), 99–111.

[243] Wright, J. D., Hughes, J. P., Ostchega, Y., Yoon, S. S., & Nwankwo, T. (2011). Mean systolic and diastolic blood pressure in adults aged 18 and over in the United States, 2001-2008. *National Health Statistics Reports*, (35), 1–22– 24.

[244] Wyatt, K. E. K., Bourne, J. W., & Torzilli, P. A. (2009). Deformation-dependent enzyme mechanokinetic cleavage of type I collagen. *Journal of Biomechanical Engineering*, 131(5), 051004.

Acknowledgements

Science and art belong to the whole world, and the barriers of nationality vanish before them.

Johann Wolfgang Goethe – remark to a German historian, 1813

Completing one's PhD thesis is a special journey, and I am grateful that I had supportive friends, family, and mentors along the way. Science is more than numbers, more than experiments, more than equations. It is most of all about people. I will always be grateful for the colleagues, friends, and family who accompanied me on my journey. I cannot help but wonder how different this thesis would have looked like if not for you.

First and foremost, Sandra, Carlijn, and Frank, whose guidance and mentorship go back well beyond the last four years. I can only hope I have repaid the trust you have placed in me. Frank, you were the one who sparked my interest in tissue engineering and heart valves, and provided me with the opportunities to pursue these interests. Perhaps even more importantly, you were the one who motivated me to make life-changing decisions I never thought I would make. Living in (or even visiting) the US never appealed to me, and pursuing a PhD degree in Eindhoven was never high on my list. Yet, here I am in Charlottesville, Virginia, where I now call home, writing this acknowledgment for my TU/e PhD thesis Sandra, our weekly meetings (I estimate well over two hundred) were the cornerstone of my research. Your dedication, honesty, integrity, and competence were a big part in the making of the scientist and person I am today. The period you enabled us to spend together at Stanford were surely the highlight of my PhD journey. I have no doubt you will be as inspiring as a mum to Lars as you have been a mentor to me. Carlijn, you have always been an invaluable resource in the biological aspects of my research. When Frank stepped down, your role only grew in importance, and I am most grateful for all the time you invested in me and the rest of the group. Your personal touch and feedback as a promotor have been a big factor in the development of this thesis as well as my own personal development.

I would like to extend my personal gratitude to professors Gerhard Holzapfel, Simon Hoerstrup, Hans van Oosterwyck, and Frans van de Vosse for carefully critiquing the thesis and being willing to make the journey to be a part of the defense committee. This truly means a lot to me.

Mathieu, how could I have done this without you? Little did I know, five years ago, that the person who I skied down the alps and who got me mysterious green drinks would be the same person with whom I would eventually co-author two complete chapters/papers. I am grateful to have shared our PhD journeys and many beers, offices in both Eindhoven and Stanford, memorable vacations, etc., etc. Our many shared hours in the lab were never boring, always fruitful (OK, mostly). It will be reassuring to have you on my side one more time, this time as a paranimf.

I will always recommend the PhD degree at TU Eindhoven for the endless amount of helpful people. The only downside to this is that I will surely not manage to thank everyone in this acknowledgement. But I can try. Cees, for your ever present mentorship, shared passion for music, and endless anecdotes — "you are faster if you are working slowly" is a mantra I will always (try to) live by. Jurgen, "de man die alles maken kan", for your enthusiasm and inventiveness in making everything we ever asked for and more. Marcel, for your help with devising the bioreactor. Richard, Niels, Maarten, Emiel and the rest of the PULS/e lab for sharing your knowledge and equipment on ultrasound and eagerness to frequent many a bar. Marloes, Marc, and Moniek, for your help and knowledge of everything that I am (still) clueless about in the lab. Yvon, for your cheerfulness and inventiveness in solving the complicated puzzles that are called professor agendas. Daphne, for the foundation you laid down to study native human heart valves. Tommaso, pastavreter, for the many discussions, road trips and wine wisdom. STEM group and cel lab members, thank you for providing such a comfortable and open work environment and for providing help and feedback whenever needed.

My fellow 4.12 office residents, for serious and less serious talks, snacks, lunches, office socials, and many foosball matches. Thank you Stéphanie, Renate, Thomas, Irene, Emanuela, Bart, Anne, Stefan, Stefan, Mathieu Maike, Nicole, Suzanne, Laura, Ronald, Marc, Marjan, and Dylan.

To all the students that I had the privilege in mentoring: Guus, Leon, Wouter, Guusje, Yeshi, Luuk, Lissa, Jeroen, and Jolijn, and all the others. Thank you for allowing me to help you through my own mistakes and perhaps sometimes competence, but always dedication.

From outside of Eindhoven: Ellen, your generous hospitality at Stanford University allowed for the most rewarding and inspiring period of my PhD journey. I am indebted to you and Maria for the making of Chapter 3. Everyone else in the Kuhl lab, Johannes, Francisco, Rijk, Mona, Caitlin, and Cedric: thank you for making me feel at home in the Bay Area. Antoon van den Bogaerdt and Marie-José Goumans, thank you for providing the human heart valves that provided the foundation of Chapters 2 and 3.

No journey was ever undertaken for free, and as such, no research can be performed without financial support. In my case, this was mainly provided by the ImaValve consortium, part of the European Union's Seventh Framework. I thank everyone within the consortium for so openly sharing their ideas and expertise.

Let us not pretend that the last four years have only been about academic research. Life outside the university is just as important. Many readers may know of my passion for music. The Biosonix have been a great outlet all these years. Cees, Eline, Ginny, Marja, René, Richard, know that I blame you for ever having to sing and play Meat Loaf. Our weekly rehearsals (starting out in the polymer lab in the department's basement) and shows were always something to look forward to. Never stop making music.

Patrick, Niek, Rob, my friends for so long, the only constant amongst a life full of variables. You know how much you mean to me, our friendship goes so far beyond road trips and endless rounds

of card games. Rob, I am glad to have you with me as a paranimf for the final episode of this journey — surely it can not be more perilous than braving arctic temperatures to see the aurora?

At the end of this journey, I am ready to thank the most important people in my life: my parents, pa en ma. Woorden schieten tekort voor alles wat jullie voor mij betekenen, voor mij gedaan hebben, gelaten hebben. Ik zeg het veel te weinig, maar nu staat het in ieder geval op papier gegrift: ik had me geen betere ouders kunnen wensen. Geen afstand ter wereld kan daar verandering in brengen. Deze thesis is voor jullie, ik hou van jullie.

With the utmost gratitude,

Pim

Curriculum vitae

Pim Oomen was born on August 8, 1990, in Rotterdam and raised in the small town of Hoeven. In 2008, he completed the gymnasium at the Markland College in Oudenbosch, after which he moved to the Eindhoven University of Technology. He earned a BSc and MSc in Biomedical Engineering at the Eindhoven University of Technology under the supervision of prof. Frank Baaijens. During these degrees, he developed an interest in biomechanics and tissue engineering, and performed parts of his research at Queen Mary University of London and University of Texas at Austin.

In 2014, he started his pursuit of a PhD degree in Biomedical Engineering, under supervision of prof. Carlijn Bouten, dr. Sandra Loerakker, and prof. Frank Baaijens. Part of his research has been performed at Stanford University in collaboration with prof. Ellen Kuhl, supported by a Young Talent Award from the Dutch Heart Association. His PhD research concerned the mechanics of growth and remodeling of native and tissue-engineered cardiovascular tissues, which resulted in this thesis. For his research on heart valve growth and remodeling, he was awarded the 2017 Student Award of the European Society of Biomechanics.

After completing his doctoral research in 2018, he once more moved to the US, this time to perform postdoctoral research at the University of Virginia with prof. Jeffrey Holmes. In close collaboration with both engineers and clinicians, he now spearheads the development and testing of a new software platform that allows clinicians to customize cardiac resynchronization therapy for individual patients.

List of publications

Journal publications

Van Kelle, M.A.J.*, Oomen, P.J.A.*, Janssen-van den Broek, M.W.J.T., Lopata, R.G.P., Loerakker, S. & Bouten, C.V.C. Initial scaffold thickness affects the emergence of a geometrical and mechanical equilibrium in engineered cardiovascular tissues. *Submitted* (2018).

Oomen, P.J.A., Holland M.A., Bouten C.V.C., Kuhl E. & Loerakker S. Mechanical models suggest that growth and remodeling play opposing roles during the development of human heart valves. *Scientific Reports 8*, (135), 1–13 (2018).

Oomen, P.J.A., van Kelle, M.A.J., Oomens, C.W.J., Bouten, C.V.C. & Loerakker S. Nondestructive mechanical characterisation of developing biological tissues using inflation testing. *Journal of the Mechanical Behavior of Biomedical Materials* 74, 438–447 (2017).

Van Kelle, M.A.J.*, Oomen, P.J.A.*, Bulsink, J.A., Janssen-van den Broek, M.W.J.T., Lopata, R.G.P., Rutten, M.C.M., Loerakker, S. & Bouten, C.V.C. A Bioreactor to Identify the Driving Mechanical Stimuli of Tissue Growth and Remodeling. *Tissue Engineering: Part C* 23(6), 377–387 (2017)

Oomen, P.J.A., Loerakker, S., van Geemen, D., Neggers, J., Goumans, M.J.T.H., van den Bogaerdt, A.J., Bogers, A.J.J.C., Bouten, C.V.C. & Baaijens, F.P.T. Age-dependent changes of stress and strain in the human heart valve and their relation with collagen remodeling. *Acta Biomaterialia 29*, 161–169 (2016).

Van Geemen, D., Soares, A.L.F., Oomen, P.J.A., Driessen-Mol A., Janssen-van den Broek, M.W.J.T., van den Bogaerdt, A.J., Bogers, A.J.J.C., Goumans, M.J.T.H., Baaijens, F.P.T. & Bouten, C.V.C. Age-Dependent Changes in Geometry, Tissue Composition and Mechanical Properties of Fetal to Adult Cryopreserved Human Heart Valves. *PLOS ONE* 11(2), 1–20 (2016).

*Co-first author

Conference contributions

Oomen, P.J.A., van Kelle, M.A.J., Janssen–van den Broek, M.W.J.T., Lopata, R.G.P., Loerakker, S, & Bouten, C.V.C. Emergence of a geometrical and mechanical equilibrium in engineered cardiovascular tissues. *World Congres of Biomechanics*, Dublin (2018).

Oomen, P.J.A., Bouten, C.V.C, Kuhl, E. & Loerakker, S. The interplay of growth and remodeling in human heart valves during somatic growth (Plenary presentation, award lecture). *European Society of Biomechanics Conference*, Sevilla, Spain (2017).

Oomen, P.J.A., Bouten, C.V.C, Kuhl, E. & Loerakker, S. Predicting age-dependent changes in human native heart valves due to growth and remodeling (Oral presentation). *VII International Conference on Computational Methods for Coupled Problems in Science and Engineering Coupled Problems*, Rhodes Island, Greece (2017).

Oomen, P.J.A., Bouten, C.V.C, Kuhl, E. & Loerakker, S. Predicting age-dependent changes in human heart valves due to growth (Oral presentation). *Euromech colloquium: advanced experimental methods in tissue biomechanics*, Warberg, Germany (2017).

Oomen, P.J.A., Oomens, C.W.J., Bouten, C.V.C & Loerakker, S. Real-time Monitoring of the Mechanical Properties of Engineered Tissues During Growth And Remodeling (Oral presentation). *Summer Biomechanics, Bioengineering and Biotransport Conference*, National Harbor, MD, USA (2016).

Oomen, P.J.A., Loerakker, S., van Geemen, D., Neggers, J., Goumans, M.J.T.H., van den Bogaerdt, A.J., Bogers, A.J.J.C., Bouten, C.V.C. & Baaijens, F.P.T. Age-dependent changes in stress and strain in the human native heart valve and their relation with collagen remodeling (Oral presentation). *Summer Biomechanics, Bioengineering and Biotransport Conference, Salt Lake City*, UT, USA (2015).

Oomen, P.J.A., Loerakker, S., van Geemen, D., Goumans, M.J.T.H., van den Bogaerdt, A.J., Bogers, A.J.J.C., Bouten, C.V.C. & Baaijens, F.P.T. Unraveling Collagen Remodeling In Human Native Heart Valves (Poster presentation). *Heart Valve Society 1st Annual Meeting*, Monte Carlo, Monaco (2015).

Oomen, P.J.A., Loerakker, S., van Geemen, D., Neggers, J., Goumans, M.J.T.H., van den Bogaerdt, A.J., Bogers, A.J.J.C., Bouten, C.V.C. & Baaijens, F.P.T. Causes and consequences of collagen architecture remodeling in human native heart valves (Oral presentation), *Computational Methods in Biomechanics and Biomedical Engineering*, Amsterdam, Netherlands (2014).